PAUL SCHERRER INSTITUT

PSI

ABSTRACTS

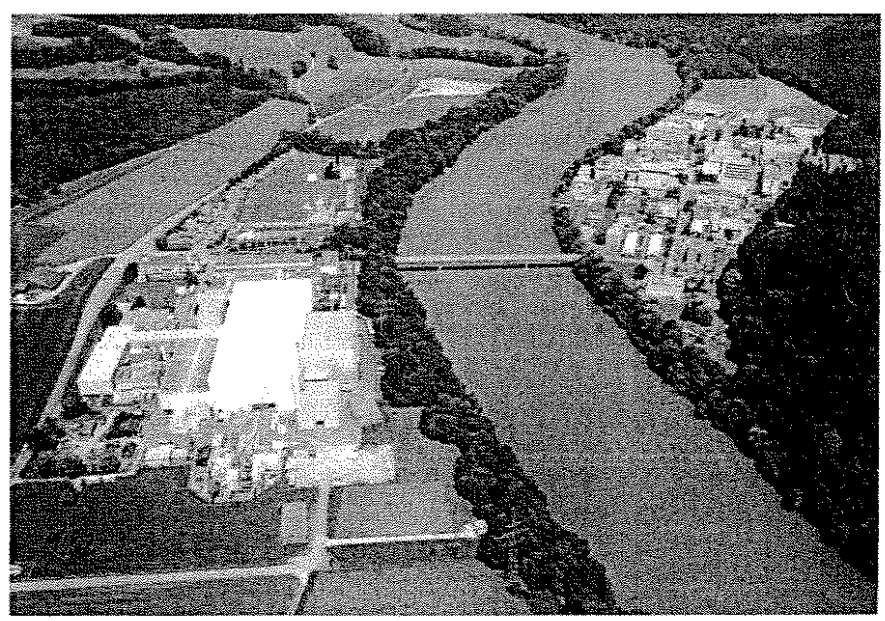

Second International Symposium on Ultrasonic Doppler Methods for Fluid Mechanics and Fluid Engineering

Paul Scherrer Institute, Villigen, Switzerland
20. - 22. September, 1999

Second International Symposium on Ultrasonic Doppler Methods for Fluid Mechanics and Fluid Engineering (2. ISUD)

20. - 22. September, 1999

Paul Scherrer Institute

Villigen, Switzerland

Scientific Committee

Dr. M.P. Chauve (IRPHE, Univ. Marseille II, Physics)
Prof. M. Aritomi (Tokyo Inst. Technol., Fluid Engineering/Nuclear)
Prof. E. Windhab (ETHZ, Fluid Engineering/Non-Newtonian)
Dr. G. King (Univ. Warwick, Physics)
Dr. M. Mori (TEPCO, Industrial Application)
Dr. Y. Takeda (PSI, Fluid Engineering/Mechanics)
Dr. A. Tokuhiro (PNC, Nuclear)

Organizing Committee

Dr. G. King (Univ. Warwick)
Dr. P. Le Gal (IRPHE, Univ.Marseille II)
Dr. Y. Takeda, (PSI, Chairman)
Dr. H. Kikura (TIT)
Dr. G. DeCesare (EPFL)

2. International Symposium on Ultrasonic Doppler Method for Fluid Mechanics and Fluid Engineering

Paul Scherrer Institute

20.9. (Monday)		21.9. (Tuesday)		22.9. (Wednesday)	
Time	Session/Presentation	Time	Session/Presentation	Time	Session/Presentation
9:00	***Registration* w/ Coffee**	9:00	***Plenary Lecture 2***	9:00	***Civil and Geo Science***
			Prof. T. Mullin (Manchester)		Best
					Laveli
10:00	***Opening***	10:00	**Coffee**		DeCesare
10:30	***Plenary Lecture 1***	10:30	***Rheology & Liquid Metals***		Bollaert
	Prof. P. Monkewitz (EPFL)		Uriev	11:00	**Coffee**
11:30	***Space Time Flow 1***		Sawada	11:30	***Fluid Mechanics 2***
	Lusseyran		Kikura		Murakoso
	King		Pinton		Taishi
12:30	**Lunch**	12:30	**Lunch**		Kuze
				13:00	***Closing***
14:00	***Space Time Flow***	14:00	***Industrial Applications***		
	Inoue		Mori		
	Stocks		Furuichi		
	Le Gal	15:00	**Discussion session**		
15:30	**Coffee**				
16:00	***Fluid Mechanics 1***	16:00	***Excursion***		
	Yamanaka		***Met-Flow Dinner***		
	Furuichi				

10.08.99/

2. International Symposium in Ultrasonic Doppler Method in Fluid Mechanics and Fluid Engineering

Tentative Program

(*: Cairman)

20.9.1999

Time	Presentation
9:00-10:00	Registration
10:00-10:30	Opening
10:30-11:30	**Plenary Lecture (1) *M. Aritomi** Prof. P. Monkewitz, EPFL
11:30-12:30	**Space and Time Flow 1 *T. Mullin**
11:30-12:00	Lusseyran F, Izrar, Audemar, Skali-Lamy, LEMTA Time-space characteristics of stratified shear layer from UVP measurements
12:00-12:30	King G, Takeda, U.Warwick Characterizing the Taylor-couette reactor
12:30-14:00	*Lunch Break*
14:00-15:30	**Space and Time Flow 2 *F. Lussyran**
14:00-14:30	Inoue Y, Kondo, Yamashita, Gifu The UVP measurement of flow structure in the near field of a square jet
14:30-15:00	Stocks N. G, Shaw, King, U.Warwick Low frequency instability of the Karman vortex street : An experimental study of the secondary wake instability
15:00-15:30	Eloy C, LeGal, IRPHE Intermittent behavior of a vortex in a deformed cylinder
15:30-16:00	*Coffee Break*
16:00-17:00	**Fluid Mechanics 1 *G. DeCesare**
16:00-16:30	Yamanaka G, Kikura, Takeda, Aritomi, TIT Flow measurement on oscillating pipe flow near the entry using UVP method
16:30-17:00	Furuichi N, Kumada, Gifu Spanwise structure around a reattachment region of a two-dimensional backward-facing step flow

21.9.1999

Time	Presentation
9:00-10:00	**Plenary Lecture (2) *G. King** Prof. T. Mullin (Manchester) Sidewall convection in liquid Gallium
10:00-10:30	*Coffee Break*
10:30-12:30	**Rheology and Liquid Metal *Y. Takeda**
10:30-11:00	Ouriev B, Windhab, ETH Study of flow processes of conventrated suspensions using in-line non invasive rheological technique
11:00-11:30	Ohira Y, Sawada, Tada, Keio Sloshing behavior of a magnetic fluid in a cylindrical container
11:30-12:00	Kikura H, Takeda, Bauer, TIT Flow mapping of the mercury flow
12:00-12:30	Pinton JF, CNRS Acoustic spectroscopy of vorticity and temperature fluctuations
12:30-14:00	*Lunch Break*
14:00-15:00	**Industial Applications *G. DeCesare**
14:00-14:30	Mori M, Takeda, Furuichi, Aritomi, Kikura, TEPCO Development of a new flow metering system using UVP (1) Principle, configuration and laboratory experiments
14:30-15:00	Takeda Y, Furuichi, Mori, Aritomi, Kikura, PSI Development of a new flow metering system using UVP (2) Comparison with weight measurement at NIST
15:00-16:00	**Discussion session *Y. Takeda / G. King**
16:00	Excursion Met-Flow Dinner

22.9.1999

Time	Presentation
9:00-11:00	**Civil and Geo Science**
9:00-9:30	Best J
9:30-10:00	Boillat JL, Lavelli, LCH Surface roughness determination based on velocity profile measurements
10:00-10:30	DeCesare G, Schleiss, LCH Turbidity current monitoring in a physical model flume using ultrasonic Doppler method
10:30-11:00	Boillat JL, Bollaert, LCH Modeling and measurement of muddy debris-flows
11:00-11:30	*Coffee Break*
11:30-13:00	**Fluid Mechanics 2**
11:30-12:00	Murakoso H, Suzuki, Aritomi, Mori, TIT Liquid flow structure around bubbles -Effect of channel width-
12:00-12:30	Taishi T, Kikura, Aritomi, TIT Effect of control volume of UVP method on turbulent pipe flow measurement
12:30-13:00	Kuze M, Furuichi, Kumada, Gifu The structure of flow over the heated rotating plate
13:00	Closing

2. ISUD
2nd International Symposium on Ultrasonic Doppler Methods
for Fluid Mechanics and Fluid engineering
September 20-22, 1999
Paul Scherrer Insitut, 5252 Villigen PSI, Switzerland

Plenary Lecture 1

Some thoughts on where flow diagnostics should be heading.

Prof. P. Monkewitz
Institute of Hydraulic Machines and Fluid Mechanics (IMHEF)
Swiss Federal Institute of Technology - Lausanne (EPFL)

2. ISUD
2nd International Symposium on Ultrasonic Doppler Methods
for Fluid Mechanics and Fluid Engineering
September 20-22, 1999
Paul Scherrer Insitut, 5252 Villigen PSI, Switzerland

"Time-Space characteristics of stratified shear layer from UVP measurements"

Lusseyran F., Izrar B., Audemar C., Skali-Lamy S.

Introduction

The flow pattern studied, is a stratified shear layer, consisting of a fresh water flowing on a salted water bed. The instabilities developing under the effect of the velocity gradient are mainly convective and thus develop with time and space during their propagation downstream. A European contract[1] on the estuaries of rivers constitutes the framework of this study, which deals in particular on the interaction between fresh water and sea water, zone in which occur, under the control of the hydrodynamic conditions, the main part of the physicochemical and biological phenomena. The measure of a velocity profile in space and time, as given by Ultrasonic Doppler Method (UVP device from Met-Flow), is well adapted to analysed the stability of such a flow and allows a comparison between the waves properties experimentally observed and the theoretical results given by a linear stability analysis.

Experimental conditions

The experiment is performed in a water channel schematically represented in figure 1. Two layers of equal depth (D=10 cm) and different densities are initially superposed and progressively sheared. The tunnel is 20 cm wide, 30 cm deep and 300 cm long. In the upper layer, the fresh water flows from the left side to the right side of the tunnel at a given flow rate corresponding to the mean velocity U_1. In the under layer, the salty water (initial concentration of NaCl : 10g/l) is coming from the right side and its flow rate is driven by a fixed pressure condition.

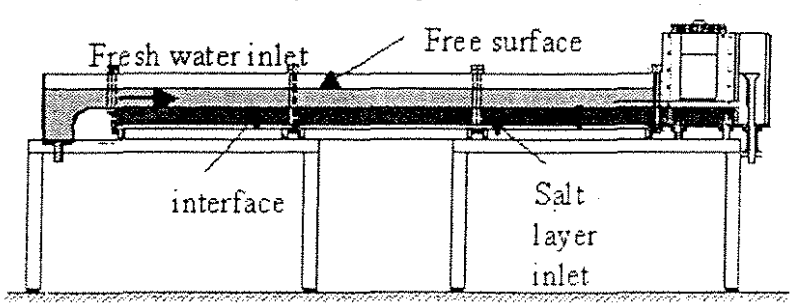

Figure1 : *Experimental loop*

[1] Financial supported by the European program MAS3-CT96-0049

The ultrasonic probe is placed horizontally in the meddle of the shear layer. The zero of the spac co-ordinate is located at 4 cm from the entrance. The specifications of the UVP used, are tabulate below:

Basic ultrasonic frequency	4 MHz
Spatial resolution	2.22 mm
Number of points in space	128
Number of points in time	1024
Acquisition frequency	16.39 Hz

Results

The development of the instabilities is illustrated figure 2. Rodamine is added to the salty wate which appears red in the laser sheet. The local gradient of concentration is still very steep, while th waves are developed enough for the expression of non linearity. The initial conditions $\{U_1,\rho\}$ of th layer are characterised by a global Richardson number $Ri_D = \frac{g}{\rho}\frac{\Delta\rho}{\Delta U_1^2} D$.

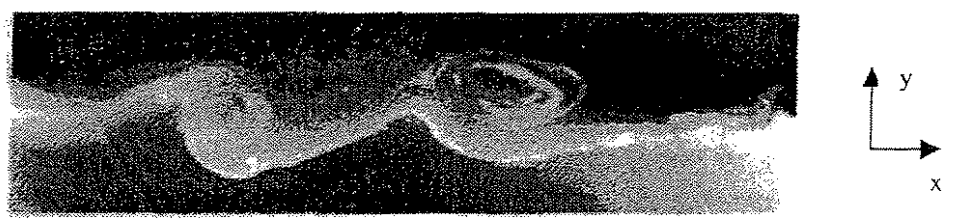

Figure 2 : *Interface between fresh and salty water under unstable conditions.*

The ultrasonic probe gives the longitudinal (horizontal) component $u(x,t)$ of the velocity. On example of the velocity field is given (Figure 3), for $Ri_D = 8.14$. The instabilities of th concentration gradient layer are clearly visible on the longitudinal component of the velocity. A large spectrum of wave length and celerity is observable, even some waves which propagat upstream. In order to measure the dispersion relationship $f(\omega,k)=0$ the 2D Fourier transfor $\tilde{u}(k,\upsilon)$ of $u(x,t)$ is applied (Figure 4). $f(\omega,k)=0$ is given by the line of the maximum of energy i the Fourier plan, which then appears as a very powerful tool for analysing the dynamics of th instabilities.

This experimental dispersion relationship is compared, with success, to the theoretical dispersio relationship, obtained from a linear stability model derived from the temporal model proposed b Lawrence et al. [1991] (Figure 6). The velocity and concentration profiles used are given figure 5.

Different analysis of the signal $u(x,t)$ are processed using the combinations between the variables of the 2 conjugated planes $P\{x,t\}$ and $\tilde{P}\{k,\nu\}$. Figure 7 gives an example of the measure of the spatial growth rate k_i of a given frequency υ using the plan $\tilde{\tilde{u}}(x,\upsilon)$.

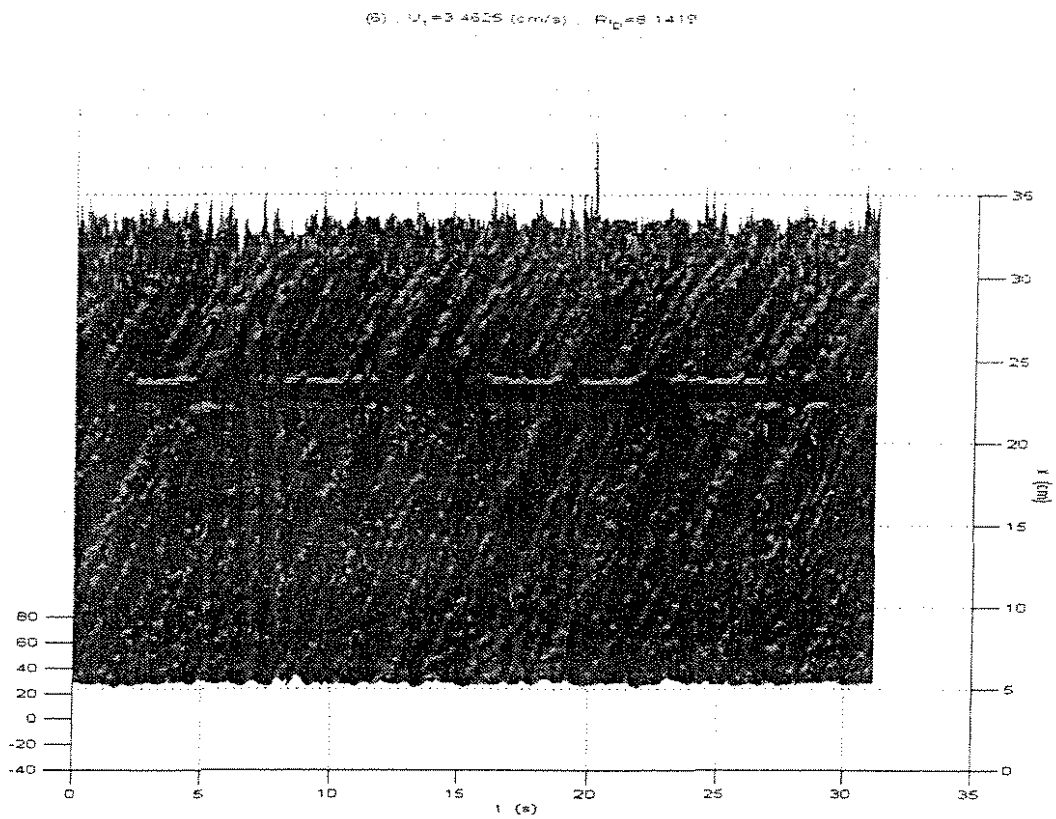

Figure 3 : *Velocity profiles versus time and space for a concentration of 10g/l NaCl and a velocity U_1=3.46cm/s.*

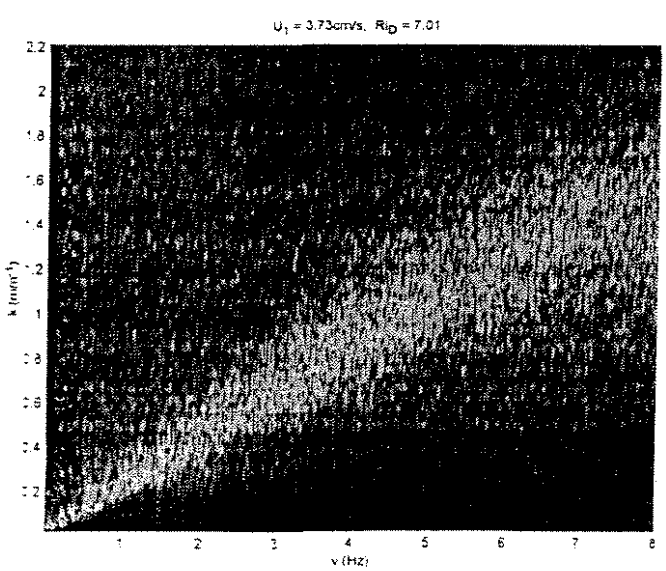

Figure 4: *Velocity amplitudes $\tilde{u}(k,\upsilon)$ in the Fourier plan.*

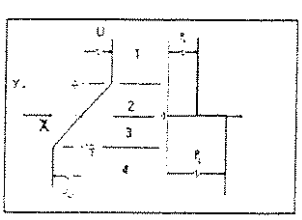

Figure 5: *From Lawrence 1991*

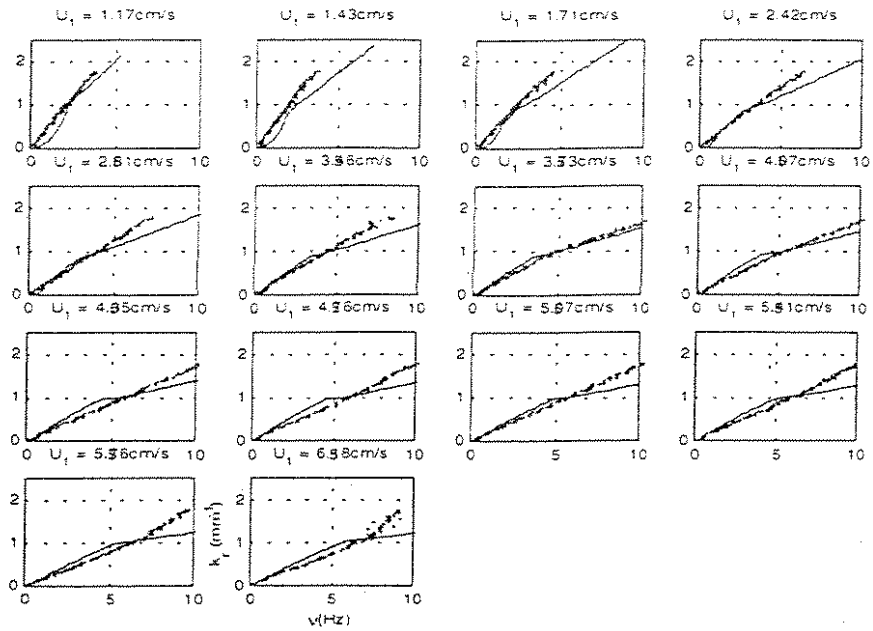

Figure 6: *Dispersion relationship for 14 values of U_1 corresponding to Ri_D={71.4,47.7,33.4,16.7,12.3,8.14,7.01,5.89,5.16,4.31, 3.79,3.33,2.94, 2.55} :- dotes results from the experimental Fourier plan,-line results from the linear stability analysis*

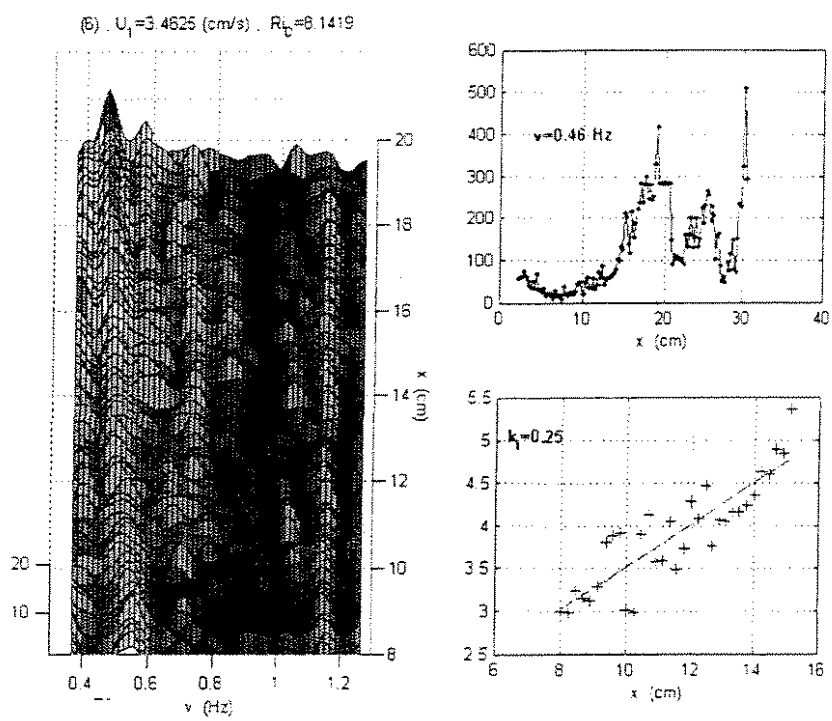

Figure 7 : *Measure of* the spatial growth rate k_i of a given frequency $\upsilon = 0.46\,Hz$ using the plan $\widetilde{\widetilde{u}}(x,\upsilon)$ for Ri_D=8.14.

Reference

Lawrence et al. J. of Fluid Mechanics, 1991.

2.ISUD
2nd International Symposium on Ultrasonic Doppler Methods
for Fluid Mechanics and Fluid Engineering
September 20–22, 1999
Paul Scherrer Institut, 5232 Villigen PSI, Switzerland

Characterizing the Taylor-Couette Reactor

G.P. King[1], Y. Takeda[2]

[1] Fluid Dynamics Research Centre, School of Engineering, University of Warwick, Coventry CV4 7AL, UK.
[2] Paul Scherrer Institut, 5232 Villigen PSI, Switzerland.

1 Introduction

In this contribution we will describe recent progress on understanding the mixing characteristics in pre-turbulent Taylor-Couette flows, and our progress in characterizing flows in the eccentric Taylor-Couette geometry. We are interested in the eccentric geometry because we expect mixing to be more homogeneous there.

Some years ago Kataoka proposed time-independent Taylor vortex flow as an ideal plug flow mixing system [1]. Since then other applications have been proposed as well as studies to parameterize the mixing properties [2, 3, 4, 5, 6, 7]. For the engineer it comes something of a surprise to discover that the mixing in three-dimensional time-independent Taylor vortex flow is not very good. In the next flow regime, wavy Taylor vortex flow, the mixing is much better, but the ideal plug flow property is lost. That is, there is significant axial transport. Even though the mixing is better, it is not always homogeneous throughout a vortex. These results come from the recent studies of chaotic advection by Ashwin and King [8] and Rudman [2]. A fundamental understanding of the mixing properties of wavy vortex flow has recently been achieved [9] based on the approach described in Ref. [10].

After describing the results in Ref. [9], we turn our attention to the eccentric Taylor-Couette system. First the basic result in Ref. [11] will be described which shows that near homogeneous mixing can be achieved in eccentric Taylor vortex flow. Unlike the concentric geometry, there are few results on the structure of flows in the eccentric geometry. As a result our experimental programme has the aim of studying the evolution of flows with increasing Reynolds number for different eccentricities. Our progress using the UVP will be described.

References

[1] K. Kataoka, H. Doi, T. Hongo, and M. Futagawa. Ideal plug flow properties of Taylor vortex flow. *J. Chem. Eng. Japan* 8 (1975) 472-476.

[2] M. Rudman. Mixing and particle dispersion in the wavy vortex regime of Taylor-Couette flow *AIChE J.* 44 (1998) 1015-1026.

[3] N.H. Thomas and D.A. Janes. Fluid dynamic considerations in airlift and annular vortex bioreactors for plant-cell culture. *Annals of The New York Academy Of Sciences* 506 (1987) 171-189

[4] C.M.V. Moore and C.L. Cooney. Axial dispersion in Taylor-Couette flow. *AIChE J.* 41 (1995) 723–727.

[5] R.M. Lueptow and A. Hajiloo. Flow in a rotating membrane plasma separator. *Am. Soc. Artif. Int. Organs J.* 41 (1995) 182–188.

[6] G. Desmet, H. Verelst, and G.V. Baron. Local and global dispersion effects in Couette-Taylor flow - I. Description and modeling of the dispersion effects. *Chem. Engng. Sci.* 51 (1996) 1287–1298; II. Quantitative measurements and discussion of the reactor performance. *Chem. Engng. Sci.* 51 (1996) 1299 1309.

[7] R.J. Campero and R.D. Vigil. Axial dispersion during low Reynolds number Taylor-Couette flow: intra-vortex mixing effects. *Chem. Engng. Sci.* 52 (1997) 3303–3310.

[8] P. Ashwin and G. P. King. A study of particle paths in nonaxysymmetric Taylor-Couette flow. *J. Fluid Mech.* 338 (1997) 341–362.

[9] G.P. King, I. Mezic, M. Rudman, G. Rowlands, and A.N. Yannacopoulos. Can particle transport coefficients be extracted from symmetry measures? Preprint, 1999.

[10] A.N. Yannacopoulos, I. Mezić, G. Rowlands, and G.P. King. Eulerian diagnostics for Lagrangian chaos in three-dimensional Navier-Stokes flows *Phys. Rev. E* 57 (1998) 482-490.

[11] P. Ashwin and G. P. King. Streamline Topology in Eccentric Taylor Vortex Flow. *J. Fluid Mech.* 285 (1995) 215-247.

2. ISUD
2nd International Symposium on Ultrasonic Doppler Methods
for Fluid Mechanics and Fluid Engineering
September 20-22, 1999
Paul Scherrer Institut, 5232 Villigen PSI, Switzerland

The UVP Measurement of Flow Structure in the Near Field of a Square Jet

Yoshihiro INOUE*, Kunikazu KONDO† and Shintaro YAMASHITA*

* Dept. Mechanical and Systems Engineering, Gifu University, Gifu 501-1193, Japan
† Dept. Mechanical Engineering, Suzuka College of Technology, Suzuka 510-0294, Japan

ABSTRACT

Coherent structures in the near field of a three-dimensional jet have been investigated. The experiments were carried out for a free jet issuing from a square nozzle into a water channel. Instantaneous velocity profiles were measured in the streamwise and cross-stream directions using an ultrasonic velocity profile monitor. From power spectra, two dominant frequencies were found out with respect to the flow structures, and it is indicated from the wavelet transform that a coherency of vortical structures was changed in time as well as in frequency domain.

1. Introduction

Flow characteristics of various kinds of a jet have been extensively examined by many workers because of their wide applicability in the industry. Control of the turbulent mixing and diffusion and reduction of the noise have also been investigated, and interactive control of the jet is carried out in recent years.

The present study intends to examine the spatiotemporal flow structure in the near-field of a square jet. It is produced by a mixing layer between the jet stream and a surrounding still fluid, and there are sharp corners in the shear layer of the square jet. A very large curvature of the shear layer induces an intensive deformation of a vortex ring, and therefore, its understanding is not sufficient only by analogy from a circular jet [1] and an elliptic jet [2]. The square jets have been investigated by Tsuchiya et al. [3], Quinn and Militzer [4], Toyoda et al. [5], Grinstein and DeVore [6], Wilson and Demuren [7], and so on.

2. Experimental apparatus and procedure

The flow field and coordinate system are shown in Fig. 1. The x-axis is taken to coincide with the jet center line. The y-axis and z-axis are normal to each side of the nozzle, and the y_1-axis and z_1-axis are along the diagonals, respectively.

The test channel is an open channel which is 0.7 m wide, 0.64 m depth and 3 m length. The nozzle is square with its side length of H = 100 mm. The jet velocity U_j remains constant in 100 mm/s, and the Reynolds number is $Re_j = U_j H / \nu \approx 1 \times 10^4$. From the results

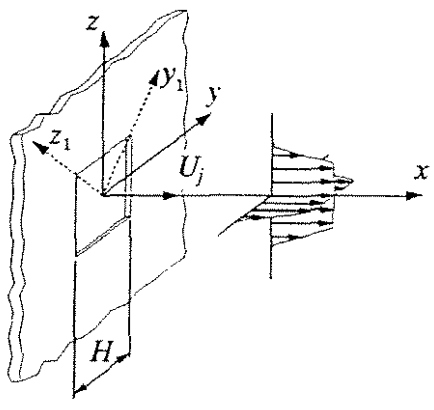

Fig. 1 Flow field and coordinate system.

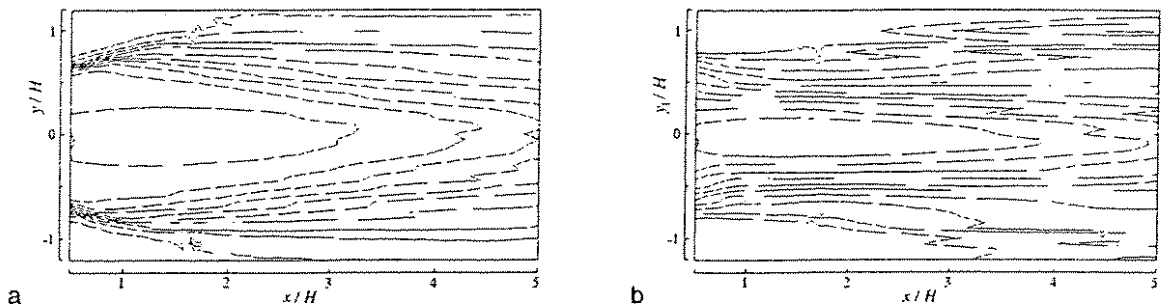

Fig. 2 Contour map of mean velocity in the streamwise direction. a x-y plane and b x-y_1 plane.

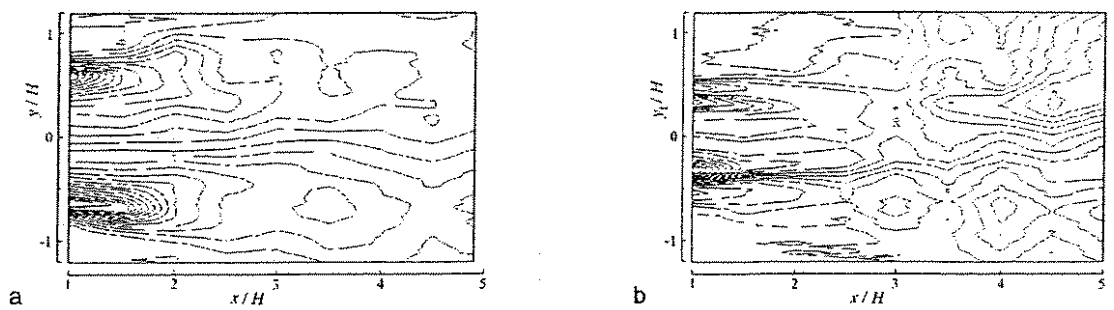

Fig. 3 Contour map of mean velocity in the lateral direction. a x-y plane and b x-y_1 plane.

obtained by hot-film measurements, the turbulence intensity in the jet core is about 1.1 % of the efflux velocity, and the momentum thickness of the shear layer is $\theta = 1.02$ mm at $x = 0.2\,H$.

UVP measurements are performed in the x-y plane and x-y_1 plane with an ultrasonic transducer of fundamental frequency of 4 MHz. Hydrogen bubbles are continuously generated from a platinum wire in the measuring plane, and are used as scattering particles for the ultrasound. The measuring time is about 57 ms for one velocity profile, and an interval time between the adjacent profiles is 160 ms.

3. Results and discussion

3.1 Mean flow fields

Figures 2 and 3 show contour maps of mean velocity in the streamwise direction and in the lateral direction in the x-y and x-y_1 planes, respectively. The mean velocity in the streamwise direction (Fig. 2) shows that the flow goes outside in the x-y plane, i.e., the opposite side direction, and the jet width rapidly extends. In the x-y_1 plane, the flow goes toward the center axis just behind the nozzle, and the jet width is gently extended in the downstream. This feature has also appeared well in the contour maps of mean velocity component in the cross-stream directions (Fig. 3). In the diagonal direction shown in Fig. 3b, the regions of the positive and the negative velocities are adjacent to each other at $|y_1 / H| \approx 0.4$ in the interval of $x / H < 1.5$. It seems that features of this flow are caused by axis-switching of the vortex ring formed in the initial shear layer.

3.2 Instantaneous velocity field

Spatiotemporal contour maps of the instantaneous velocity components in the lateral directions are shown in Figs. 4a-d at $x / H = 1$ and 3. In the upstream section of $x / H = 1$, the velocity fluctuation is relatively inactive near the jet axis, while it is developed in the mixing layer. Significant patterns of the contour line are visible about $|y| = 0.6\,H$ and $|y_1| = 0.4\,H$, and they correspond to the vortex structure in the mixing layer. In the normal direction to the nozzle side (Fig. 4a), the velocity in the mixing layer is positive for $y > 0$ and negative for $y < 0$, and in the diagonal direction (Fig. 4b), the regions of positive and negative velocities are arrayed with an

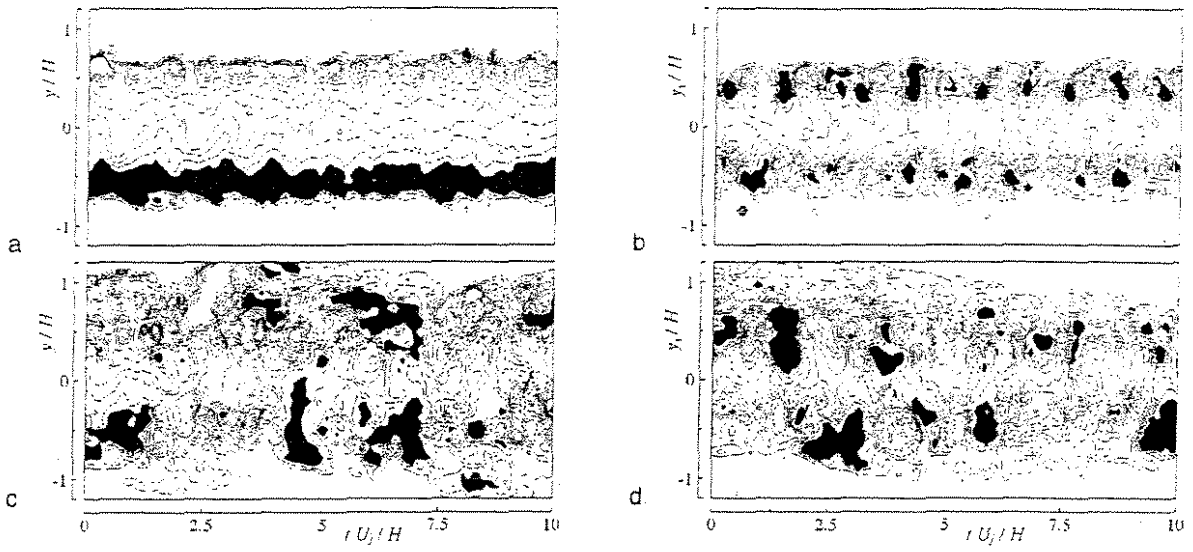

Fig. 4 Spatiotemporal velocity field in the lateral direction. **a** y-t plane at x/H =1, **b** y_1-t plane at x/H =1, **c** y-t plane at x/H =3, **d** y_1-t plane at x/H =3

organized pattern in each layer. In the downstream section of $x / H = 3$ shown in Figs. 4c-d, there is no remarkable difference between both directions, and the regions with various velocity and length scales are scattered spatiotemporally.

3.3 Power spectrum

Figure 5 shows power spectra of fluctuation velocity u at $y = 0$ and $z = 0.4\,H$. The spectrum is obtained by Fourier transforming a time-series data set of 512 points, and ensemble averaged values are shown. In the upstream sections of $x / H = 1$ to 2, there exist two spectral peaks at normalized frequencies of $St_H = f H / U_j = 0.80$ and 1.12. Also, the frequency corresponding to the jet column mode is $St_H \approx 0.41$ from the result on the jet axis. Figure 6 shows the streamwise distribution of power spectral density at these three frequencies. The values at $St_H = 0.41$ are outstanding in $x / H > 2$, and are relatively weakened in $x / H > 3.5$. The distribution related to $St_H = 0.80$ takes a peak at $x / H \approx 1.3$. The dimensionless frequency of 0.80 seems to be consistent with a time scale based on the advection of the vortex ring structure.

3.4 Coefficient of Wavelet transform

Figure 7 represents the wavelet transform of fluctuating velocity at $x / H = 1.5$ and 3. Only the positive value of the real part of the transformed results is shown. The wavelet for the analysis is Morlet wavelet [8], and k_ψ is a constant of 6. Here, a is the scale of the wavelet and b the translation on the time axis.

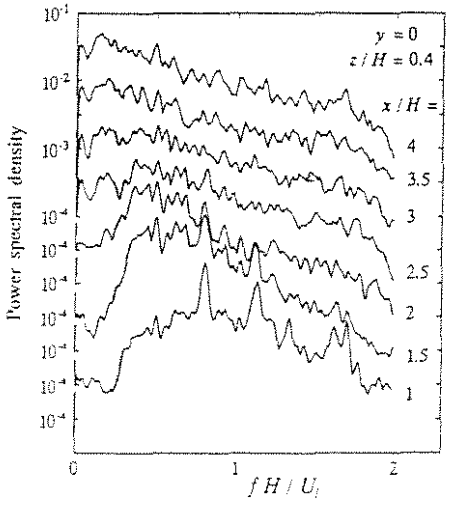

Fig. 5 Power spectrum at various streamwise-positions.

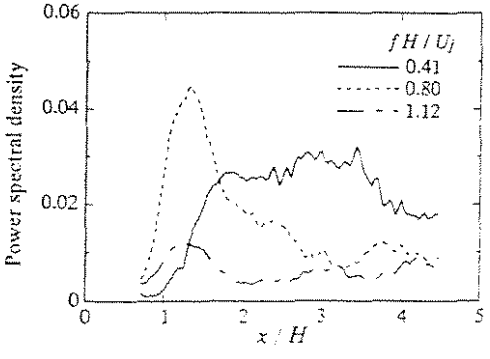

Fig. 6 Streamwise distribution of power spectral density at various frequencies.

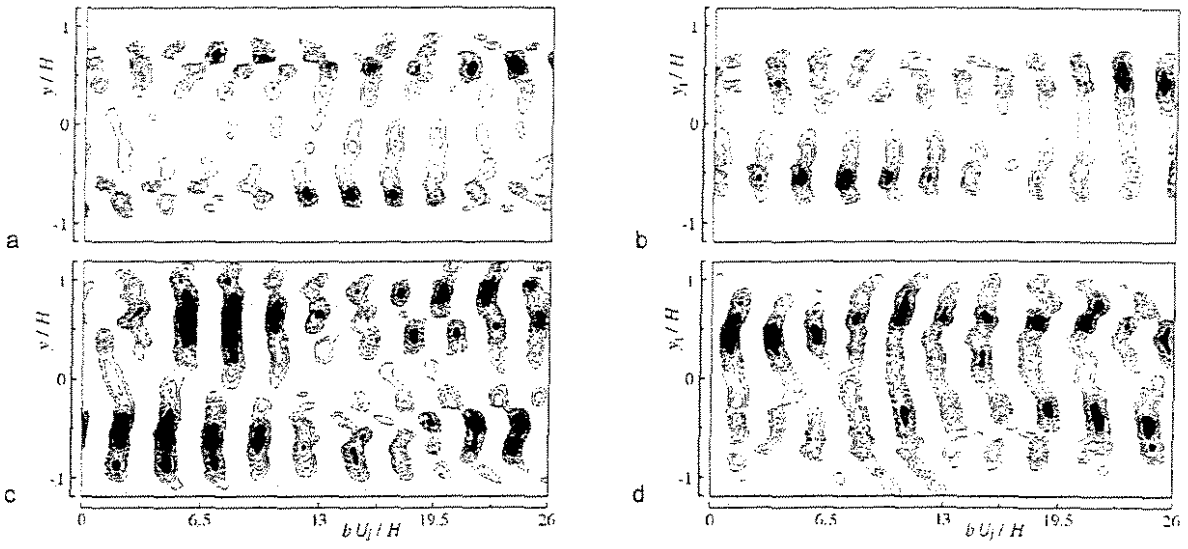

Fig. 7 Spatiotemporal map of wavelet transform with a scale of $a\,U_j/H = 2.4$. **a** y-b plane at $x/H = 1.5$, **b** y_1-b plane at $x/H = 1.5$, **c** y-b plane at $x/H = 3$, **d** y_1-b plane at $x/H = 3$

Wavelet coefficients of the velocity component normal to the jet axis are shown in Figs. 7a-d at $x / H = 1.5$ and 3. The dimensionless scale of the wavelet is fixed at $a\,U_j / H = 2.4$, which is nearly equal to a time scale of the jet column instability. Figures 7a-b in the upstream section show that the velocity perturbations with this scale occur in the mixing layers about $|y| = 0.6\,H$ and $|y_1| = 0.4\,H$, respectively. On the other hand, at $x / H = 3$ (Figs. 7c-d), the velocity fluctuations by the jet column mode are developed across the jet. The aspect of the flow field is educed by the wavelet transform, which cannot been seen clearly in spatiotemporal contour maps of the instantaneous velocity component (Figs. 4c-d). In addition, the spatiotemporal instability of the column mode can be found.

4. Concluding remarks

The spatiotemporal flow structure in the near-field of a square jet were investigated by UVP monitor. Mean flow pattern were given for the contour maps of mean velocity in the streamwise direction and in the lateral direction. Instantaneous flow pattern, power spectral density of fluctuation velocity and the wavelet transform of fluctuating velocity were analyzed from data set measured by the UVP monitor. These quantities made clear the structural properties in the near-field of a square jet.

References

[1] Hussain, A. K. M. F., *J. Fluid Mech.*, **173** (1986), 303.
[2] Husain, H. S. and Hussain, F., *J. Fluid Mech.*, **248** (1993), 315.
[3] Tsuchiya, Y. et al., *Exp. Fluids*, **4** (1986), 197.
[4] Quinn, W. R. and Militzer, J., *Phys. Fluids*, **31** (1988), 1017.
[5] Toyoda, K. et al., *Trans. JSME Ser. B*, **58** (1992), 7 (in Japanese).
[6] Grinstein, F. F. and DeVore, C. R., *Phys. Fluids*, **8** (1996), 1237.
[7] Wilson, R. V. and Demuren, A. O., *Trans. ASME J. Fluids Eng.*, **120** (1998), 285.
[8] Farge, M., *Annu. Rev. Fluid Mech.*, **24** (1992), 395.

Low frequency instability of the Karman vortex street: An experimental study of the secondary wake instability

N.G. Stocks, C.T. Shaw and G.P. King
Fluid Dynamics Research Centre, Department of Engineering, University of Warwick, Coventry CV4 7AL

SUMMARY

The flow in the wake of a finite-length cylinder has been studied experimentally as it undergoes its secondary instability. This instability occurs at Reynolds numbers around 180-190. The energy content of four main frequency modes appearing in the wake was measured before and after transition. For three of the modes, the energy content remains largely unchanged by the transition process. However, after transition, a low frequency (turbulent) mode appears which exhibits energy four orders of magnitude greater after transition than before. By considering the downstream growth rate of this mode, evidence is presented which suggests that transition to turbulence may occur as a result of wake transition in the central downstream plane of the cylinder.

INTRODUCTION

The flow of a fluid around a circular cylinder has long served as one of the archetypal systems used for the study of wake formation in bluff body flow. The evolution of the wake up to Re$\sim$ 180 is now relatively well understood (Huerre and Monkewitz, 1990, Williamson, 1996a) but the secondary instability of the Karman vortex street, which for an infinitely long cylinder is known to occur at Re=188.5 (Henderson and Barkley, 1996) is still the subject of much discussion (Zhang et al, 1995, Williamson, 1996b, 1992). This secondary instability is of some importance because it is at this stage that turbulence, in the form of stochastic fluctuations of the velocity field, is first observed globally in the wake.

The presence of boundary conditions introduces complications that are now known to be of considerable importance. They influence the flow structure across the whole span of the cylinder, even in the case of large aspect ratios. In the work presented here experiments are carried-out on the wake of a finite-length cylinder placed in a boundary layer with the other end terminating in open flow (free end). Such a situation is more typical of engineering applications. Although, at first sight, these boundary conditions seem quite different with respect to other work carried out on cylinder flows, in practice it was found (Stocks et al, 1996) that they gave rise to a rather simple and stable wake structure that is similar in form to wake structures observed in other studies. This system is therefore ideal for the study of transition when oblique (rather than parallel) vortex shedding predominates.

Recent work by Williamson (1992, 1996b) suggests that natural transition to turbulence in cylinder wakes is a consequence of an amplification of vortex dislocations that are generated in the near wake of the cylinder. Experimentally it is known that at the secondary instability of the wake a new spatial mode is observed. This is often referred to as mode-A and is characterised by the appearance of streamwise vortices with a wavelength of approximately four cylinder diameters in the spanwise direction. It is at this secondary instability that additional randomly occurring dislocations seem to appear along the span of the cylin-

der and, hence, turbulence is first observed. These dislocations grow as they propagate downstream. The results presented here seem to be consistent with this picture. It appears that the wake itself undergoes transition, resulting in the amplification of low frequency disturbances in the near wake.

THE WAKE STRUCTURE

Prior to transition, the wake has a rather simple structure that is now well understood. Directly behind the cylinder the flow is split into three separate spanwise frequency cells, a dominant central cell that corresponds to the main vortex shedding mode and two end cells which have lower shedding frequencies. Physically, this cellular structure arises through vortex dislocations at the cellular interfaces and is a direct consequence of the finite-end boundary conditions (Konig et al, 1992). These cellular modes can be thought of as the primary modes generated in the near wake. All other frequencies observed in the spectra (prior to transition to turbulence) are linear combinations of the frequencies of these modes The Strouhal frequency of the central cell was measured to be 163Hz, which corresponds to a Strouhal number ($S = fd/U$) of $S = 0.180$, this is to be compared with the predicted value for parallel shedding (Williamson, 1988) of 0.186. The discrepancy is due to the oblique nature of the shedding (this has been confirmed using measurements with two probes) which, using the formula (Williamson, 1988) $S_{obl} = S_{par}\cos(\theta)$, is calculated to have an angle $\theta = 14°$. At the interface between the cellular modes, a mode at their difference frequency (about 31Hz), is generated through nonlinear mixing. As this frequency is significantly smaller than the main vortex shedding frequency, it is found to be easily propagated downstream whilst the higher frequencies are rapidly filtered out (Williamson, 1992, Stocks et al, 1996). Consequently, it is this mode, generated by the vortex dislocations, that organises the far-wake region

After transition, a new low frequency mode appears which gives rise to a zero frequency peak in the power spectral densities. The magnitude of this peak is not small and surpasses the magnitudes of the main vortex shedding modes. Such a peak has recently been observed in another cylinder flow experiment (Williamson, 1996b), where large scale, low frequency fluctuations are observed to grow downstream of the cylinder. Evidence was presented that indicated that these low frequency fluctuations were a result of vortex dislocations which spontaneously appeared after the wake had undergone its secondary transition to spatial mode-A. However, the energy content of this peak was not studied in detail.

ENERGY CONTENT OF THE MODES

The evolution of the modes with downstream position, Figures 1, illustrate the variation of the average span-wise energy, $\langle E \rangle$, of each mode as a function of downstream position for $y/d = 0.0$. The energy of the centre cell mode, the end-cell modes, and the difference mode, Figs. 1(d,c,b) respectively, are seen to behave similarly both before (circles) and after transition (crosses). Hence these modes appear to be largely unaffected as the wake undergoes transition. This contrasts with the behaviour of the energy in the low frequency (turbulent) mode, shown in Fig. 1(a). After transition the energy in this mode increases by nearly four orders of magnitude. It is this increase in turbulent energy in the centre-plane that accounts for the greater part of the total energy in the wake.

The rapid growth (appearance) of the low frequency mode after transition results in

the whole far-wake region becoming turbulent. Effectively, after transition, the turbulent fluctuations, already present in the near-wake region, become present in the rest of the wake. However, if the increase in turbulence were solely due to an increase in the fluctuational energy in the near wake, then one would not expect different growth rates before and after transition. This tends to suggest that the wake itself has undergone transition.

If one tries to interpret these results within the framework of Williamson's vortex dislocations picture, then one would speculate that it is the secondary instability of the vortex street, giving rise to transition to mode-A, that modifies the properties of the wake. This transition results in the central plane region becoming unstable to low frequency fluctuations. Hence, these fluctuations, which already exist in the near wake region prior to transition, are selectively amplified and give rise to large scale vortex dislocations. Whilst this is obviously a simplified view of what is a complicated spatiotemporal effect, we believe it may encompass the main features of the transition process

CONCLUSIONS

In conclusion we would propose that these results, taken with the mechanism proposed by Williamson (1992,1996b), suggest that the occurrence of turbulence is due to the selective amplification of low frequency fluctuations in the near wake. Our results also indicate that this amplification mechanism arises due to a transition of the wake itself. However, it appears that the wake properties are only strongly affected by this transition in the central downstream plane of the cylinder. We postulate that it is the transition to mode-A that actually causes the modification of the wake properties and hence to the appearance of the amplification mechanism. This would suggest that naturally occurring turbulence can only be observed after the formation of this mode.

REFERENCES

Henderson, R. D. and Barkley, D (1996), 3-Dimensional Floquet stability analysis of the wake of a circular cylinder *Journal of Fluid Mechanics*, **322**, 215-241

Huerre, P. H. and Monkewitz, P. A. (1990), Local and global instabilities in spatially developed flows *Annual Review of Fluid Mechanics*, **22**, 473-537

Konig, M., Eisenlohr, H., Eckelmann, H. (1992), Visualisation of the spanwise cellular structure of the laminar wake of wall-bounded cirular cylinders *Physics of Fluids*, **4**, 869-872

Stocks, N. G., Shaw, C. T. and King, G. P. (1996), Dynamical characterisation of the spatiotemporal structures in the wake of a bluff body *Journal of Fluids and Structures*, **10**, 21-31

Williamson, C. H. K. (1988), Defining a universal and continuous Strouhal-Reynolds number relationship for the laminar vortex shedding of a circular-cylinder *Physics of Fluids*, **31**, 2742-2744

Williamson, C. H. K. (1992), The natural and forced formation of spot-like vortex dislocations in the transition of a wake *Journal of Fluid Mechanics*, **243**, 393-441

Williamson, C. H. K. (1996b), Three-dimensional wake transition *Journal of Fluid Mechanics*, **328**, 345-407

Williamson, C. H. K. (1996a), Vortex dynamics in the cylinder wake, *Annual Review of Fluid Mechanics*, **28**, 477-539

Zhang, H. Q., Fey, U., Noack, B. R., Konig. M. and Eckelmann, H. (1995), On the transition of the cylinder wake *Physics of Fluids*, **7**, 779-794

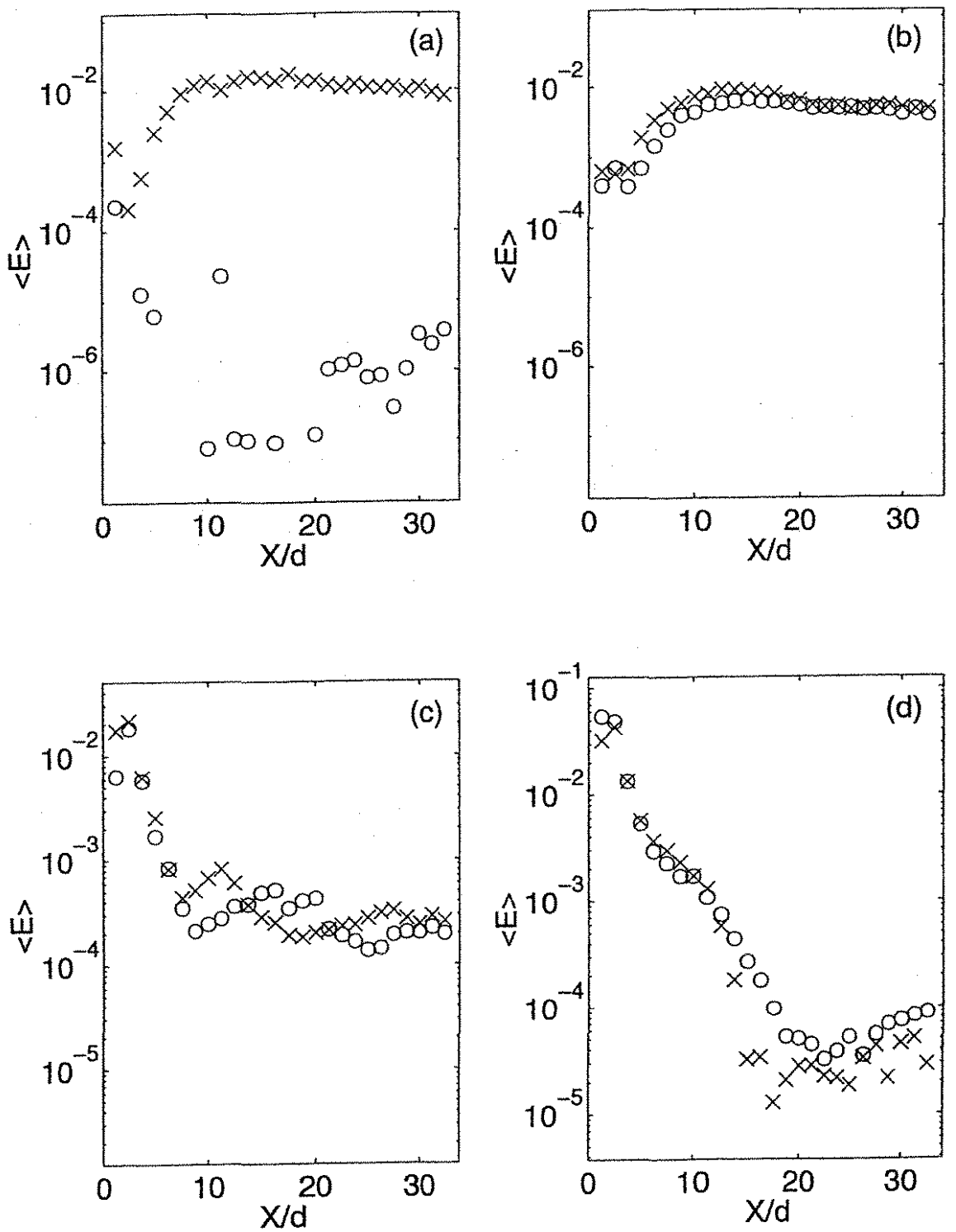

1. Average spanwise energy, $\langle E \rangle$, of modes as a function of downstream position in the centre-line plane $y/d = 0$. Four modes are shown: (a) the low frequency mode, (b) the difference frequency mode, (c) the end-cell mode and (d) the centre-cell mode. Circles represent the energy in a mode at Re=158. Crosses represent the energy in a mode at Re=189.

2. ISUD
2nd International Symposium on Ultrasonic Doppler Methods
for Fluid Mechanics and Fluid Engineering
September 20–22, 1999
Paul Scherrer Institut, 5232 Villigen PSI, Switzerland

Flow measurement on Oscillating pipe flow near the Entry using UVP method

Yamanaka,G.[1)], Kikura,H.[1)], Takeda,Y.[2)] and Aritomi,M.[1)]

1) Tokyo Institute of Technology, 2-12-1 Ohokayama, Meguro–ku, Tokyo 152, Japan
2) Paul Scherrer Institut, 5232 Villigen PSI, Switzerland

1. Introduction

Purely oscillating flow is the most simple unsteady flow, and it is the basic flow of blood flow in the arteries, oil pressure engineering and reciprocating compressor. So many researchers investigated this problem theoretically and experimentally.

Hino et al.[1] investigated the critical Reynolds number of laminar to turbulence in oscillating pipe flow, and they pointed out that there are 4 types of the flow. Merkri & Thoman[2] determined the similar result in the resonance tube. The investigations of the entrance region in unsteady flow has recieved some attention. Avula[3, 4] investigated the entrance region in flow started from rest. About the entrance region in the oscillating pipe flow, theoretical work was performed by Atabek et al.[5] and experimentally by Gerrard & Hughes[6]. They showed that laminar flow in front of an oscillating piston is fully developed at a distance $L = 0.3\delta R_\delta$, where R_δ is Reynolds number defined by Stokes layer thickness δ as a characteristic length.

In the present experiment, the velocity profiles in the entrance region of the oscillating pipe flow was investigated by the mean of ultrasonic velocity profile method (UVP)[7], and compared the measured data with Gerrard & Huge's results.

2. Experiment

Fig. 1 shows the schematic diagram of the experimental apparatus of an oscillating pipe flow. Test fluids are the solutions of glycerol, whose concentrations are 18vol% and 68vol%. The present work is performed in circular tube made of plexiglass having inner diameter 46mm, outer diameter 48mm and length 3000mm. The fluid motion is induced by an oscillating piston at the one end of the pipe. The oscillating piston is driven by a crank–gear system connected to a constant–speed electric motor. In the present experiment, oscillatory frequency is changeable. The frequency of the electrical motor is measured by the rotational meter. The motion of the oscillation piston is measured with the laser rangefinder. The pipe is connected to a water tank at the other end to reduce disturbance of water head. The pipe is placed inside a rectangular tank filled with water.

The water is used to reduce the reflection of the ultrasonic beam from the pipe wall and as a acoustic coupler between pipe and transducer, and its temperature is controlled to keep the temperature of the test fluid. The test fluid is set to be at a constant temperature of 25°C.

The velocity profile is measured by a UVP monitor model X-3 PS (Met-Flow SA). We measured the two kinds of velocity profiles, which are the axial velocity components to radial position and the axial relative velocity along the center axis of the pipe. In the measurement of the axial velocity to radial position, the transducer is positioned along the axis at various positions, and fixed onto the pipe with an angle of 15° between the transducer axis and the vertical line to the pipe axis. In the axial relative velocity measurement, the transducer is setted on the oscillating piston and moved with the oscillating piston. As the reflectors of ultrasonic, MB-100 made of plymetacril with the 68vol% glycerol solution and SB-100 made of polysthylene with the 18vol% glycerol solution are mixed. The averaged diameter of MB-100 is 100μm and SB-100 is 80μm respectively.

3. Result

Fig. 3 shows the developed velocity profiles to the non-dimensional position r/R, where r is the distance from the center axis and R the radius of the test pipe. The axis of the ordinate is the non-dimensional velocity by the averaged velocity amplitude U_0.

Fig. 4(a)~(c) shows the developing process of velocity with respect to the normalized distance x/D, where x is the distance from the piston at the upper dead point ($\varphi = \pi$) and D the diameter of the pipe. It seems that the velocity developed in the region farther than $x/D = 5$. However, the difference of velocity profiles in the relatively large distance ($x/D > 5$) is not clear from the figure. Hence Fourier analysis of the time dependent velocity on the center line of the pipe was attempted, and the results are plotted the component of the oscillation frequency of the piston and its harmonic (2nd and 3rd) components with respect to x/D in Fig. 4(e)~(f). It can be seen from the figure that the velocity in the region $x/D > 10$ is developed.

References

[1] Hino, M., et al., Experiments on transition to turbulence in an oscillatory pipe flow, *J. Fluid Mech.*, 75, pp. 193–207, (1976).

[2] Merkli, P. and Thomann, H., Transition to turbulence in oscillating pipe flow, *J. Fluid Mech.*, 68, pp. 567–576, (1975).

[3] Avula, X. J. R., Analysis of suddenly started laminar flow in the entrance region of a circular tube, *Appl. Sci. Res.*, 21, pp. 248–259, (1969).

[4] Avula, X. J. R., A combined method for determining velocity of starting flow in a long circular tube, *J. Phys. Soc. Japan*, 27, No. 2, pp. 497–502, (1969).

[5] Atabek, H. B., et al., Oscillatory flow near the entry of a circular tube, *Z. Angew. Math. Phys.*, 12, pp. 185–201, (1961).

[6] Gerrard, J.H. and Hughes, M.D., The flow due to an oscillating piston in a cylindrical tube: a comparison between experiment and a simple entrance flow theory, *J. Fluid Mech.*, 50, pp. 97–106, (1971).

[7] Takeda, Y., Velocity profile measurement by ultrasound Doppler shift method, *Int. J. Heat Fluid Flow*, 7, pp. 313–318, (1986).

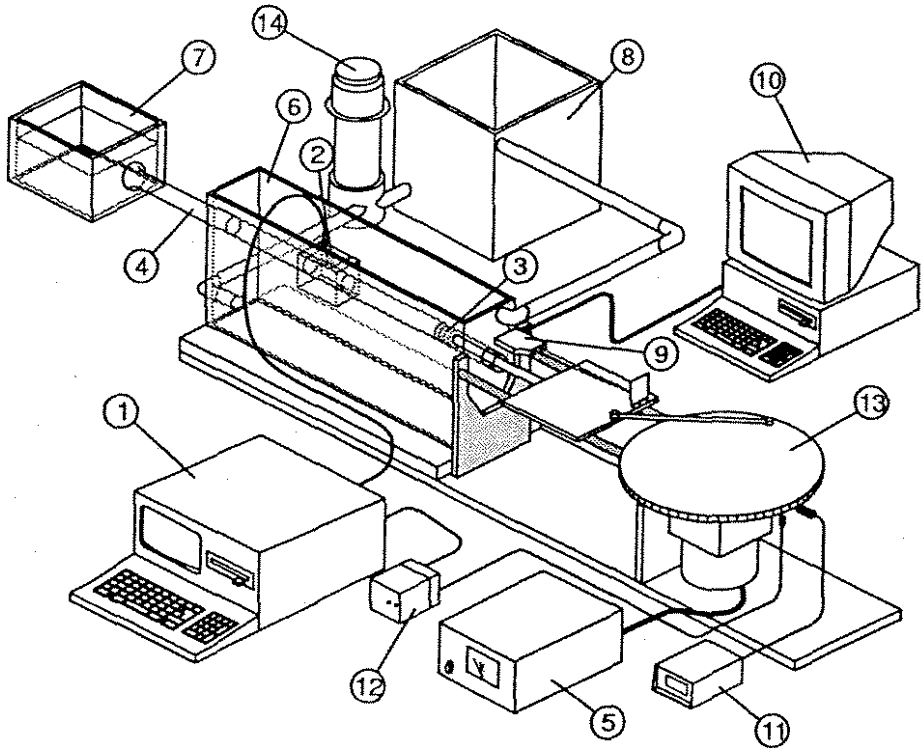

1.	UVP monitor	8.	Tank
2.	U.S. transducer	9.	Laser rangefinder
3.	Piston	10.	Parsonal computer
4.	Test pipe	11.	Rotational counter
5.	D.C. supply	12.	Relay circuit
6.	Tank	13.	Rotating disk
7.	Reserver Tank	14.	Pump

Fig.1 Experimental apparatus

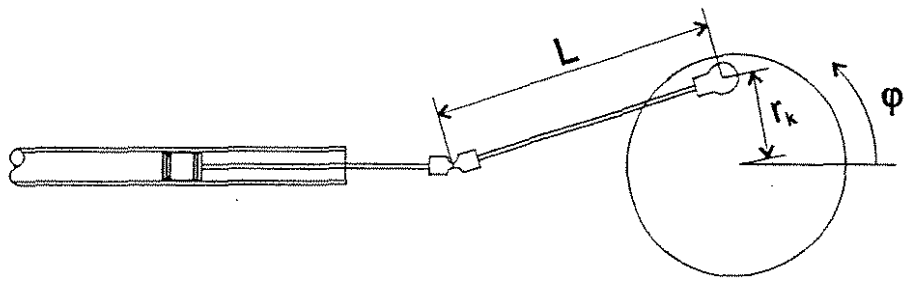

Fig.2 Schematic survey of the oscillating system

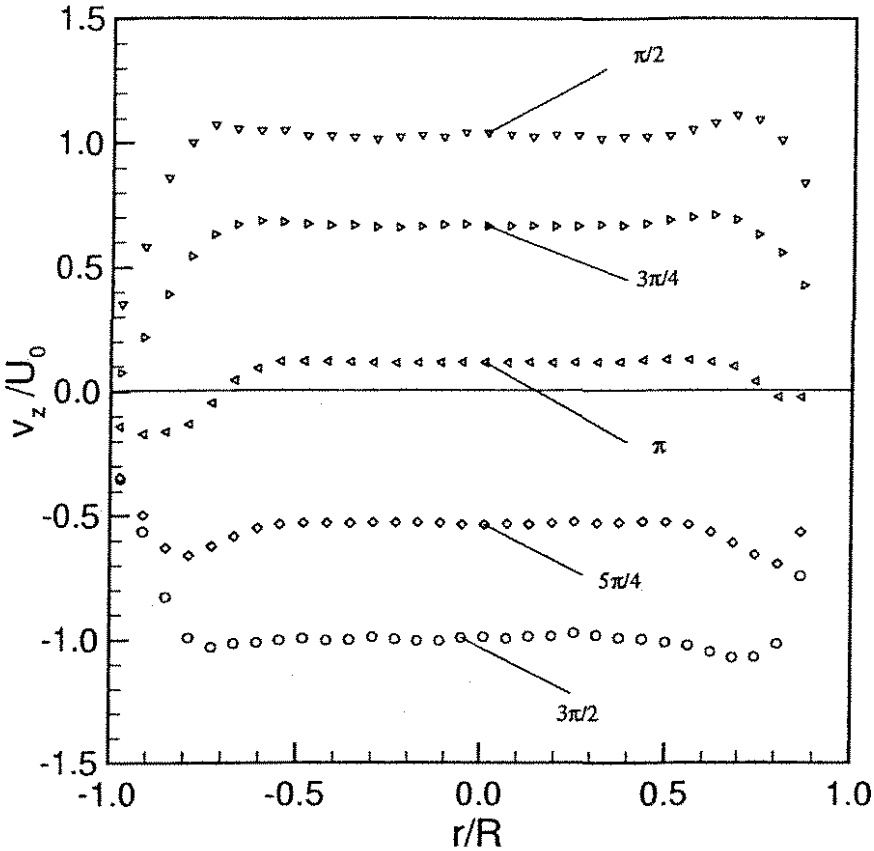

Fig.3 Time dependent velocity profiles in the developed region

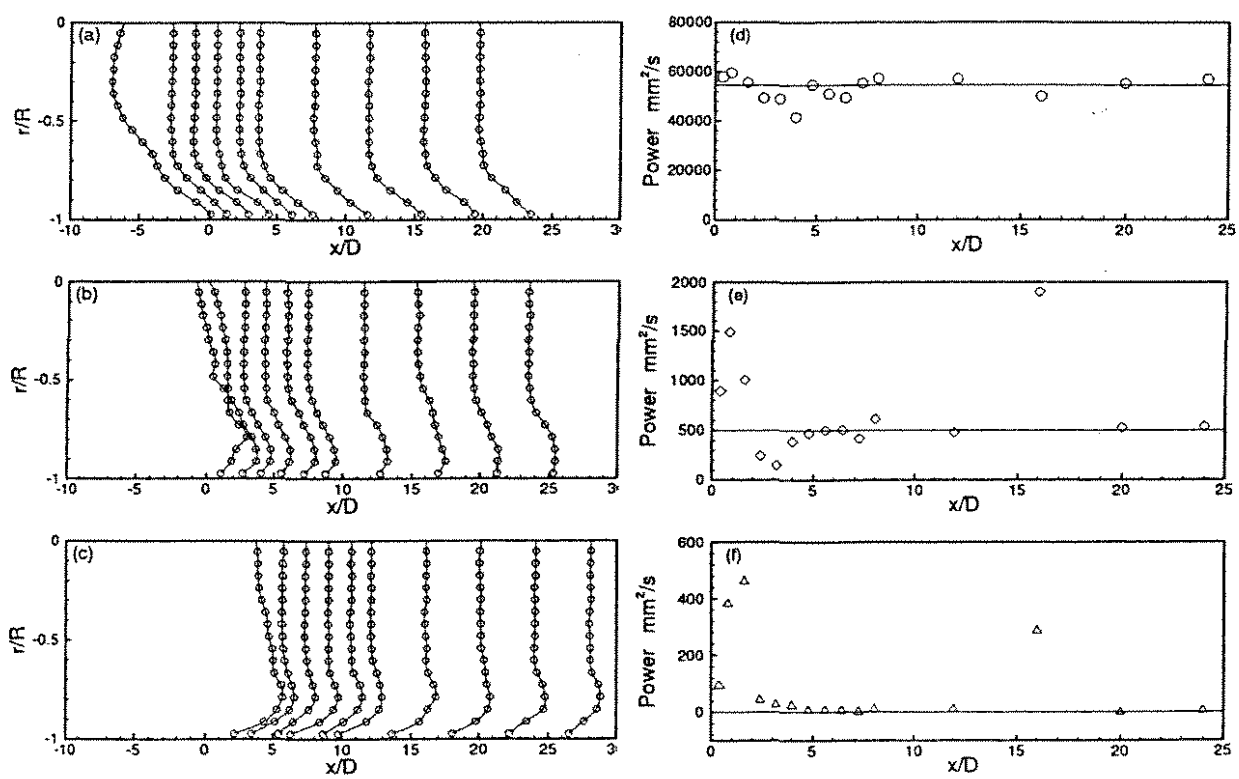

Fig.4 Velocity profiles in the entrance region at (a) $\varphi = -\pi/4$, (b) $\varphi = 0$, (c) $\varphi = \pi/4$, and the change of the spectram components of (d) 1st peak, (e) 2nd peak, (f) 3rd peak

2. ISUD
2nd International Symposium on Ultrasonic Doppler Methods
for Fluid Mechanics and Fluid Engineering
September 20-22, 1999
Paul Scherrer Insitut, 5252 Villigen PSI, Switzerland

Spanwise Structure around a Reattachment Region of a Two-dimensional Backward-Facing Step Flow

N. Furuichi[1] and M. Kumada[2]

1,2. Gifu University, 1-1 Yanagido, Gifu, 501-1193, Japan

1. INTRODUCTION

Many experiments have been performed to study around a separated shear layer and a reattachment region of a two-dimensional backward-facing step flow. A two-dimensionally flow field to streamwise direction is usually assumed to analyze flow structure, on the other hand, it is well known that this flow field exhibits a three-dimensional vortex structure and low-frequency fluctuation around a reattachment region such as many previous investigation were reported. Kasagi et al.[1] showed a three-dimensional vortex-like structure in the scale of the step height around reattachment region by the smoke-wire visualization method. Neto et al.[2] and Le et al.[3] visualized the three-dimensional vortex that has strong longitudinal vorticity in streamwise direction by numerical experiments. Hijikata et al.[4] visualized a instantaneous pressure field of the step wall by the holographic method and showed that there are some large-scale eddy around the reattachment region. However, the results of visualized vortex structure were only shown in these investigations and it was not clarified enough the three-dimensional structure in quantitative. Especially, it is suggested that the flow structure such as a low-frequency fluctuation around a separated shear layer and a reattachment region is governed by the deformation of the separated shear vortex, however there is less report about this mechanism.

It is difficult to clarify that three-dimensional structure around a reattachment region because there is not a measuring method that can be measured three-dimensional velocity component over a flow field. However, such as Kasagi et al.[5] indicated that the velocity fluctuation of w-component becomes greatest of the three-component near the step wall around the reattachment region using PTV method, it is necessary that w-component velocity is measured over a reattachment region to clarify the three-dimensional structure. In this investigation, we measure instantaneous velocity profile of spanwise direction by UVP and discussed spanwise structure and large-scale fluctuation around a reattachment region of a two-dimensional backward-facing step flow.

2.EXPERIMENTAL APPARATUS

The flow field and coordinate system are shown in Fig.1. The closed-loop water channel has working section of 240x60mm in cross sectional area

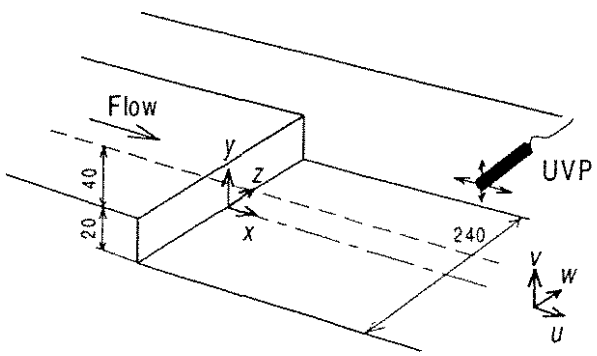

Figure 1. Experimental apparatus and coordinate system

[1] Present address : Paul Scherrer Insitut, CH5232 Villigen PSI, Switzerland

and 2300mm length. The backward-facing step (with a step height of 20mm) was formed below the floor plate at a point 250mm downstream from the construction nozzle exit. The expansion rate is ER=1.5 and the aspect ratio is AR=12. The mean velocity of main flow is fixed at Uc=0.25m/s in all experiment (Re_h=5000). The turbulence intensity of the main flow is Tu=0.6%. The mean velocity distribution of u-component upstream of the step is in agreement with the Blasius theory. The boundary thickness upstream of the step is about 4.6mm. Time-averaged velocity distribution of u-component behind a step at z=0 is in good agreement with other previous studies (Kasagi et al.[5]). The time averaged reattachment length, determined by the fraction of forward flow at y/h=0.05 is x_R=6.0 in this experiment apparatus. The mean velocity distribution of u-component and reattachment length is almost same over a channel in spanwise direction. These results were obtained by using LDV system[6].

The transducer of UVP was set the outside wall of the test section to measure spanwise w-component velocity profile. The distance of each measuring point is 1.48mm. The measuring interval is 44msec.

3.RESURLTS AND DISCUSSION

The contour map of mean w-component velocity at a time-averaged reattachment point is shown in Fig.2. The solid and dotted line means positive and negative flow direction, respectively. The positive velocity means that the flow direction is right and negative means left in this figure. It can be observed that the flow structure around reattachment region is different with one of y/h>0.4. Especially, vicinity of the step wall, there is a typical flow pattern that a flow of positive and one of negative direction exist alternately in this experiment. On the other hand, it can not be observed typical structure at y/h>0.4. A spanwise structure like this figure has not been clarified so that we can not compare this result with other one directly as mentioned above. However reflecting a reattachment phenomena, it is suggested that there is a strongly three-dimensional structure exists around reattachment region.

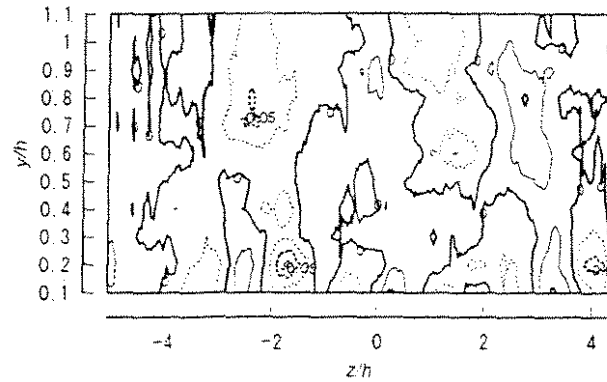

Figure 2. Mean velocity distribution of spanwise component in vertical plate at x/h=6

Typical gradation map of instantaneous velocity which measuring region is at x/h=6, y/h=0.1 is shown in Fig.3. The white color means negative (flow upward in this figure) and black means positive (downward). The horizontal axis means dimensionless time. As shown in this figure, a behavior of instantaneous w-component velocity is very complex such as it can be observed that a flow direction frequently changes in same region and that some longitudinal structure exist around tUc/h=75. It is also seemed that a lump of different flow direction forms like staggered rows. Hijikata et al.[4] showed these structure around the reattachment region in the pressure field and they indicated the these lumps are generated by the roll up of the spanwise voticies. To show this structure in quantitative, a map of two-point correlation is shown in Fig. 4. The vertical axis means a lag time and the fixed point is z/h=1.0. It can be observed a staggered-like structure and especially, a property of these structure is more clear at upward side of the fixed point (z/h>1.0) than downward. In this region, a correlation

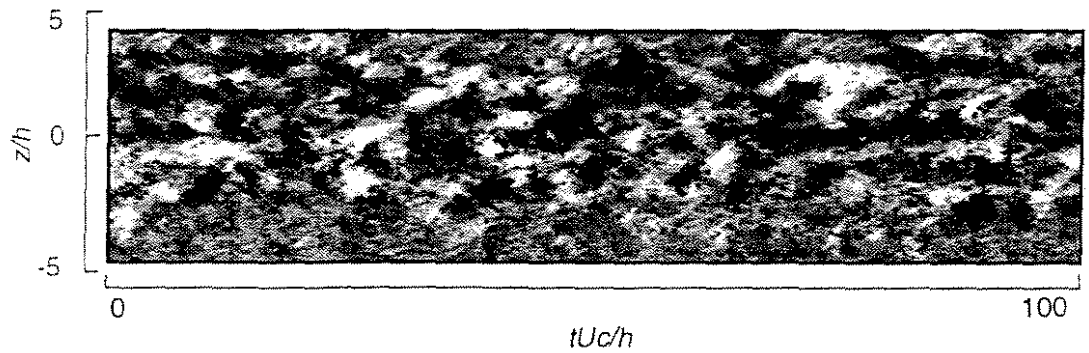

Figure 3. Time series representation of the spanwise component of instantaneous velocity at x/h=6, y/h=0.1

coefficient is negative around z/h=2 or lag-time is zero. It is suggested that the each flow direction of these region is opposite one reflecting a reattachment phenomena. No periodical structure exists at the fixed point because a flow field is unsteady, however it can be observed some islands at about tUc/h=4-5 which corresponds to the frequency of vortex generation at separated shear layer. Thus, it is suggested that the flow direction of spanwise around a reattachment region change alternately like a staggered structure.

The streamwise variation of an integral length scale is shown in Fig.5. Upstream of a reattachment region, the showing point is on the dividing stream line and downstream is the vicinity of the step wall. The integral scale increases forward to a reattachment region at a separated shear layer and it slightly increases downstream of reattachment region. Especially, it is noted that integral scale does not change drastically near the step wall at reattachment region. To pay an attention to the spanwise structure of a reattachment region, spanwise variation of integral scale at x/h=6 is shown in the Fig.6. The distribution of correlation coefficient around a fixed point is different between positive and negative side in spanwise direction so that each side integral scale is shown separately. The solid line means positive side and the dotted line negative side integral scale. An integral scale is not uniform in spanwise location and one of each direction shows a peak alternately. As suggested in the Fig.4, there is some lumps around a reattachment region.

There is a possibility that the operation of the long time correlation eliminates the property of the instantaneous structure. In Fig.7, the temporal variation of the correlation coefficient is shown to consider the instantaneous structure around reattachment region. The time period for the reference is 1.8sec (fh/Uc=0.045) that means the frequency of the large-scale structure of the separated shear layer such as flapping[7]. The reference point is at z/h=-1.2 and calculating point is z/h=-1.8 (the solid line) and z/h=0.3 and -0.5 (the dotted line). These points are the peaks in Fig.6. The horizontal axis means the lag-time and vertical axis means the correlation coefficient. It can be observed the large-scale fluctuation periodically that frequency is about fh/Uc=0.01 in dimensionless time and more small fluctuation that considered a flapping is fh/Uc=0.1. A frequency of large-scale fluctuation is larger than that of flapping. This fluctuation of correlation coefficient means that the instantaneous flow direction change alternately same or opposite between reference point and calculating one. As shown in figure, the solid line and the dotted are 180 out-of-phase so that this fluctuation exists over a reattachment region. To more clear this mechanism, we calculated the power spectrum of the velocity fluctuation. Reflecting many scale fluctuations, it can be observed many peaks of the power spectrum over the flow field, however we paid attention to the low frequency around

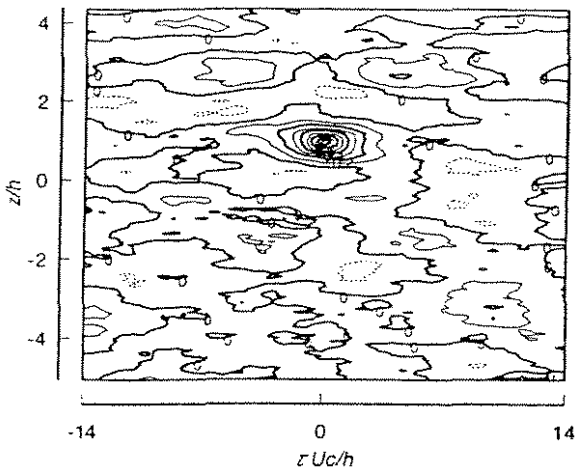

Figure 4. Contour map of two-point correlation at x/h=6, y/h=0.1

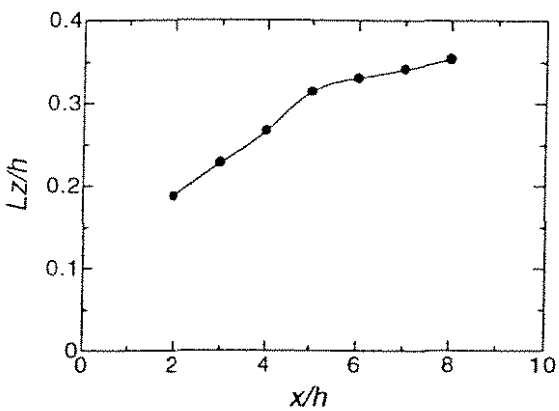

Figure 5. Streamwise variation of integral scale

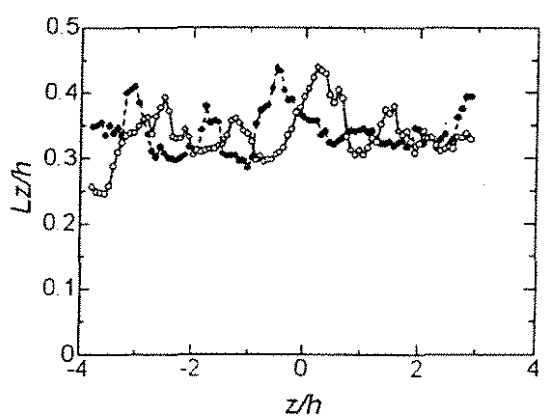

Figure 6. Spanwise variation of integral scale at x/h=6, y/h=0.1

the 0.18Hz. In Fig.6. the spanwise distribution of the power spectrum is shown around 0.18Hz (fh/Uc= 0.01) at x/h=6,7. At x/h=6, several typical peaks can be observed such as indicate by arrows. The position of these peaks is good agreement with the one of the cross point of integral scale in Fig.6. On the other hand. more downstream at x/h=7, typical peak can not be observed. Therefore, it is considered a typical spanwise fluctuation over the flow field at a time-averaged reattachment region.

Around a reattachment region, it is well known that low frequency fluctuation becomes larger than at the separated shear layer. Kondo et al.[8] showed the fluctuation of pressure field around reattachment region and they indicated that there was a large scale fluctuation which frequency is about fh/Uc=0.01. Eaton and Johnston[9] also indicated that 30% energy of the u-component velocity exists fh/Uc<0.1. It has not been clarified that a large scale fluctuation of spanwise velocity component in quantitative in previous study, however in our experiment, low frequency fluctuation around a reattachment region becomes larger than that at the separated shear layer same as one of u-component velocity. Especially the component of fh/Uc=0.015 shows a typical behavior. These phenomena can be observed clearly only the vicinity of the step wall around a time-averaged reattachment point. It is suggested that this large scale fluctuation is concerned to the one of instantaneous reattachment point over a channel and it might contribute largely to w-component fluctuation.

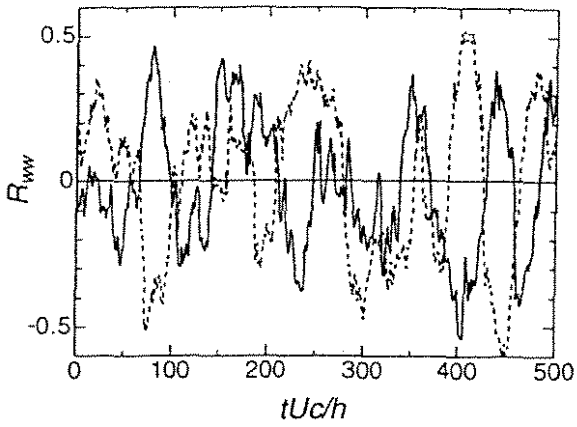

Figure 7. Temporal variation of the two-point correlation coefficient between z/h=-1.2 and z/h=-1.8 (solid line), z/h=0.3 and z/h=-0.5 (dotted line)

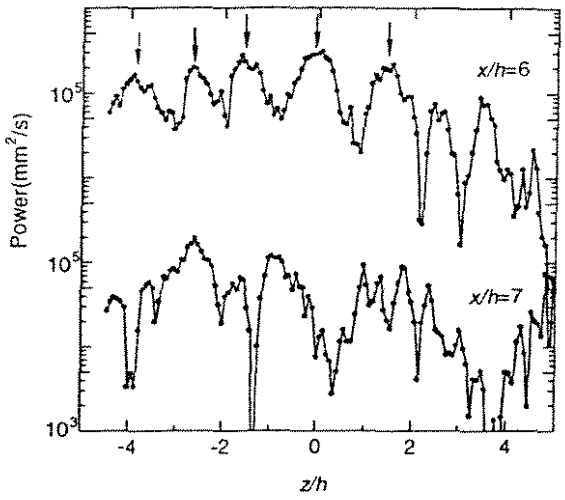

Figure 8. Spanwise variation of power spectrum of the fh/Uc=0.015.

4.CONCLUSION

A spanwise structure of a two-dimensional backward-facing step flow around a reattachment region is clarified by using UVP. As a result, around reattachment region, it is found that the spanwise structure is not uniform to spanwise direction and there is some lump that is staggered-like structure vicinity of the step wall. A fluctuation of the w-component velocity around reattachment region is larger in a low-frequency than that of the separated shear layer. Especially the component of fh/Uc=0.015 in dimensionless time shows a typical behavior which fluctuate to spanwise direction over a channel.

REFERENCES

[1] Kasagi. N., Hirata, M. and Yokobori, S., Proc. The Int. Symposium on Flow Visualization, pp245, 1977

[2] Neto. A. S., Grand, D., Metais, O. and Lesieur, M., J. Fluid Mech.. 256. pp1, 1993

[3] Le. H.. Moin, P. and Kim, J., J. Fluid Mech., 330, pp349, 1997

[4] Hijikata, K., Mimatsu. J. and Inoue, J., AEME-FED Exp. and Numerical Flow Visualization, 128, pp61, 1991

[5] Kasagi. N. and Matsunaga, A., J. Heat and Fluid Flow, 16, pp477, 1995

[6] Furuichi, N., Hachiga, T., Hishida, K. and Kumada, M., Proceeding 9th International Symposium on Application of Techniques to Fluid Mechanics, pp22-1, 1998

[7] Furuichi. N., Hachiga, T., Hishida, K. and Kumada, M., 1st Turbulence and Shear Flow Phenomena, 1999

[8] Kondo. T. and Nagano, Y., JSME-B, 54-505, pp2114, 1988 (in Japanese)

[9] Eaton. J. K. and Johnston, J. P., Stanford Univ. Rep. MD-39, 1980

2. ISUD
2nd International Symposium on Ultrasonic Doppler Methods
for Fluid Mechanics and Fluid Engineering
September 20-22, 1999
Paul Scherrer Insitut, 5252 Villigen PSI, Switzerland

Sidewall Convection in Liquid Gallium

T. Mullin
Dept. of Physics and Astronomy
University of Manchester

Introduction

Side wall convection in liquid metals is an important problem in the semiconductor crystal growing process known as the Bridgman technique. In this a crucible of molten material is slowly drawn from a furnace and solidification takes place as the container is exposed and cools.

This technique is used in the growth of high-quality materials for optoelectronic applications, for example. The industrial process may involve dendrite growth and the distribution of dopants and is thus a complicated problem. However, insights can be gained from studying the basic fluid dynamics that result from the differential heating of the sample since other processes are strongly influenced by the induced motion. For small temperature differences, the convection is steady and primarily consists of a large, single circulation. However, the bulk flow in a confined cavity evolves considerably for larger values of the driving force, as the interaction between the different regions of flow becomes significant. Thus, the mechanisms underlying the transitions to time-dependent and eventually turbulent flow are often complex. In crystal growth processes the temperature gradient between the melt and the solid gives rise to buoyancy driven convection. In most practical situations the motion so induced is found to be highly disordered or even turbulent. It is known that these flows can produce irregular distributions of dopant called striations in the host material and this inhomogeneity is undesirable if one wants to grow good quality semiconductor crystals. Hence there is considerable interest in methods of suppressing or controlling fluid convection.

One method of controlling the convection is to apply an external magnetic field. This induces an electromotive field which can be non--uniform in regions in the melt. Hence electrical currents can flow, and these interact with the applied magnetic field to damp the convective motion. These effects can be calculated explicitly for simple geometries but laboratory and practical flows are extremely complicated and require numerical computations. It is the aim of the present study to

investigate the fundamental magnetohydrodynamic interactions in a simplified crystal growth geometry using a combined experimental and numerical approach. By doing this we hope to gain insight into the basic fluid mechanical processes and thereby provide a platform on which to build an understanding of more practical flows.

An investigation of the effects of a magnetic field

We will first discuss the results of an experimental and numerical study of the effects of a steady magnetic field on side wall convection in molten gallium. The magnetic field is applied in a direction which is orthogonal to the main flow. The convection is reduced by the magnetic field and good agreement is found for the scaling of this effect with the relevant parameters. Moreover, qualitatively similar changes in the structure of the bulk of the flow are observed in the experiment and the numerical simulations. In particular, the flow is restricted to two dimensions by the magnetic field, but it remains different to that found in two-dimensional free convection calculations. We also show that oscillations found at even greater temperature gradients can be suppressed by the magnetic field.

An investigation of structure of the flow field

Next we will report the results of an experimental and numerical investigation of the steady flow of molten gallium in a differentially heated rectangular enclosure. Excellent agreement is found between the experimental results and those from a full three-dimensional numerical simulation based on a Boussinesq model. Qualitative differences are uncovered between these new findings and published results obtained from analytical and two-dimensional models. Detailed features of the flow are examined and the significance of cross-flows in the centre of the cavity is revealed. Specifically, we show that the transition to time-dependent flow will be different in two and three-dimensional models.

Secondary flows are found to be important and these show a strong dependence on the Prandtl number emphasising the role of this parameter in the problem. Some discrepancies are found between the results from the numerical centro-symmetric model and the experiment which arise from unavoidable external influences.

Juel, A., Mullin, T. Ben Hadid, H. & Henry, D. 1999 Magnetohydrodynamic convection in molten gallium. J. Fluid Mech., 378, 119-144.

Juel, A., Mullin, T. Ben Hadid, H. & Henry, D. 1999 Three-dimensional free convection in molten gallium. J. Fluid Mech.(Submitted)

2.ISUD
2nd International Symposium on Ultrasonic Doppler Methods
for Fluid Mechanics and Fluid Engineering
September 20-22, 1999
Paul Scherrer Institute, 5232 Villigen PSI, Switzerland

STUDY OF FLOW PROCESSES OF CONCENTRATED SUSPENSIONS USING IN-LINE NON INVASIVE RHEOLOGICAL TECHNIQUE

Boris Ouriev and Erich J. Windhab

ETH Zürich, Institute of Food Science/Food Engineering, CH-8092 Zürich

Introduction

To detect changes in the quality of food materials, related to the microstructure of the food system already in the production process, the rheological flow behaviour of the in general non-Newtonian, highly concentrated and non–transparent fluid is a powerful "tool" if it can be measured in-line. Commercial process rheometers are usually not suitable for this purpose because of their size, cost and destructive methods they are based on.

In our approach we mainly consider pressure driven laminar shear flows of highly concentrated non-transparent food suspensions which are transported in the most of the production processes of interest in cylindrical tubes. An emphasis made on development of measurement cell accommodating an Ultrasound Velocity Profiler (UVP X3, Met-Flow SA) Doppler system and two micro pressure transducers for in-line viscosity sensing.

As one of application solutions the authors introduce direct inline measurements conducted in transporting pipe of chocolate crystallisation process. In particular case the process influences the crystal fraction in the chocolate suspension, and thus strongly affects the flow properties (rheology) as well as a variety of quality characteristics like stability, texture, spreadability and taste of the final product.

The crystallisation process is sensitive to slight modifications of the structure of the chocolate suspension mainstream. Injection of defined type and amount of crystals into the liquid phase of the chocolate suspension influence the final quality of the product. Since the product is non-transparent and very sensitive to slight temperature, flow velocity and applied deformation changes, no other alternative could be found for precise on-line structure state monitoring.

Experiments

The developed in-line measured cell was adapted and installed in an industrial chocolate crystallisation process. The cell consists of a straight pipe section with 32-mm diameter (DIN 32). A 4 MHz UVP X3 was used for in-line flow visualisation in the sectional tube channel which is a part of the process transporting pipe (see Figure 1).

Simultaneously, the wall shear stress was measured using so-called pressure difference method with two flush-mounted pressure transducers. Besides, temperature sensors incorporated in the pressure transducers are used for temperature measurement in the flow channel.

A new data acquisition system with software was created for precise rheological on-line calculations and monitoring (see Figure 2).

The shape of the measured velocity profiles was approximated using the power law model and was correlated with the crystals concentration in the chocolate suspension. The shear rate distribution was computed from the UVP velocity profile values. The fit velocity profile was

used for volumetric flow rate calculation. A pressure difference was calculated from the mean values of smoothed raw pressure signals. Further calculations of the wall shear stress and shear stress distribution along the diameter distance was performed. During the last step the shear viscosity function is composed from shear rate and shear stress distributions.

The process consists of two production procedures. During the first one, a fixed amount of 0.14 % *Cm* (mass concentration) crystals is injected into the liquid phase of the chocolate suspension. During the second one, an amount of 0.05 % *Cm* was injected. The influence of only 0.1 % *Cm* additional crystals could be recorded as a change in power law exponent *n* (see Figure 5) and shear viscosity function (see Figure 6).

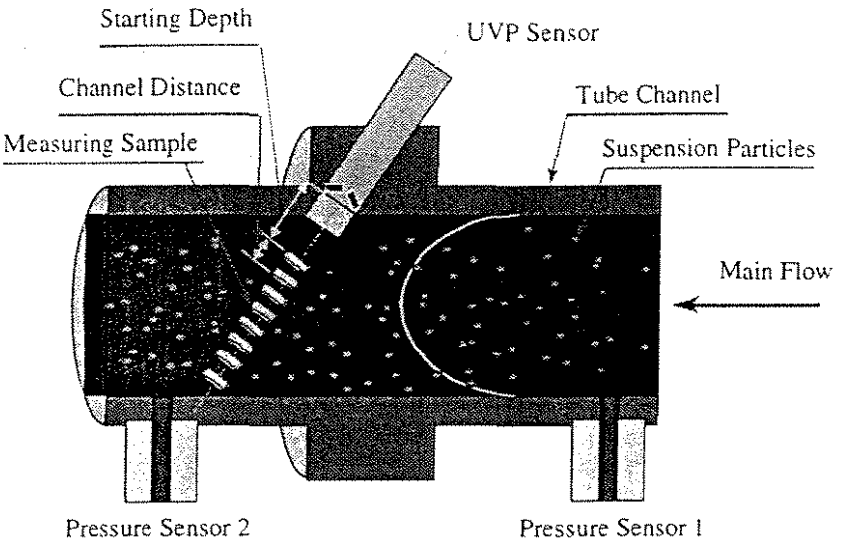

Figure 1: Schematic of the shear stress adapter with pressure sensors installed in the sectional transporting pipe with the distance L = 990 [mm] apart. It also shows a basic parameters used in flow visualisation set-up of the UVP sensor

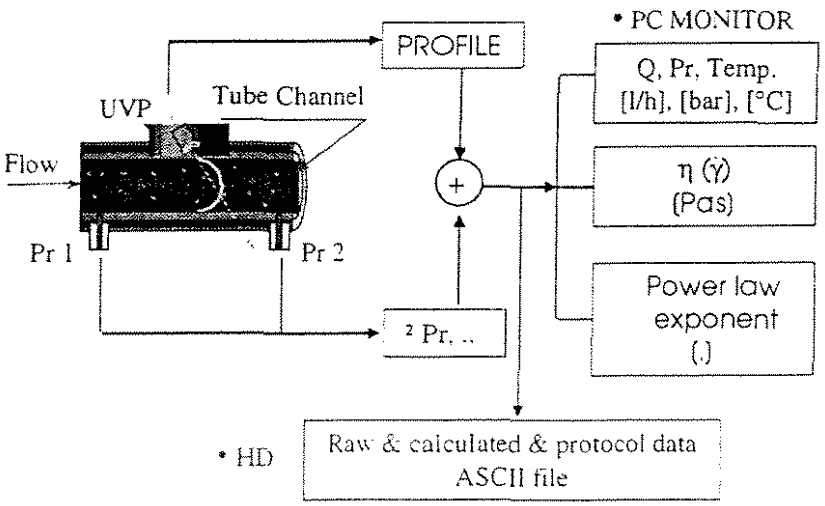

Figure 2: General data flowchart of In-line Rheometer: measurement, real time monitoring and storage of raw and calculated data.

A general data flowchart is shown in Figure 2. The on-line monitor (see Figure 2) is active throughout the measuring sequence. The information on the monitor is renewed consequently with the new incoming data file from the UVP monitor.

Results and Discussion

The measured time averaged flow velocity *Vx(r)* profiles along the diameter distance *Dd* are shown in Figure 3. The result of the on-line power law fit procedure is introduced (see Figure 4) in a form of calculated velocity profile. Using a Herschel-Bulkley approximation a yield stress could be derived from the averaged raw velocity profile and compared with the measurement of conventional rotational rheometer.

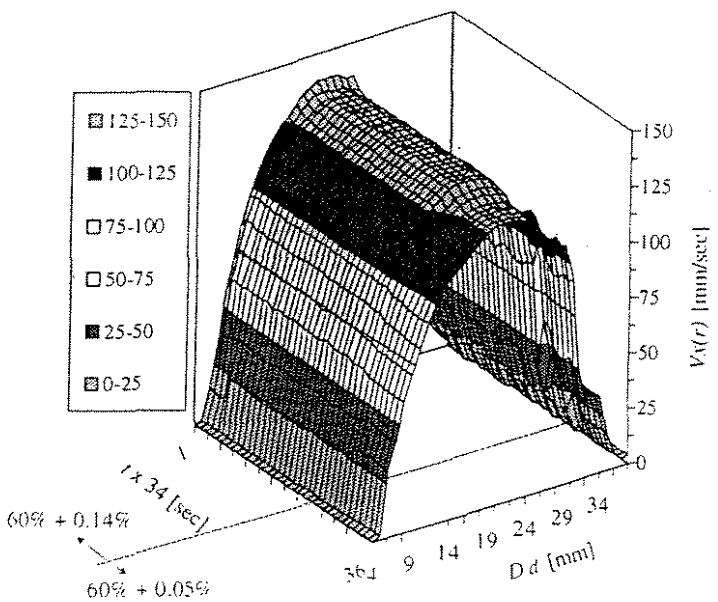

Figure 3: A 3D time series chart of raw velocity profiles of concentrated chocolate suspension (solids concentration greater than 60 % Cm); the average time between two velocity profile recordings varies between 30 and 34 sec.

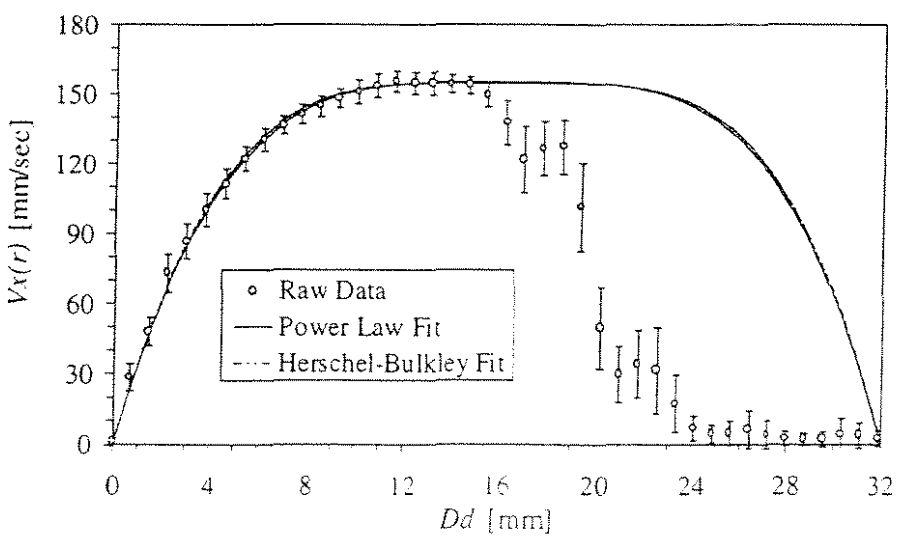

Figure 4: A 1D raw velocity 'Vx(r)' profile of chocolate suspension: power law and Herschel-Bulkley fit are shown as a solid and dashed lines and measured values as symbols.

According to shown in Figure 4 Herschel-Bulkley fit gives an output parameters as radius of the plug $R^* = 1.5$ [mm] and power law exponent $n = 0.4$. The wall shear stress and the yield stress value could be approximated from the pressure head loss $\Delta P = 0.057$ [bar] measured along the length distance $L = 990$ [mm]. The yield stress measured in-line exceeds value of $\tau_0 = 4.32$ [Pa] in comparison with the off-line rotational rheometer measurement of yield stress approaching $\tau_0 = 4.52$ [Pa].

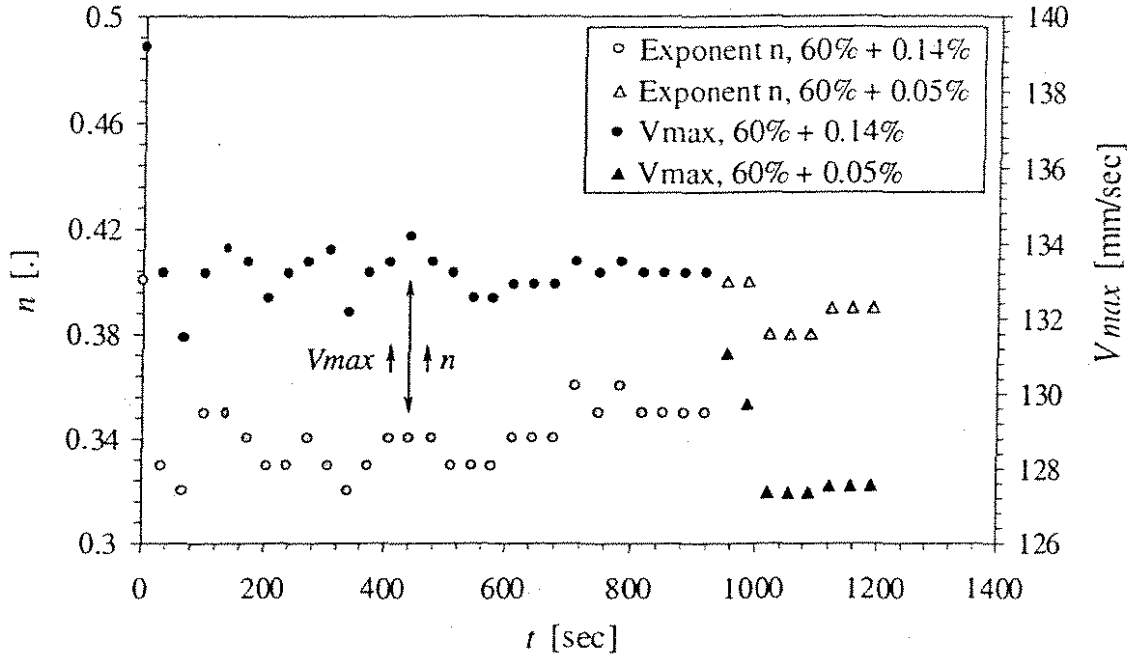

Figure 5: Comparison between maximum flow velocity 'Vmax' and power-law exponent 'n' as a function of time 't'.

With increasing of the flow velocity *Vx(r)* the structure of chocolate suspension is exposed to faster deformation rate, which is followed by slightly delayed dispersing of the structural network. The opposite reaction of the structure is found during decrease of the flow velocity. This can be observed on-line from the "in phase" fluctuations of the power law exponent *n* with the maximum flow velocity fluctuations.

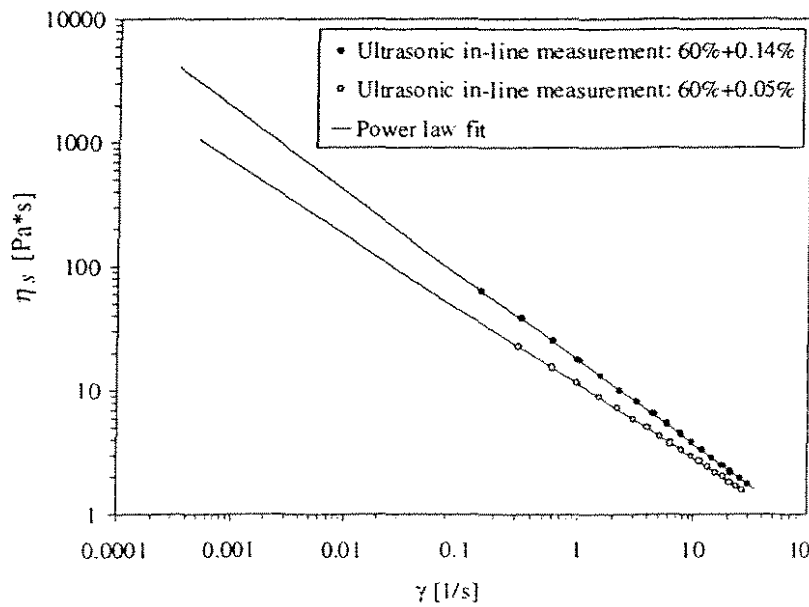

Figure 6: Shear viscosity function 'η_s' computed and monitored on-line every 30 sec.

An increase in effective concentration of solids on 0.1 % Cm distinguishably changes the slope and offset of the shear viscosity function (see Figure 6).

The measured rheological quantities, namely the shear viscosity function (see Figure 6) and power law exponent n (see Figure 5), described the structural state of the chocolate suspension in the industrial crystallisation process and enable a continuous process monitoring.

Acknowledgement

The authors wish to thank the workshop ETH LMVT and Dr. Takeda with Mr. Gogniat for their support in present research.

Literature

Takeda, Y
Measurement of flow phenomena using the ultrasonic velocity profile method in a simulated Cyochralski crystal puller. Journal of crystal growth, 1993 June.

E. Windhab, B. Ouriev, T.Wagner, M. Drost
Rheological study of non-Newtonian fluids
(Abstract) Proceedings of the 1st International Symposium on Ultrasonic Doppler Methods for Fluid Mechanics and Fluid Engineering, Villigen PSI, Switzerland (1996)

B. Ouriev, Prof. E. Windhab.,"Slit rheometry for testing of a new on-line measuring system", proceedings of the Food Rheology Congress, March 1997, Zurich.

Ouriev. B, Windhab E.
Slit rheometry for testing of a new on-line measuring system
Proceedings of the Food Rheology Congress, pp. 378-383, (March 1997), Zurich

Ouriev B., Windhab E.
In-line rheological measurements and flow visualisation using Doppler ultrasound method.
5th European Rheology Conference, Extended Abstract, Proceedings (, September 6-11, 1998), Ljublijana, Slovenia.

Ouriev B., Windhab E.
On-line rheological measurements and process monitoring using flow visualisation of non-transparent highly concentrated multiphase systems using Doppler ultrasound method.
International Conference on Colloid Chemistry and Physical-Chemical Mechanics, Abstract, Proceedings, pp. 232 (October 4-8, 1998), Moscow, Russia.

2. ISUD
2nd International Symposium on Ultrasonic Doppler Methods
for Fluid Mechanics and Fluid Engineering
September 20-22, 1999
Paul Scherrer Insitut, 5252 Villigen PSI, Switzerland

Sloshing Behavior of A Magnetic Fluid in A Cylindrical Container

Y.Ohira[1)], T.Sawada[1)] and M.Tada[2)]

1) Department of Mechanical Engineering, Keio University
3-14-1 Hiyoshi, Kohoku-ku, Yokohama 223-8522, Japan
2) Tokyo Motor Vehicle Works, Mitsubishi Motors Corporation
10, Ohkura-cho, Nakahara-ku, Kawasaki 211-8522, Japan

1 Introduction

The magnetic fluid is a stable colloidal dispersion of rather small surfactant-coated magnetic particles in a liquid carrier. It is developed in order to control a position of liquid fuel under a gravity-free state. Its characteristics such as strong magnetism and liquidity are paid attention, and fundamental studies have been carried out.

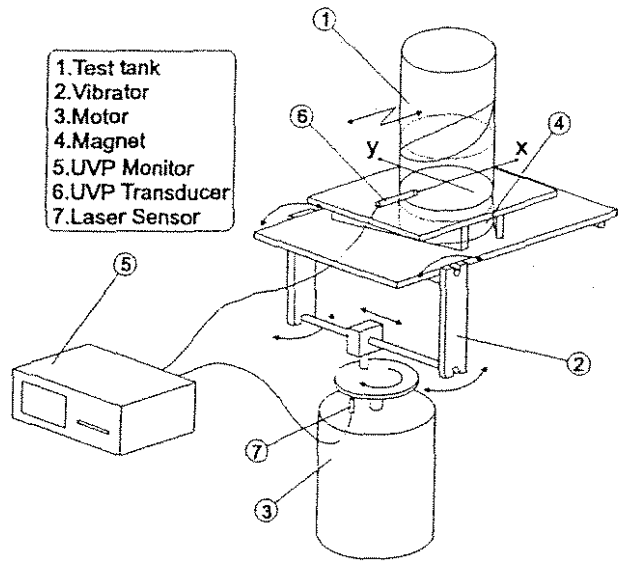

Fig. 1: Experimental Apparatus

"Sloshing" is a phenomenon that the liquid with a free surface is agitated severely in liquid storage tanks. Zelazo and Melcher[1] studied dynamic behavior of a magnetic fluid in an oscillated container. Dodge and Garza[2] demonstrated a simulation of liquid sloshing in low-gravity by using a magnetic fluid. Omori. et al.[3] analyzed swirling phenomenon as a turning phenomenon of steady-state vibration solution which results from nonlinear coupled vibration.

The sloshing problem is not easy from a mathematical point of view. Obvious nonlinearities are occurring especially in the vicinity of the resonant frequency. In an axisymmetric container the inner liquid oscillates with rotational movement around the center axis of

the container in spite of the lateral excitation. It has been called "swirling phenomenon". The direction of the rotation is not fixed. The direction is changed irregularly. Moreover, the stop of the rotation is sometimes observed. In order to understand and to explain this complex problem, detailed measurement of internal velocity profiles is necessary. However, magnetic fluid is opaque. Thus, optical methods like laser Doppler anemometry or the flow visualization technique like particle image velocimetry can not be applied. We performed an ultrasonic velocity profile(UVP) measurement. It is a method for measuring a velocity profile on a line with respect to the velocity component along this line, which can be applied to opaque fluid. Kikura, et al.[4] measured velocity profile of the Taylor vortex flow of a magnetic fluid using by UVP. Sawada, et al.[5] examined flow behavior of a magnetic fluid sloshing in a rectangular container. In the present experiment, we also used UVP method. We attempt to measure the velocity profile of the magnetic fluid sloshing in order to clarify "swirling phenomenon".

2 Experiments

Figure 1 shows the schematic diagram of the experimental apparatus. The cylindrical container is made of transparent acrylic resin, and its inner diameter and height are 94 mm and 300 mm, respectively. The adjustable crank is mounted on the output shaft of the motor. Rotation of the motor is changed to horizontal motion by crank mechanism. The rotational frequency of the motor is continuously controlled by an inverter, and the shaking table is oscillated sinusoidally. The amplitude of the oscillation is X_0=1.5 mm for all experiments. We used a water-based magnetic fluid W-40 with 27 wt%. The fluid depth is h=47 mm in the present experiment. Magnetic field is applied by a cylindrical permanent magnet whose diameter is 110 mm. We used several permanent magnets in order to change the magnetic field intensity. Since magnetic particles in the magnetic fluid are too small to reflect ultrasonic waves, we add porous SiO_2 powders with a mean diameter of 0.9 μm (MSF-10M, Liquidgas Co., Ltd.). An ultrasonic(US) transducer is fixed on the side wall of the container. Its position is changed in order to measure the horizontal velocity profiles along the same (V_x) and orthogonal (V_y) lines with the direction of the forced oscillation. A nominal diameter of the US transducer is 5 mm, and the measuring volume has a thin-disc shape, ϕ5 mm×0.71

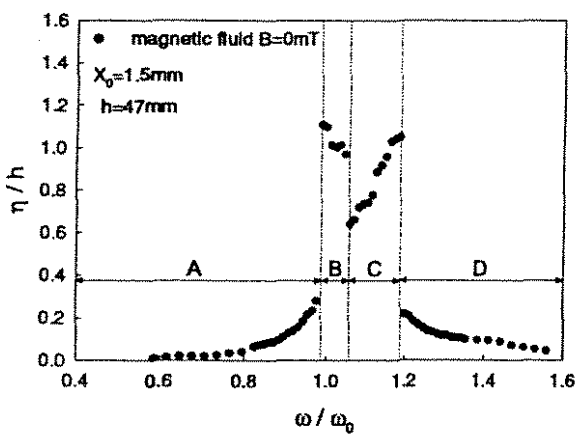

Fig. 2: Frequency responses of the free surface of a magnetic fluid for B=0 mT

mm. The UVP monitor is an Model X-2 manufactured by Met-Flow SA. The basic frequency is 4 MHz. Experiments are carried out changing motor frequencies, magnetic field intensities, and heights of fixed US transducer.

3 Results and Discussions

Figure 2 shows the frequency response of the free surface of a magnetic fluid when the forcing frequency varies. The surface magnetic field induction at the center of the permanent magnet is indicated by B, η is the maximum free surface elevation at the inner wall and ω_0 is the first resonant angular frequency for B=0. In the region of A, the free surface vibrates with the direction of the forced oscillation. As the forcing frequency increases, the surface elevation also increases until the free surface is intensively shaken near the resonant frequency (border between A and B). At the resonant frequency, the free surface forms the collapse wave, and after the resonant frequency (in the region of B), rotation around the center axis of the container occurs. The direction of the rotation is not fixed, and the direction is changed irregularly. Because of the above phenomena, it has been called "unstable swirling phenomenon"(see Fig.3). As the forcing frequency increases in the region of B, the surface elevation decreases with unstable swirling phenomenon. On the border between B and C, unstable swirling phenomenon changes to stable rotation whose direction is fixed. It has been called "stable swirling phenomenon". In the region of C, the stable swirling phenomenon is kept and its direction depends on the direction of unstable swirling phenomenon on the border between B and C. As the forcing frequency increases, the surface el-

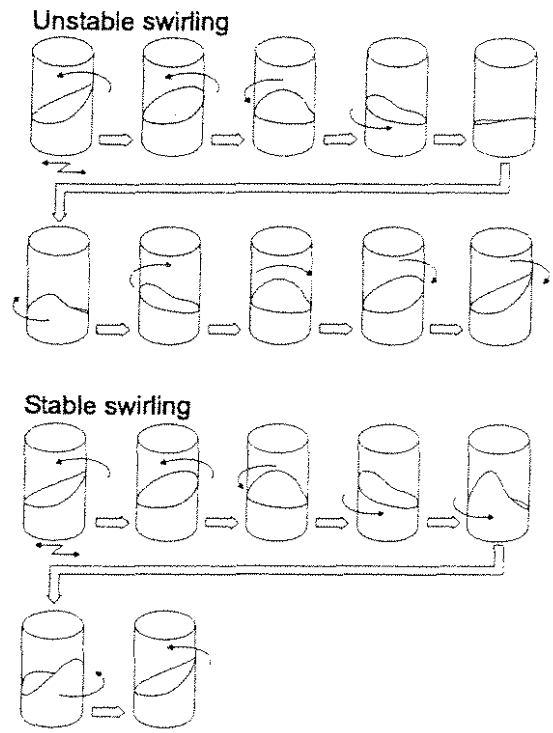

Fig. 3: Unstable swirling and stable swirling

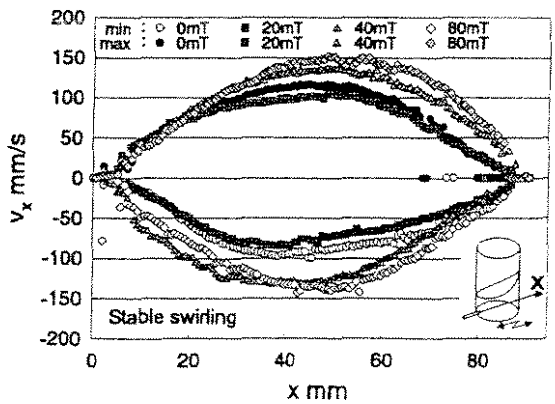

Fig. 4: Maximum velocity profiles for the second resonant angular frequency at h_0=10 mm

evation also increases. The surface elevation is maximum on the border between C and D, and the surface elevation rapidly decreases after the border between C and D. In the region of D, the free surface vibrates as well as region A.

UVP measurements were mainly carried out near the second resonant angular frequencies(border between C and D). Figure 4 shows maximum velocity profiles for several applied magnetic fields. There are 128 measurement points along the measurement axis. Here x is the distance from the inner wall where the US transducer is fixed, and h_0 is the position of the US transducer from the bottom wall. When the magnetic field increases, the velocity also increases because of the magnetic force. We can not have data near the opposite inner wall away from the US transducer. We suppose that it comes from the clustering and chaining of the magnetic particles of a magnetic fluid formed under an applied magnetic field. As a result, we suppose that the US echo signal diminishes.

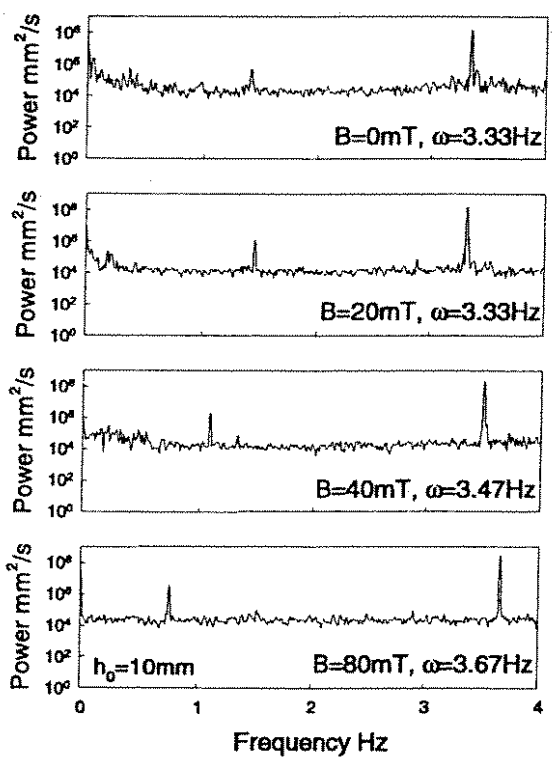

Fig. 5: Power spectra for the second resonant angular frequency over 12.65 mm$\leq x \leq$19.04 mm at h_0=10 mm

From measured velocity data, we calculated power spectra by using a fast Fourier transform in time domain. Figure 5 shows the power averaged over a region of 12.65 mm$\leq x \leq$19.04 mm at h_0=10 mm. The most dominant peak for each applied magnetic field corresponds to the forcing frequency. For each applied magnetic field, the second dominant peak exists. We can not understand what it means, but it is observed that the second dominant peak is shifted to the low frequency region as the magnetic field intensity becomes large. We consider that there is some relation between the second dominant peak and swirling. It is a theme in the future that we carry out detailed experiments for this problem.

This work was partly supported by Grant-in-Aid for Scientific Research (B) of The Ministry of Education, Science, Sports and Culture.

References

[1] R.E.Zelazo and J.R.Melcher, *J.Fluid Mech.* **39** (1969),1.
[2] F.T.Dodge and L.R.Garza, *NASA Tech.Rep.* **9** (1970),1.
[3] H.Omori, T.Matui, K.Kato and K.Hujiwara, *J.Struct.Constr.Eng.* **385** (1988),69.
[4] H.Kikura, T.Takeda and F.Durst, *Expt.Fluids* **26** (1999),208.
[5] T.Sawada, H.Kikura and T.Tanahashi. *Expt.Fluids* **26** (1999),215.

2. ISUD
2nd International Symposium on Ultrasonic Doppler Methods
for Fluid Mechanics and Fluid Engineering
September 20–22, 1999
Paul Scherrer Institut, 5232 Villigen PSI, Switzerland

Flow mapping of the mercury flow

Kikura,H.[1)], Takeda,Y.[2)] and Bauer, G.[2)]

1) Tokyo Institute of Technology, 2-12-1 Ohokayama, Meguro-ku, Tokyo 152, Japan
2) Paul Scherrer Institut, 5232 Villigen PSI, Switzerland

1. Introduction

Measurement of a flow, a velocity at any point or its spatial and temporal distribution, has been one of the most difficult tasks in using liquid metals and, because of it, its application to the study in physics and to industrial devices has been largely limited. Also for many of the rheological liquids which are mostly opaque, investigation of their flow behaviour was limited only to a measurement of total volume flow and pressure. For overcoming such difficulty, a new measuring method has been developed using ultrasound technique, Ultrasonic Velocity Profile method (UVP), and has been established in the field of fluid mechanics and fluid engineering[1][2]. The UVP has been developed at Paul Scherrer Institut(PSI) in Switzerland for investigating liquid metal flow in the geometry of the target of the neutron spallation source (SINQ). This method uses a pulsed echography of ultrasonic beam. In this paper, we present our latest results of the measurement of mercury flow.

2. Experimental set-up

2.1 Mercury loop A full scale mock-up container of the lower part of the SINQ target geometry has been installed in the Hg loop of the Institute of Physics of the Latvia University (IPLU) at Riga, Latvia. The mercury is a model liquid to Pb-Bi-Eutectic (LBE) to be used in the SINQ liquid target. The SINQ target test section is illustrated in Fig.1. It consists of double coaxial cylinders and has two buffle chambers at the top for inlet and outlet flow respectively. The mercury is fed into this chamber through 6 inlet tubes connected to it. It then flows down in an annular channel toward the bottom part called "window" which has a hemispherical shape. The fluid turns there into a inner circular channel inside the inner guide tube and flows up to the second chamber for outlet. The diameter of the outer tube is 207 mm and the total length of the test section including these chambers is ca. 2.3m[2]. Since the geometry of the bottom part such as the shape of the bottom plate and of the edge of inner tube as well as the gap distance between inner tube and bottom plate is most important in designing the target, investigation of the flow in various geometry for this part is under progress. In this paper, we present results of experiments for the axisymmetric configurations of inner tube and for the flow configuration under the different gap distance and different flow rate.

2.2 Instrumentation Flow measurement was made using UVP method. Based on the results of ultrasound transmission[3], the wall thickness of stainless steel was selected as 2.87mm. The ultrasound transducers(TDX) were set on the outside of the container wall. Figure 2 shows the test window region with transducers that were fixed by a special transducer holder. With this holder we can measure maximum on 20 measuring lines. Prior to the measurement, gas bubbles were injected as a tracer, which reflect the ultrasound pulse. By this method, the measurement was successful to observe the spatial and temporal behaviour of the flow. When many measuring lines are aligned non-parallel, it is possible to obtain two velocity components at the crossing points of measuring lines, so that we can obtain the vector field

3. Results

In the present experiment we made two different types of flow mapping; time-averaged flow mapping and time-dependent flow mapping. Fig. 3 shows the typical measuring lines for time-averaged and time-dependent flow mapping. For the time-averaged velocity profiles, the data set for one measurement consists of 512 instantaneous velocity profiles. The vector field was then computed for a series of measurements which consists of 36 measuring lines. This generates in total 126 vectors in the field, when eliminating the points where the crossing angle is less than 15°. The computed vector field is plotted in Fig. 4. It is seen that the flow is not necessarily symmetric with respect to the target axis especially to gap:8. It is considered to be due to the generation of large vortex and its time dependent nature as a chaotic flow. The effect of flow rate is seen in Fig. 4 such that it becomes more symmetric for the large flow rate, although it is not a strong effect. A feature in the vector fields appears similar for three flow rates studied here when the gap distance is constant. Again the flow is very non-symmetric for 8 cm gap distance,

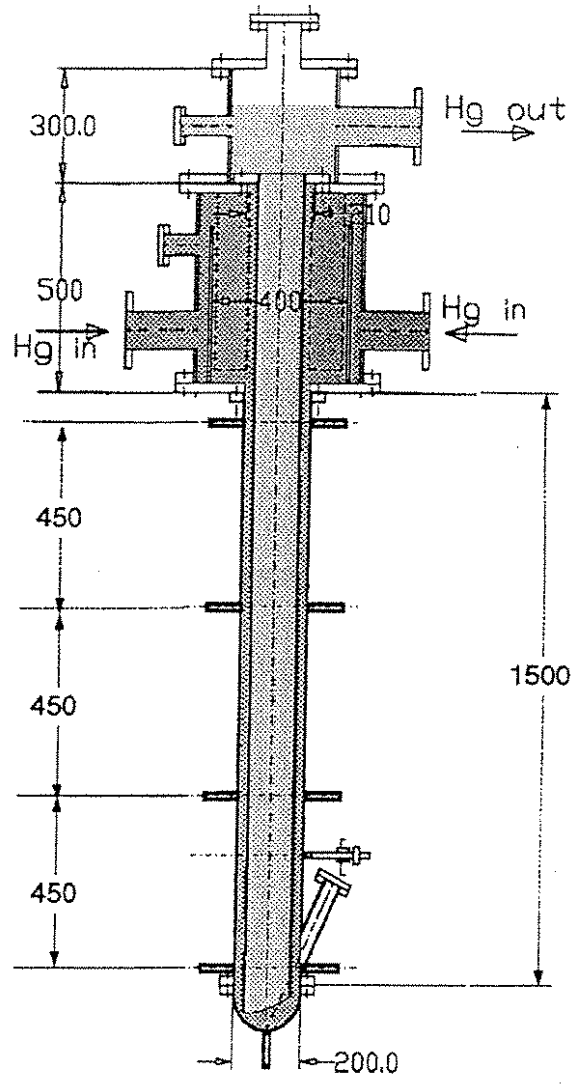

Fig.1 Test section

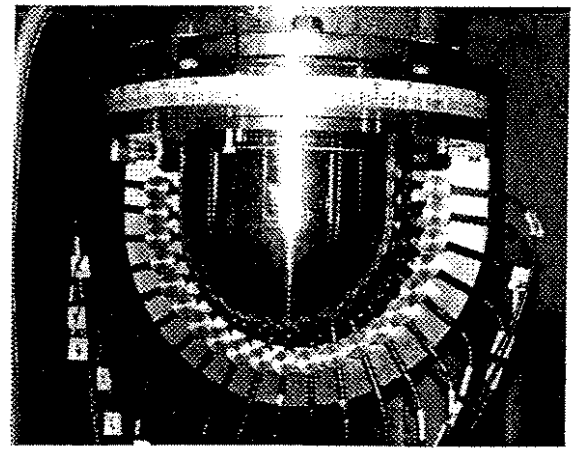

Fig.2 The hemispherical window

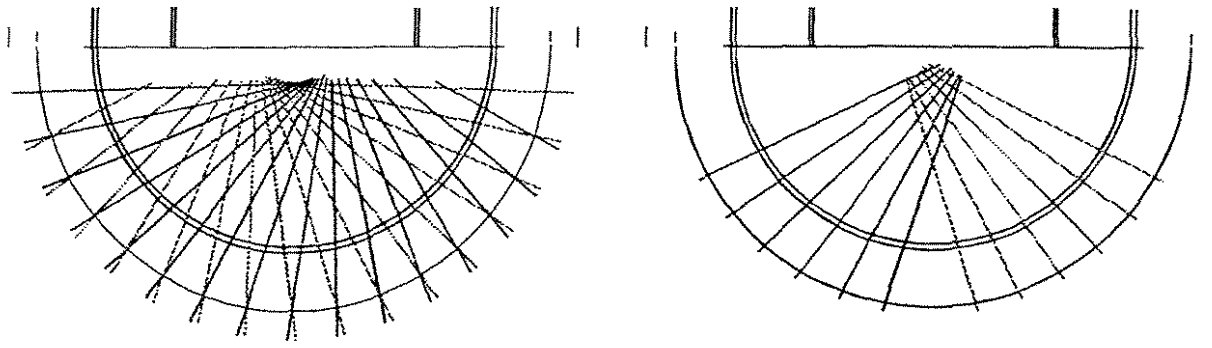

(a) Time averaged (b) Time dependent

Fig.3 Measuring lines

but it is similar to other cases. The effect of gap distance is significantly large as seen above. Even for the smallest flow rate with gap distance 2 cm, the flow appears quite symmetric. It is also seen that the region of very low velocity (dead layer) becomes smaller. It is obvious because the inlet flow velocity at the exit of the annular channel is larger.

Using the high speed measuring mode of present equipment, we can obtain the time-dependent flow mapping. Unfortunately, for the time-dependent flow mapping, present measuring area is very small because of restricted alignment of the measuring lines. Fig. 5 shows the flow field for the cases of two different gap distances in the hemispherical window. In these cases, measuring time for one line was 44ms and total measuring time for a vector map was 0.525 sec. In this figure, we also found that the gap distance has a very strong influence on the flow behaviour.

REFERENCE

1. Y.Takeda, *Experimental Thermal and Fluid Science*, Vol.10, (1995), pp444-453.
2. Y.Takeda, *JSME Int.J., Fluids and Thermal Engineering*, Vol.38, No.1, (1995), pp8-16.
3. Y.Takeda and H.Kikura, *Proc. 1998 ASME Fluid Engin. Div. Summer meeting*, Washington (1998), FEDSM98-5074.
4. H. Kikura, Y.Takeda, M.Aritomi and M.Mori, *Proc. 1998 Fall Meeting of the Atomic Energy Society of Japan*, II, Fukui, Japan (1998-9), p.344, in Japanese.

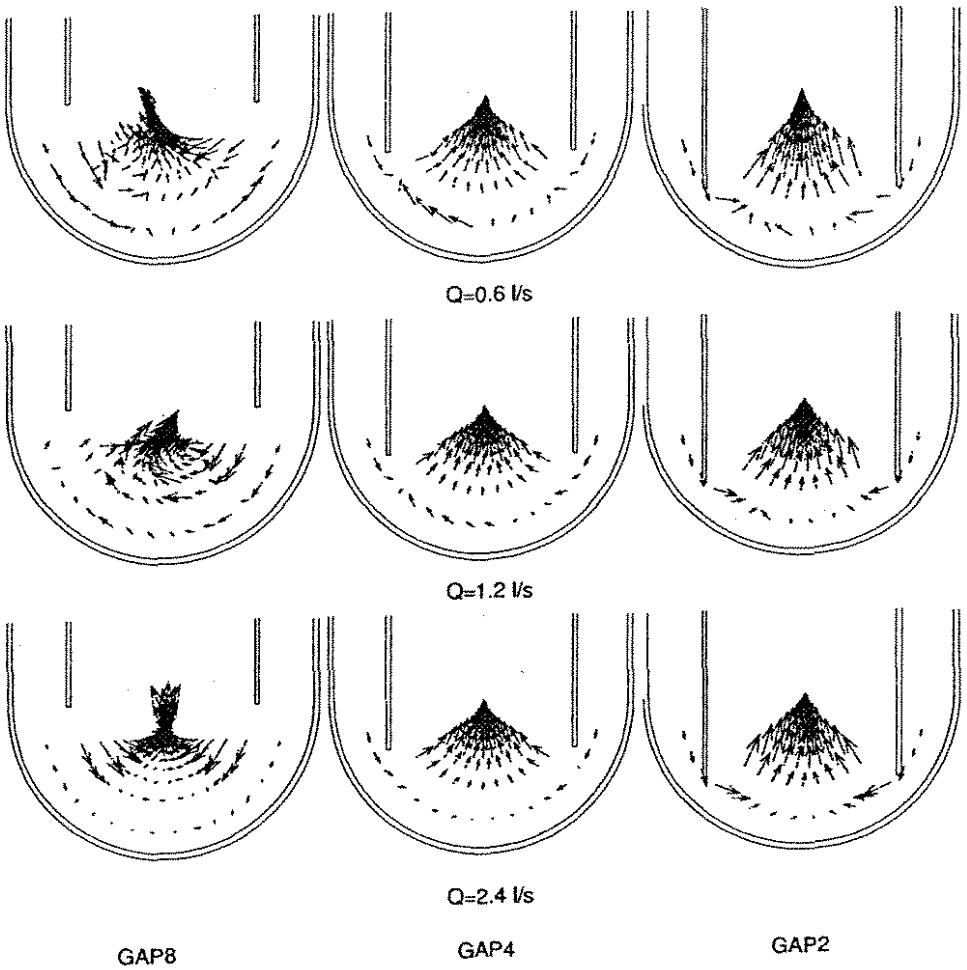

Fig.4 Vector fields for different gap distance

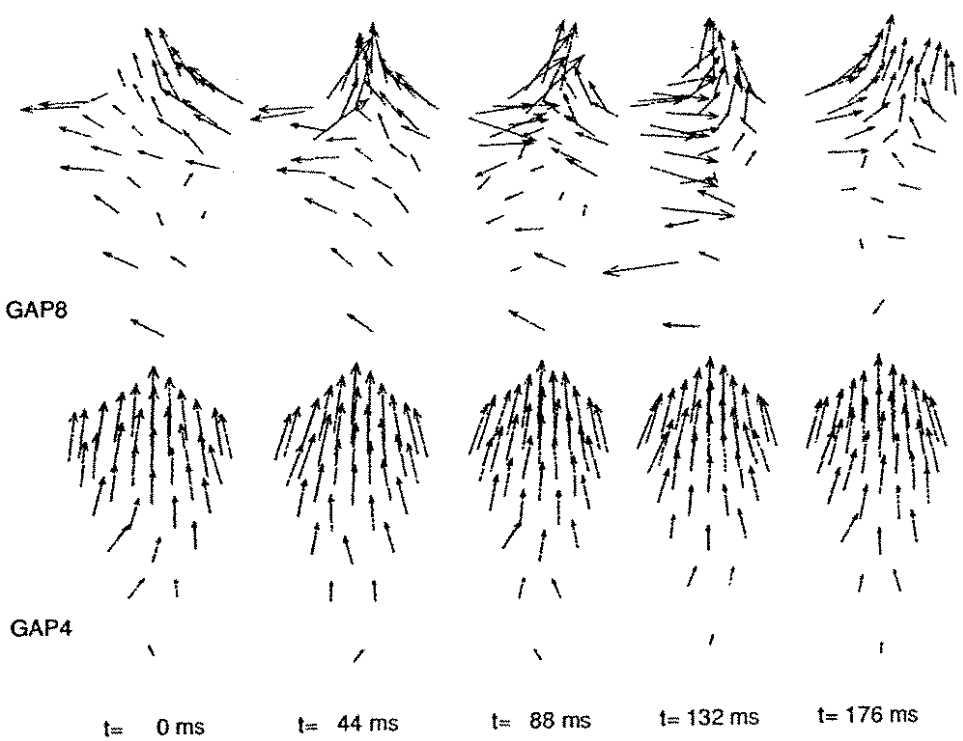

Fig.5 time dependent flows

2nd International Symposium on Ultrasonic Doppler Methods for Fluid Mechanics and Fluid Engineering
September 20-22, 1999 Paul Sherrer Institut, 5252 Villigen PSI, Switzerland

Acoustic spectroscopy of Vorticity and Temperature fluctuations

Jean-François Pinton

Laboratoire de Physique, CNRS, École Normale Supérieure de Lyon
46, allée d'Italie 69364 Lyon cedex 07, France

1 Introduction

This method was originally developped to obtain vorticity measurements. Indeed, in the study of hydrodynamics instabilities and turbulence, a flow is often described in terms of dynamics of vortical structures. Furthermore, in this context, interpetations are often given via mode (or Fourier components) interactions. However, vorticity measurements are scarce, and mostly indirect [1]. There was thus a strong motivation for the development of a direct, non-intrusive and spectral measurement of the vorticity.

The principle is that of classical spectroscopy: when a medium is exposed to an incoming wave the total scattered amplitude, far from the flow, is proportional to Fourier transform of the spatial disctribution of scatterers[1]. The nature of the wave choses the physical quantity being probed. Electromagnetic waves respond to density variations; sound waves couple with both with density variations and velocity gradients:
- in the case of density inhomogeneities, the speed of sound is locally modulated; the resulting scattering has a dipolar angular dependance,
- velocity variations are felt through inhomogeneities in the vorticity. Indeed, vortices scatter sound waves; the mechanism may be pictures as follows: a vortex is advected by the incoming wave and, being set into a non-stationary motion it radiates sound (in much the same manner as accelerated charges emit electromagnetic waves). The scattered wave has a quadrupolar structure.

Measurement of the forward scattered wave yields a measurement of the Fourier components of the vorticity, for an isothermal flow. When temperature fluctuations are present, they may be singled out by measurements of the backscatterd wave.

2 Theoretical background

The scattering a an ultrasonic wave by an inhomogeneous flows results from the non-linear coupling, through the Navier-Stokes equation, of the three hydrodynamics modes sound, entropy and vorticity [2, 3]. Although expressions for the scattered amplitude have been derived by a number of authors [4, 5, 6, 7]. compact and elegant formulations are given bay Lund and co-workers [8, 9]. For a plane incoming sound wave with frequency ν_0:

$$P_{\text{scat}}^{\text{vort}}(\vec{D},\nu) = P_0^{inc}\frac{e^{i\nu r/c_0}}{r}\,\frac{-\cos\theta\sin\theta}{1-\cos\theta}\,\frac{i\pi^2\nu}{c_0^2}\tilde{\Omega}_\perp(\vec{q},\nu-\nu_0)\;, \qquad (1)$$

[1] It is assumed that thepopulation of scatterers is diluted so that Born's first approximation is justified.

$$P_{\text{scat}}^{\text{temp}}(\vec{D},\nu) = P_0^{inc}\frac{e^{i\nu\tau/c_0}}{r}\frac{\pi^2\nu^2}{c_0^2 T_0}\cos\theta\,\tilde{T}(\vec{q},\nu-\nu_0)\,, \tag{2}$$

at distance $\vec{D}$ from the flow, where $\vec{q} = \vec{k}_d - \vec{k}_i$ is the scattering wavevector, θ the scattering angle, c_0 the speed of sound at temperature T_0, $\Omega_\perp(\vec{r},t)$ the component of the vorticity field perpendicular to the scattering plane and $T(\vec{r},t)$ the temperature field (we write $\tilde{F}$ the Fourier transform of a function F).

3 Experimental implementations

Generalities
The scattering wavenumber choses the scale at which the flow is probed, $q = 4\pi\nu_0\sin(\frac{\theta}{2})/c$. In experiments, this is conveniently achieved by tuning the frequency of the incoming sound wave. In laboratory flows the scales of motion are in the range 10cm to 100μm; they are resolved using ustrasonic transducers which emit in the band 100kHz to 50MHz for flows in liquids (commercially available) or in the band 5kHz to 400kHz for flows in gases (custom made [10]). The transducers must be as large as possible to define a scattering wanuber with precision[2]; typical values are $\Delta q/q \sim 2\%$.

Validation
We have extended the early work of the 60s russian acoustic school [11, 12] to develop sound scattering as a spectroscopic tool for flow investigation. First equations (1) and (2) have been validated in simple flows where scatterers are periodically spaced. For vorticity such is the case of the von Kármán vortex street; for thermal perturbations we have used the thermal wake above a heated wire. In each case [13, 14, 15], we have established the spectral nature of the measurement and shown that this scattering technique allows original contributions to the study of spatio-temporal instabilities.

Applications to turbulence
We have studied a heated jet [16], in a case where temperature may be regarded as a passive scalar. The scattering technique gives a direct measurement of the spectrum, in space, of the temperature fluctuations; we have observed a spectral density $T^2(q) \propto q^{-5/3}$ in agreement with the Corrsin-Obhukov theory. We have also shown the intermittency increases at small scale in agreement with the formation of scalar fronts.

Vorticity measurements in a jet [17] have shown that the enstrophy spectrum has a $q^{1/3}$ inertial behavior, in agreement with Kolmogorov's mean field theory. Regarding intermittency, we have shown [18, 19] that the Fourier components of vorticity have a trivial behavior at all scales, save for a band around the Taylor microscale where intense filaments are formed.

Current research is oriented towards simultaneous dynamical analysis at several wavenumbers, to probe directly the triad interactions that underly the turbument cascade [20, 21].

[2] But the measurement volume must remain in the far field.

References

[1] Wallace J., *Experiments in fluids*, 4, 61-71, (1986).

[2] Obukhov, A. M., *Izv. Akad. Nauk Seriya Geofiz.* **2**, 155-165 (1953), ou *Waves in Random Media* 4, 9-19 (1994).

[3] Chu, B. T. and Kowaznay, L. S. G., *J. Fluid Mech.* **3**, 494- (1958).

[4] Lighthill, M. J., *Proc. Camb. Phil. Soc.*, **49**, 531-551 (1953).

[5] Pitaevskii, L. P., *Sov. Phys. JETP* **8**, 888 (1959).

[6] Ferziger, J. H., *J. Acoust. Soc. Am.* **56**, 1705-1707 (1974).

[7] Fabrikant, A. L., *Sov. Phys. Acoust.* **28**, 410-411 (1982); **29**, 152-154 (1983).

[8] Lund, F. and Rojas, C., *Physica* **D 37** 508-514 (1989).

[9] Contreras H., Lund F., *Phys. Lett. A*, **149**(2-3), 127-130, (1990).

[10] Anke D., *Acistica*, **30**, (1974).

[11] Kallistratova, M. A. and Tatarskii, V. I., *J. Acoust. Soc. Am.* **6**, 503-505 (1960).

[12] Gromov, P. R., Ezerskii, A. B. and Fabrikant, A. L., *Sov. Phys. Acoust.* **28**, 452-455 (1982).

[13] Baudet C., Ciliberto S. and Pinton J.-F., *Phys. Rev. Lett.*, **76**(2), 193, (1991).

[14] Pinton, J. F. and Baudet, C., in *Turbulence in spatially extended systems*, Les Houches Series, Basdevant, C., Benzi, R. and Ciliberto, S. editors, Nova Science Publishers (1993).

[15] Pinton J.-F., Baudet C., Laroche C. and Fauve S.*J. Phys II France*, **3**, 767-773,(1993).

[16] Petrossian A. and Pinton J.-F., *J. Phys II France*, **7** ,(1997).

[17] Baudet C. and Hernandez R., in *Advances in Turbulence VI*, Eds. Gavrilakis S., Machiels L. and Monkewitz P., Kluwer Academic Publishers, (1996).

[18] Pinton J.-F., Dernoncourt B., Fauve S., in *Advances in Turbulence VI*, Kluwer, S. Gavrilakis, L. Machiels and P.A. Monkewitz eds., 437-440, (1996).

[19] B. Dernoncourt, J.-F. Pinton, S. Fauve. *Physica D*, **117**, 181-190, (1998).

[20] Mordant N., Pinton J.-F., *Graduate Report*, ENS-Lyon, (1997).

[21] Michel O., Baudet C., Friedt J.-M., in *Colloque Gretsi*, Grenoble (1997).

2.ISUD
2nd International Symposium on Ultrasonic Doppler Methods
for Fluid Mechanics and Fluid Engineering
September 20-22, 1999
Paul Scherrer Institute, 5232 Villigen PSI, Switzerland

Development of a new type flow metering system using UVP

- (1) Principle, Configuration, and Laboratory experiments -

M. Mori[1], Y. Takeda[2], N. Furuichi[2],
M. Aritomi[3] and H. Kikura[3]

1 Tokyo Electric Power Company, Inc., Tsurumi-ku, Yokohama 230-8510, Japan
2 Paul Scherrer Institute, CH-5232 Villigen, Switzerland
3 Tokyo Institute of Technology, 2-12-1 Ohokayama, Meguro-ku, Tokyo 152-8550, Japan

1. INTRODUCTION

The flow velocity profile measurement by the ultrasonic-Doppler velocity profile(UVP) method [1-4] exhibited an outstanding potential in an accurate measurement of flow rates because of the advantage of the UVP method instantaneously measuring a spatiotemporal velocity profile over the flow channel. The conventional ultrasonic measuring techniques are based on a spatially averaged fluid velocity measurement, the fact of which causes inaccuracy in flow rate measurements due to the inevitable assumption of the flow velocity profiles. This paper summarizes the measurement methods of the velocity profile and flow rate using UVP, and its characteristics of ultrasonic wave propagation through the metallic wall to place the transducer on the outside wall of the pipe for industrial application. Using a small pipe test stand, we showed the UVP method to be very feasible in order to measure the transient flow rate with high accuracy and with fast response. We also performed the measurement of flow rates using larger stainless steel pipes with transducers located on the outside wall of the pipe and compared the measured results of the transient flow by UVP against the measured ones by conventional measurement devices.

2. ULTRASONIC BEAM STUDY FOR APPLICATION TO METALLIC WALL

2.1 Theoretical discussion on the transmission of ultrasonic waves

The transmission of ultrasonic beams through a metallic wall was examined to clarify the effects of the ultrasonic basic frequencies against the wall thickness to enable the measurement of the flow velocity profile and flow rates from the outside surface of a metallic wall[5,6]. There occur reflection, diffraction, and absorption of the ultrasonic wave at the boundary of two materials of the different acoustic impedance. When the wall thickness is in the same order of the wave length, there occurs a sort of resonance transmission of the wave. Immersed in a fluid, a transmission coefficient of the wave is described as following:

$$D=\frac{1}{\sqrt{1+\frac{1}{4}\left(m-\frac{1}{m}\right)^2\sin^2\frac{2\pi d}{\lambda}}} \qquad (1)$$

where $m = Z1 / Z2$; Z : acoustic impedance; d : wall thickness; λ : wave length.

Due to its trigonometric characteristics, it changes as d/λ periodically, as shown in **Fig.1** with two examples of Plexiglas and steel. For Plexiglas, the amplitude of oscillation is rather small between 80 and 100% and its width is pretty broad. Whereas for steel, the resonance peak is very strong and narrow. However it is promising that for the resonant wall thickness, the transmission is 100%. It is found that the maximum transmission occurs at :

$$d/\lambda = 0, 1/2, 2/2, 3/2, 4/2, \quad = n/2 \qquad (2)$$

and the minimum (maximum reflection) at :

$$d/\lambda = 1/4, 3/4, 5/4, \quad = (2n+1)/4 \qquad (3)$$

We selected wall thickness of stainless steel using the wave length unit at a room temperature. The wall thickness was determined using 2 and 4MHz of basic frequencies. The total Doppler powers are shown in **Fig. 3**. It shows clearly that a high transmission is attained for a half-wave length of 2MHz. It is very promising that 1/2 wave length be a realistic wall thickness and would give us a solution for the measurement of the flow rate by the ultrasonic Doppler method by placing the transducer outside wall of a pipe

3. FLOW MEASUREMENT IN INDUSTRIAL STAINLESS-STEEL PIPE

3.1 Experiment

The test sections are A250 whose inner diameter is 250 mm, and A400 whose inner diameter is 400 mm stainless steel pipes connected in parallel. The length of the test section is about 10m. The smaller pipe of A250 is equipped with the orifice flow meter and the electromagnetic flow meter. The larger pipe of A400 is equipped only with the orifice flow meter.

The adopters are inclined by 5 deg., 8 deg., and 12 deg. to the normal line of the pipe axis. One adopter has a bore hole where the transducer directly contacts with water. The second adopter has a wall whose thickness is adjusted to the basic frequency but its surface is parallel to the wall. This means that the wall thickness is not constant over the total active area of the transducer. The third type has a wall of constant thickness over the active area of the transducer.

Cavitation gas bubbles were used as a reflector. Since the loop has several bent and valves, cavitation bubbles were generated when the loop is not pressurized. Hydrogen gas bubbles were also possible to use as a reflector.

3.2 Results and discussion

The steady state flow rate can be obtained by integrating the velocity profile, which is obtained with the measuring line on the diameter. There is quite a strong influence of the wall just in front of the transducer which deteriorates the shape of the velocity profile. We decided to use only the half of the velocity profile which is beyond the center of the tube, using the following equation:

$$Q = 2\pi \int_0^R V(r) r dr / \sin\theta \qquad (5)$$

where ■ is the inclination angle of the transducer.

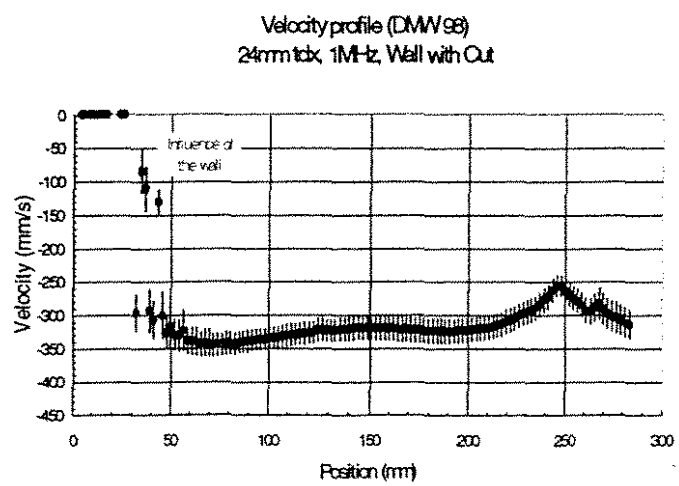

Fig. 4 Time averaged velocity profile in 250A stainless-steel pipe (1MHz, thickness of λ /2)

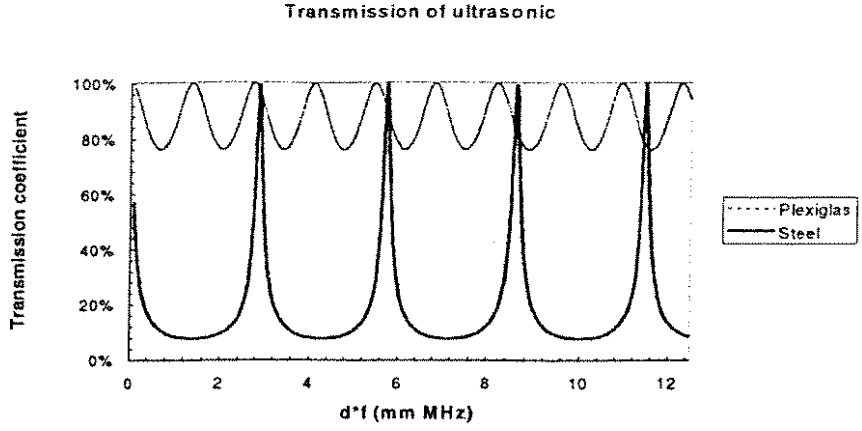

Fig.1 Transmission coefficient of ultrasonic through Plexiglas and Steel walls.

2.2 Experimental study

Fig.2 is a plot of the total Doppler power at the center of the channel with respect to the wall thickness of aluminum, whose acoustic impedance is relatively small as metals, in unit of wave length for two frequencies used here. The figure exhibits a general tendency that a large Doppler power can be observed at the wall thickness of half and one unit of wave length, the fact of which seems to enable us to have better transmission of the ultrasonic beam through metallic wall when the wall thickness is carefully selected.

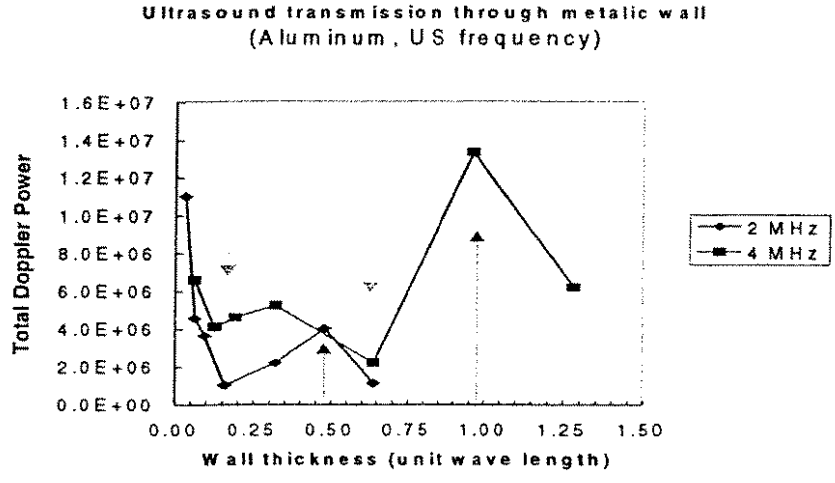

Fig. 2 Total Doppler power with unit of wave length through Aluminum wall.

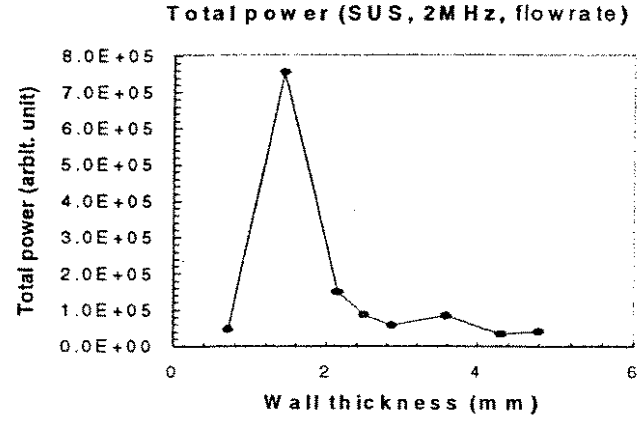

Fig.3 Total Doppler power against wall thickness of stainless steel.

Fig. 4 shows the measured results of time averaged velocity profiles of the case with 1MHz ultrasonic basic frequency.

Transient measurement means to study a response of the flow meter to the flow which fluctuates with relatively high frequency. In order to make a comparison of time-response with the orifice (ORF) and electromagnetic flow meter (EMF), these values are recorded in the computer. The results are shown in **Fig. 5**. It can be seen that the time response of UVP appears very good compared with the orifice flow meter, and that the transient behavior shows the exact correspondence with the orifice up to the small fluctuations not only transient period but also stationary period. **Fig. 6** shows a difference of the measured flow rates between UVP and the orifice. The difference ranges up to 0.2% in steady state flow condition and about up to 5% in rapid transients.

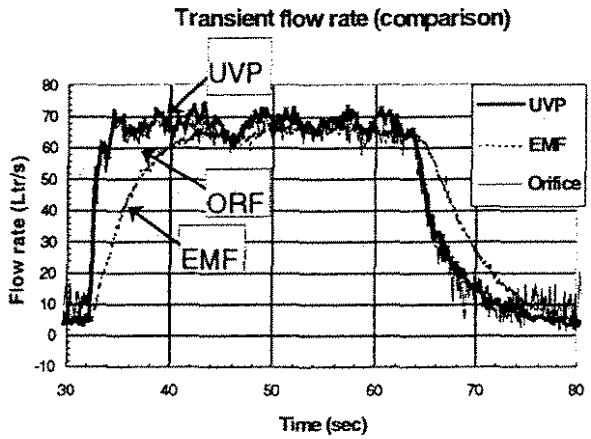

Fig. 5. Comparison of measured transient flow rates by UVP, orifice (ORF), and electromagnetic flow meters (EMF).

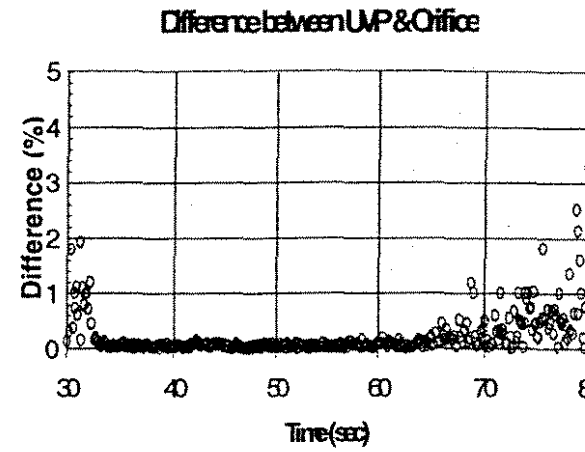

Fig. 6. Comparison of errors between measured transient flow rates by UVP and orifice flow meters.

4. CONCLUDING REMARKS

Transmission of an ultrasonic beam has been studied experimentally. The experimental results show that one half-wave length would give the most promising result for the velocity profile measurement. By one-dimensional measurement, the transient flow rate can be obtained with sufficiently high accuracy. By locating the measuring lines on the diameter at various azimuthal angles, transient flow rates can be successfully measured. Comparison with the orifice flow meter shows that the estimated flow rate is in a very good agreement with its result. The electromagnetic flow meter has a poor time response compared with other two methods.

REFERENCES

(1) Takeda, Y., Experimental Thermal and Fluid Science, 10 (1995), pp.444-453.
(2) Takeda, Y., JSME International Journal, Fluid and Thermal Engineering, B 10 (1995), pp.8-16.
(3) Kikura, H., et. al., Proc. of 1998 ASME Fluids Engineering Division Summer Meeting, June, 21-25 (1998), Washington DC, USA.
(4) Takeda, Y., et al. Proc. of the 3rd ASME/JSME Joint Fluid Engineering Conference, FEDMS99-7140, 1999
(5) Mori, M., et al. ICONE-7, D6-5, April 19-23 (1999), Tokyo, Japan
(6) Kikura, H., et al. Proc. of the 3rd ASME/JSME Joint Fluid Engineering Conference, FEDMS99-7141, 1999

2. ISUD
2nd International Symposium on Ultrasonic Doppler Methods
for Fluid Mechanics and Fluid Engineering
September 20-22, 1999
Paul Scherrer Insitut, 5252 Villigen PSI, Switzerland

Development of a new flow metering system using UVP

- (2) Comparison with weight measurement at NIST -

Y. Takeda[1], N. Furuichi[1], M. Mori[2]
M. Aritomi[3] and H. Kikura[3]

1 Paul Scherrer Institute, CH-5232 Villigen, Switzerland
2 Tokyo Electric Power Company, Tsurumi-ku, Yokohama 223, Japan
3 Tokyo Institute of Technology, 2-12-1 Ohokayama, Meguro-ku, Tokyo 152, Japan

1.INTRODUCTION

A new flow metering system using ultrasonic Doppler method (UVP) has been developed by Takeda et al [1]-[7]. In this system, a flow rate is obtained by an integration of instantaneous velocity profile measured by UVP over a pipe diameter. This system has a many advantages. One is that pressure loss is not caused because the transducer can be set outside of the wall and other one is that can be applied to opaque liquid, and so on. Especially, it is not necessary the process of interpolation or averaging which using other ultrasonic flow meter because a flow rate be estimated directly by using instantaneous velocity profile.

Kikura et al. [2] clarified a characteristic of ultrasonic propagation through the metallic wall and indicated that a flow rate can be measured from the outside of the stainless steel when the basic frequency of the ultrasonic pulse is carefully selected. Mori et al.[3] reported the result of a flow rate measurement in the stainless steel pipe (250A and 400A) which is more realistic configuration. The error rate that obtained by compare a flow rate measured by this method with that by other flow meter (orifice flow meter and electric flow mater) was less than 0.2% at steady flow condition. Taishi et al. [4] was indicated that this method has a good sensitivity for a transient flow rate. Thus, it is suggested that this method can be applied to flow metering system with a high accuracy.

For the realization this method, it is necessary the more information of the accuracy. Especially, it is necessary that the accuracy that compared absolutely flow rate is obtained. At the NIST (National Institute of Standard and Technology) in USA, there is the system that can be measured weight flow rate. In this paper we report the result that compared absolutely flow rate measured by this new method with that measured by weight flow rate by the NIST standard calibration system.

2.EXPERIMENTAL APPARATUS

The water facility of the NIST standard calibration system that consists of a reservoir, pump, meter runs and weight tank is shown in Fig.1. The system is usually operated as a constant flow facility over the test section. The junction that switches the flow channel to the weight tank or the reservoir is set at the downstream of the test section. An operation that the junction is switched does not affect to the flow condition. Flows up to 38m^3/min (10.000gal/min) can be provided and maximum Reynolds number is about 4M when the pipe 254mm in diameter is used. The weight tank capacity is about 20m^3 and weight of water inside it can be measured. The method of flow rate measurement is below. Water thorough the test section is stored in this tank in some period

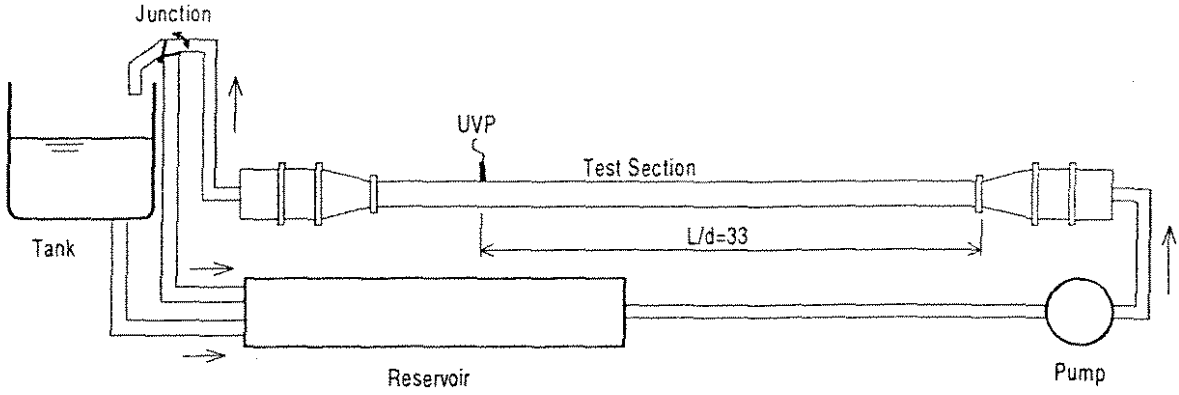

Fig. 1. Schematic of the experimental apparatus - NIST calibration standard system-

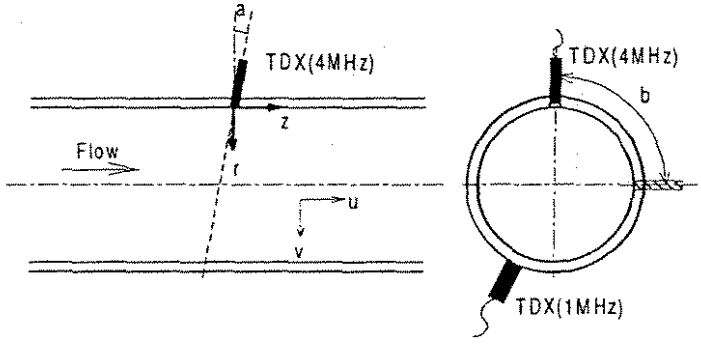

Fig. 2. Test section detail and coordinate system

Table 1. UVP parameters

Reynolds Number	400K	2.6M
Transducer	4MHz	1MHZ
Starting Depth	101mm	340mm
Channel Distance	2.22mm	1.48mm
Maximum Depth	326mm	340mm
RF gain	4,4	1,1

and a weight is measured. The weight flow rate is obtained as a result that the volume of water stored in the tank divides by that time. The relative expanded uncertainly for these facilities is 0.12%. The test section has 10.15m (400in.) length and the pipe diameter is d=253.75mm (10in.). The measuring region was set a downstream L/d=33 from the nozzle exit.

The test section with transducer setting is shown in Fig.2. Two type transducers which frequency of ultrasonic are 1MHz and 4MHz were used. The 1MHz transducer was put outside of the stainless wall and the 4MHz one was put on spatial mount made by Plexiglas which thickness is 2mm. An inclination angle of 1MHz is 5 degree and 4MHz 0-20 degree with flexibility. A particle was not used as a reflector in this experiment because there is enough small cavitation bubble that generated around the pump in water.

3.EXPERIMENTAL METHOD

Experimental procedure was according to the one of the NIST. A simultaneous measurement of flow rate by UVP and NIST system was examined five times in one running. The average flow rate was determined as the one that is averaged in each examination. A sampling of flow rate by UVP was started at the time when the junction is switched to the tank and continued over storing to the tank. The method of estimating flow rate is same one as Takeda et al[1] has reported. Reynolds numbers are 400K and 2.6M and the transducer of the UVP was used 4MHz and 1MHz, respectively. Typical UVP parameters are shown in Table 1. A mean velocity profile of U component was measured to obtain an information of flow condition. This component of velocity can not be measured directly by UVP so that it was measured according to the method of flow mapping.

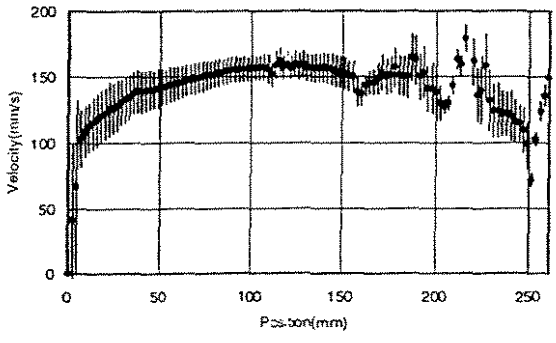

Fig. 3. Mean velocity profile (Re=400K)

4. RESULTS AND DISCUSSION

4.1 Mean velocity profile

The mean velocity profile in the pipe is shown in Fig.3. The frequency of ultrasonic is 4MHz and the inclination angle is 12 degree. Reynolds number is 400K. As shown in this figure, the velocity measured by UVP is disturbed by the reflection from the wall of the test section in this experiment so that it is difficult estimate the flow rate directly. The velocity that is measured with the ultrasonic frequency of 1MHz thorough the stainless steel is disturbed at near side of transducer by reflection such as Kikura et al.[5] reported. However, if a flow condition is symmetry, a flow rate can be calculated by using half side velocity profile. To obtain an information of the flow condition, we measured the *U*-component velocity at various positions. Mean velocity profile of *U*-component is shown in Fig.4. As mentioned above, the reflection is too strong to measure over a pipe diameter so that a velocity was measured two position which is 0 and 90 degree and the results are shown only half side from the wall of transducer side to the *r/d*=0.5. As shown in figure, velocity profile of *U*-component is good agreement with that of the 1/7 power law in various positions so that it is suggested that the velocity distribution in the pipe is almost symmetry.

4.2 Flow rate measurement

As mentioned above, the velocity profile at far side of the pipe wall can not be obtain so that a flow rate is estimated by using one of near side region at the case of using 4MHz frequency. On the other hand, the velocity profile can not be obtained at near side at the case of using 1MHz frequency because of the ringing of the stainless steel so that one of far side is used to estimate flow rate. Typical transient flow rate is shown in Fig.5. Sampling interval of flow rate is 72msec. Mean flow rate is 68.18l/s and standard deviation is 7.3%. Various frequency fluctuation can be observed and it has been clarified that these fluctuation of flow rate was good agreement with that measured by orifice flow meter[6].

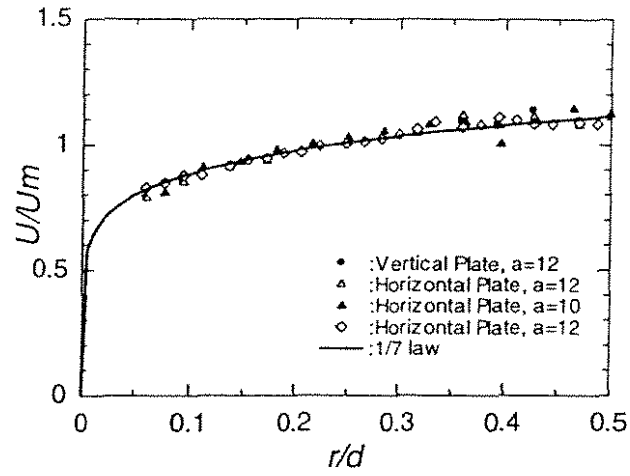

Fig. 4. *U* component mean velocity
Um is bulk velocity that measured by NIST system and "a" is inclination angle of the transducer

The result of *Re*=400K that is compared flow rate measured by UVP with that measured by NIST system is shown in Table 1. First column means data name. The value of second column is the flow rate that is measured by using UVP and the value of third column is weight flow rate by NIST system. In this table, seven data sets of measurement result that is examined five times in one experiment are shown. Especially, the number C, the average flow rate is excellent agreement with one measured by using weight flow rate and the result is 0.00%. About other data set as shown the table, the flow rate measured by this new method is good agreement with the weight flow rate by the NIST system. The error rate in all experiment is only 0.18%. The result about more high Reynolds number (=2.6M) is shown in Table 2. The error rate is a little

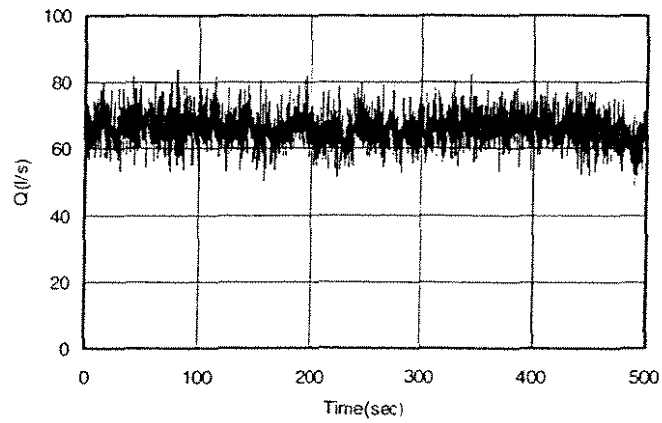

Fig. 5. Transient flow rate

larger than that of *Re*=400K because it was measured from the outside of the stainless pipe. However, when the condition of the seeding is better, the accuracy of this method is very high as shown in the table.

In this experiment, the inclination angle of transducer for 1MHz frequency is fixed 5 degree because we aimed the measurement of high Reynolds number. As a result, the reflection was too strong to measure a flow rate, however as shown in a result, it is possible that the flow rate measures using half side velocity profile in this configuration. If we examine with flexibility of the inclination angle of transducer, it is suggested that we can measure with more high accuracy.

Table 2. Flow Rate Measurement (*Re*=400K)

		UVP Average	(L/s) Deviation	Weight GPM	L/s	Difference	% error
A	1	70.60	3.25	1109.14	69.97	-0.63	-0.90%
	2	70.24	3.22	1110.27	70.04	-0.20	-0.29%
	3	70.76	3.01	1110.30	70.04	-0.72	-1.03%
	4	70.61	3.00	1110.23	70.04	-0.57	-0.82%
	5	70.23	3.12	1110.78	70.07	-0.16	-0.23%
B	6	70.20	3.31	1110.87	70.08	-0.12	-0.17%
	7	70.36	3.41	1111.42	70.11	-0.25	-0.35%
	8	70.20	3.39	1110.32	70.04	-0.15	-0.22%
	9	69.86	3.56	1109.81	70.01	0.15	0.21%
	10	69.90	3.38	1110.72	70.07	0.17	0.24%
C	11	70.21	3.17	1113.62	70.25	0.04	0.05%
	12	70.34	3.17	1113.76	70.26	-0.08	-0.11%
	13	70.38	3.39	1113.61	70.25	-0.13	-0.19%
	14	70.30	3.40	1115.04	70.34	0.04	0.06%
	15	70.16	3.41	1114.10	70.28	0.12	0.17%
D	16	69.81	3.22	1111.90	70.14	0.33	0.48%
	17	70.12	3.12	1113.85	70.27	0.15	0.21%
	18	69.67	3.25	1113.00	70.21	0.54	0.77%
	19	69.88	3.21	1112.82	70.20	0.32	0.45%
	20	70.07	3.29	1113.73	70.26	0.19	0.27%
E	21	70.20	3.29	1101.77	69.50	-0.70	-1.00%
	22	69.97	3.20	1102.62	69.56	-0.41	-0.59%
	23	70.13	3.35	1102.90	69.57	-0.56	-0.80%
	24	70.11	3.31	1102.85	69.57	-0.54	-0.78%
	25	70.36	3.38	1103.20	69.59	-0.77	-1.10%
F	26	69.76	2.96	1103.30	69.60	-0.16	-0.23%
	27	69.67	3.19	1103.51	69.61	-0.06	-0.08%
	28	69.72	3.23	1103.49	69.61	-0.11	-0.16%
	29	69.44	3.15	1103.65	69.62	0.18	0.26%
	30	69.57	3.22	1103.44	69.61	0.04	0.06%
G	31	69.96	3.07	1101.77	69.50	-0.46	-0.66%
	32	69.70	3.21	1102.62	69.56	-0.14	-0.20%
	33	69.36	3.24	1102.90	69.57	0.22	0.31%
	34	69.54	3.13	1102.85	69.57	0.03	0.05%
	35	69.71	3.22	1103.20	69.59	-0.12	-0.17%
Average		**70.03**	**0.13**	**1108.10**	**69.90**	**-0.13**	**-0.18%**

5.CONCLUSION

A new type flow metering system using ultrasonic Doppler method has been developed. In this presentation, we reported the result of comparison absolutely flow rate measured by this new method with weight flow rate by the NIST standard calibration system.

In this experiment, the pipe flow of NIST system is symmetry that is fully developed so that a flow rate was calculated using by half side velocity profile because velocity profile of another half side was disturbed by the reflection. The result of *Re*=400K is very good agreement with the flow rate measured by the weight flow rate. The error rate in all experiment is only 0.18%. The result of more high Reynolds number (=2.6M) is a little larger than the result of *Re*=400K because it was measured from the outside of the stainless pipe. However, when the condition of the seeding is better, the accuracy of this method is very high about 0.6%.

Table 3. Flow rate measurement (*Re*=2.6M)

		UVP Average	(L/s) Deviation	Weight GPM	L/s	Difference	% error
A	1	475.35	25.66	7485.94	472.24	-3.11	-0.66%
	2	478.06	25.45	7485.60	472.22	-5.85	-1.24%
	3	475.10	25.60	7494.20	472.76	-2.34	-0.50%
	4	474.44	26.95	7478.94	471.80	-2.65	-0.56%
	5	472.01	26.38	7483.13	472.06	0.05	0.01%
Average		**474.99**	**0.64**	**7485.56**	**472.21**	**-2.78**	**-0.59%**

As mentioned above, it is indicated that this new type flow metering system using by UVP has very high accuracy. And this method is multipurpose system because flow rate can be measured under high Reynolds number.

ACKNOWLEDGEMENT

We gratefully acknowledgement the supporting work made by Dr.Mattingly and NIST crew and Mr.Barbagallo in PSI.

REFERENCES

[1] Takeda, Y., et al. AESJ fall annual meeting, F16, 1998 (in Japanese)
[2] Kikura, H., et al. AESJ fall annual meeting, F17, 1998 (in Japanese)
[3] Mori, M., et al. AESJ fall annual meeting, F19, 1998 (in Japanese)
[4] Taishi, T., et al. AESJ fall annual meeting, F18, 1998 (in Japanese)
[5] Takeda, Y., et al. Proc. of the 3rd ASME/JSME Joint Fluid Engineering Conference. FEDMS99-7140, 1999
[6] Kikura, H., et al. Proc. of the 3rd ASME/JSME Joint Fluid Engineering Conference. FEDMS99-7141, 1999
[7] Mori, M., et al. ICONE-7, D6-5, 1999

Surface roughness determination based on velocity profile measurements

Dr Jean-Louis Boillat, Andrea Lavelli

Laboratory of hydraulic constructions, Swiss Federal Institute of Technology Lausanne, CH-1015 Lausanne, tel. ++41 21 6932385, fax ++41 21 6932264, email : secretariat.lch@epfl.ch

Summary

Velocity profile measurements in a channel of 0.30 m width and 8 m length were made at the Laboratory of Hydraulic Constructions at the EPF-Lausanne with a UVP probe based on Doppler's echography. The aim of this study was to determine the equivalent sand roughness k_s of the bottom. The slope of the channel is variable between 0 and 1 % and the walls are made of transparent PVC. The boundary layer's theory developed by Prandtl treats flow in the vicinity of a wall. The friction velocity is given by applying a logarithmic regression curve $u = A_1 \ln(z) + A_2$ to the velocity profile. The calculation becomes an iterative process, because the validity field of this relationship also depends on the friction velocity u_*. The results obtained for various types of bottom surface roughness make possible to draw the following conclusions:

- *The velocity fluctuations in the logarithmic part of the velocity profile are significant. This implies strong variations on the calculation of the parameters A_1 and A_2 of the logarithmic regression curve and a significant dispersion of the roughness k_s.*
- *Vertical distance z in Prandtl's law is measured from a line which passes slightly below the roughness peaks. In general $z_0 \cong -0.2\ k_s$. By measurements with UVP probe the ultrasounds can reflect on surface elements located at different levels.*
- *A solution is to measure many velocity profiles over the entire length of the channel and to determine the average value of k_s.*

1. Introduction

The pressurised tunnel is one of the significant elements of a hydroelectric power plant. It frequently extends on several kilometres between the reservoir and the surge tank marking the departure of the penstock. It is therefore of major importance to minimize the head losses due to friction in such a tunnel. This can only be done if these losses are predictable in relation with the size of the surface roughness elements. The boundary layer theory is a useful base for the determination of surface roughness which can be evaluate from velocity profile measurements.

2. Theoretical aspects

The head loss h_r [m] divided by the length of reach concerned L [m] is called friction slope J_f [-]. The common relation used to express J_f is the Darcy-Weisbach formula (1):

$$J_f = \frac{h_r}{L} = \frac{V^2}{2g} \cdot \frac{f}{D} \qquad (1)$$

D : section diameter	*[m]*
V : mean flow velocity	*[m/s]*
g : gravitational acceleration	*[m/s²]*
f : friction coefficient	*[-]*

The friction or resistance coefficient f was investigated experimentally by Prandtl [1]. An analytical relation was later proposed by Colebrook and White (2) for the expression of f in turbulent flow condition over random surface roughnesses in opposition to the uniform sand distribution used in the Prandtl experiments [2].

$$\frac{1}{\sqrt{f}} = -2 \cdot \log\left[\frac{k_s}{3.7D} + \frac{2.51}{Re\sqrt{f}}\right]$$ valid for $Re > 5000$ with (2)

$$Re = \frac{V \cdot D}{\nu}$$ (3)

k_s : *equivalent sand roughness* [m]
Re : *Reynolds number* [-]
ν : *kinematic viscosity* [m^2/s]

k_s corresponds to the sand grains diameter, homogeneous and uniformly distributed, which would cause the same pressure loss as the surface roughness of a trade conduit.

The value of k_s depends on the height, forms, density and distribution of roughness elements.
Moody was the first to propose a graphical representation of the relation of Colebrook and White (Fig. 1). This diagram give the head loss factor f as a function of Reynolds number Re and relative roughness k_s/D. The purpose of the study then becomes to determine the equivalent sand roughness k_s of a surface indifferently.

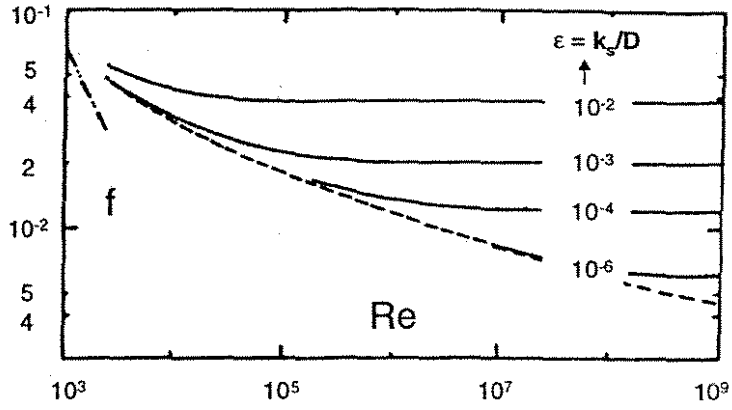

Figure 1 : Diagram of Moody-Stanton

The boundary layer theory, developed by Prandtl, treats the flow in the vicinity of a wall [1]. This flow can be subdivided in two zones:

1. the close to wall, of weak thickness, called boundary layer, where the influence of friction forces is significant;
2. the zone far away from the wall, called free fluid, where the influence of friction forces becomes negligible.

The Prandtl's law in the interior zone of the flow is given by (4).

$$\frac{u}{u_*} = \frac{1}{\kappa}\ln\left(\frac{z}{k_s}\right) + B_r$$ (4)

u_* : *friction velocity* [m/s]
z : *outdistance starting from the bottom* [m]
κ : *universal constant of Von Karman* [-]
B_r : *constant of integration* [-]

The validity field of (4) is defined as $60 \le \frac{zu_*}{\upsilon} \le 500$ which is equivalent with $0.01 \le \frac{z}{\delta} \le 0.2$, δ [m] is the distance from the bottom to which one notes maximum velocity.

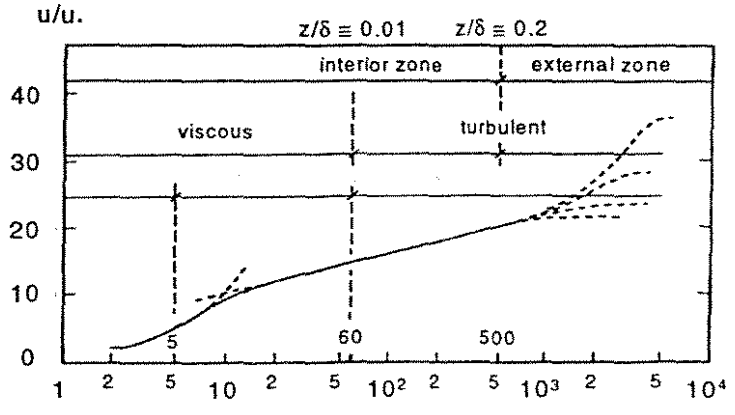

Figure 2: Validity field of the Prandtl's law

3. Experimental study

Velocity profiles measurements with a UVP X-3-PS probe [6] were made in a flume of 30 cm width and 8 m length. The data was collected at a frequency of 10 Hz and a 0.748 mm grid spacing along the axis of the transducer. This axis made an angle of 60° with the channel bottom, corresponding to one measurement every 0.648 mm along the vertical axis. The slope is variable between 0 and 1% adjustable using a crank. The side walls are made of transparent PVC and the tested bottom surfaces were following:

- smooth concrete (Fig. 3a),
- concrete with regularly bored holes representing 4.5 % of the total surface (Fig. 3b),
- Garden flagstones with some different grain sizes and forms (Fig. 3c-3e).

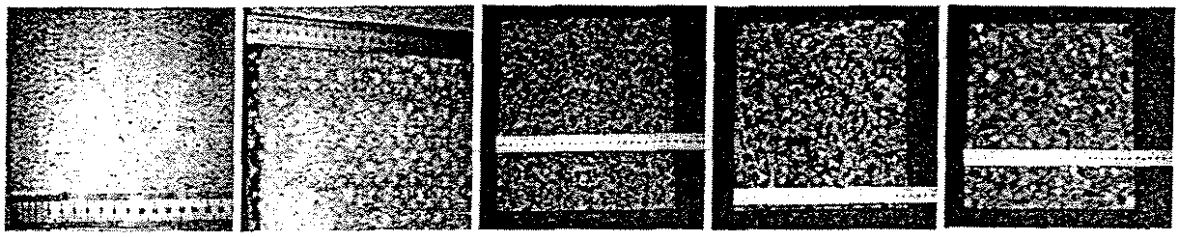

a) b) c) d) e)

Figure 3 : Tested bottom surfaces

In order to obtain a broad channel flow condition, i.e. with negligible influence of the walls, a flow discharge of 6 l/s was used.
The friction velocity u_* and roughness k_s was calculated for each basic type by applying the boundary layer theory described previously. These two steps are described hereafter:

Determination of u_*

1. First choice of the validity interval of (4) : $(z_{min}^{1} ; z_{max}^{1})$.
2. Application of the corresponding regression curve : $u = A_1^{1} \ln(z) + A_2^{1}$
3. Calculation of the friction velocity : $u_*^{1} = \kappa \cdot A_1^{1}$
4. Checking of the result validity : $\frac{z_{min}^{1} \cdot u_*^{1}}{\upsilon} \geq 60$ and $\frac{z_{max}^{1} \cdot u_*^{1}}{\upsilon} \leq 500$
5. Validity field satisfied : calculation of k_s
   Validity field not satisfied : new choice of the validity interval.

Determination of k_s

Once the friction velocity calculated, it is easy to determine the roughness k_s with (5):

$$k_s = \exp\left[\left(\frac{A_2}{u_*} - B_r\right) \cdot (-\kappa)\right] \qquad (5)$$

The B_r value in (5) is 8.5, corresponds to a rough flow condition. This is checked using the relation $\frac{u_* \cdot k_s}{\upsilon} \geq 70$ proposed by Nikuradse [3]. If not the case, the flow condition can be smooth or in transition state and the value of B_r becomes a function of $u_* k_s/v$. Two formula were proposed by Nikuradse and Krishnappan for this case [5]. The resolution must be made in a graphic way considering that an analytical solution doesn't exist.

4. Results

An example of a measured velocity profile is given on fig. 4. It is noted that the fluctuations speed in the logarithmic curve part of the profile are significant, which makes difficult a precise estimation of the friction speed u_* and roughness k_s. Figure 5 shows the Prandtl's law adjusted to the logarithmic part of the velocity profile, in the interval defined on figure 2. From the adjusted coefficients A1 = 0.0848 and A2 = 0.82, the friction velocity and the roughness values can successively be calculated.

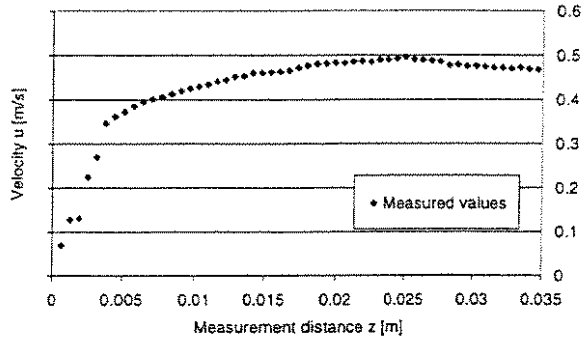

Figure 4 : Velocity profile measurement.

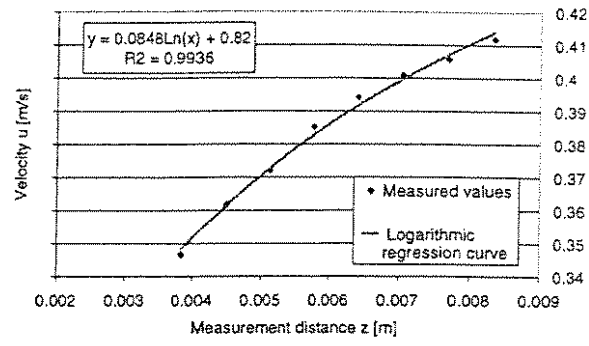

Figure 5 : Logarithmic regression curve in the interior zone.

The results of k_s for each bottom type are given in table 1.

Tested plates	k_s [mm]	Comments
Smooth concrete (figure 3a)	0.37	Good agreement with the values given in literature.
Concrete with 4.5% of holes (figure 3b)	0.59	Weak roughness increase compared to the smoothes case.
Garden flagstone VERONA (figure 3c) (A)*	15.23	For equivalent projected surfaces, roughness k_s strongly depends on the shape of the grains. Kibbled grains, with square edged boards, produce a higher value of k_s than grains with round form.
Garden flagstone RIVIERA (figure 3d) (B)*	1.67	
Garden flagstone JURA (figure 3e) (A)+(B)	5.66	

(A) : Kibbled grains ; (B) : Rounded grains.

Table 1 : Calculated k_s for different surface types.

5. Conclusions

The results obtained in the determination of the sand equivalent roughness for various types of surfaces make it possible to draw the following conclusions:

- The velocity fluctuations in the logarithmic part of the velocity profile are significant [5]. This implies strong variations on the calculation of the parameters A_1 and A_2 of the logarithmic regression curve and a significant dispersion of the surface roughness k_s.
- Vertical distance z in Prandtl's law is measured from a line which passes slightly below the roughness peaks. In general $z_0 \cong -0.2\ k_s$ [3]. By measurements with UVP probe the ultrasounds can touch parts of surface which are on different levels.

The proposed solution is to make velocity profile measurements over the entire length of the channel and to seek the average value of k_s.

Bibliographical references

[1] PRANDTL, L. et al., *Führer durch die Strömungslehre,* Fr. Vieweg et Sohn, Braunschweig, 1990.
[2] SINNIGER, R.O., HAGER, W.H., *Constructions hydrauliques, écoulements stationnaires,* Volume 15 du Traité de Génie civil, Presses Polytechniques Romandes, Lausanne, 1989.
[3] GRAF, W.H, ALTINAKAR, M.S., *Hydrodynamique,* Eyrolles, Paris, 1991.
[4] BOILLAT, J.-L., *Influence de la turbulence sur le coefficient de traînée des sphères, étude expérimentale,* Thèse n° 388 présentée au département de génie civil, EPFL, 1980.
[5] LAVELLI A., *Pertes de charge dans les galeries d'amenée, étude théorique et expérimentale,* Travail pratique de diplôme 1997-1998, EPFL, 1998.
[6] MET-FLOW SA, *Ultrasonic Velocity Profile Monitor – Operation Manual, Model UVP X-3-PS,* 1996.

Turbidity current monitoring in a physical model flume using ultrasonic Doppler method

Dr Giovanni De Cesare, Prof. Dr. Anton Schleiss

Laboratory of hydraulic constructions, Swiss Federal Institute of Technology Lausanne, CH-1015 Lausanne, tel ++41 21 6932385, fax ++41 21 6932264, email : secretariat.lch@epfl.ch

Summary

In order to clarify the flow mechanism of river-induced turbidity currents in artificial lakes, physical modelling of turbidity currents was carried out in a laboratory flume. Parallel to the laboratory study, performed at the Laboratory of Hydraulic Constructions at the EPF-Lausanne, field observations have been made in an Alpine reservoir and its main inflow river. The reproduced turbidity currents in the laboratory have been monitored using ultrasound probes functioning with the Doppler Method. Measurements were made in the flume with three different configurations of the ultrasound transducers. The flow in the laboratory flume has been simulated numerically. The results of the laboratory experiments and the numerical calculations were compared in order to check the accuracy of the numerical two-phase flow code. Comparisons were made with vertical and axial velocity profiles. The complete 3D-flow field has been computed and compared with the measured 2D-velocity distribution near the bottom of the flume. The so tested numerical two-phase flow code has then been applied to simulate river-induced turbidity currents directly in an artificial reservoir.

1. Introduction

Sediment deposition in reservoirs causes mainly loss of water storage capacity (Graf 1994, Fan and Morris 1992), the risk of blockage of intakes structures as well as sediment entrainment in hydropower schemes (Boillat et al. 1994, Schleiss et al. 1996, De Cesare 1998). Finally the sediment ends to some extent in the downstream river during flushing (Rambaud et al. 1988). The planning and design of a reservoir require the accurate prediction of sediment transport, erosion and deposition in the reservoir. For existing artificial lakes, more and wider knowledge is still needed to better understand and solve the sedimentation problem, and hence improve reservoir operation.

Turbidity currents are often the governing process in reservoir sedimentation by transporting fine materials over long distances through the impoundment to the vicinity of the dam. They are flows driven by density differences caused by suspended fine solid material. They belong to the family of sediment gravity currents. These are flows of water laden with sediment that move downslope in otherwise still waters like oceans, lakes and reservoirs. Their driving force is gained from the suspended matter, which renders the flowing turbid water heavier than the clear water above. Turbidity currents are encountered in fluvial hydraulics, most prominently if a sediment-laden discharge enters a reservoir, where, during the passage, it may unload or even resuspend granular material.

This paper presents some aspects of physical modelling and numerical simulation of turbidity currents. Special attention is drawn on the measuring technique in the laboratory using ultrasonic Doppler velocimetry.

2. Experimental set-up

Figure 1 shows the general schematic view of the flume, two adjacent mixing and storing tanks and the measuring equipment. The flume used in this investigation is 8.4 m long, 1.5 m wide and 65 cm deep. It is made of steel but has a glass wall on one side. On the bottom a 6 m PVC plate is laid which varies a slope from 0 to 6%. Water-sediment mixture is takes place in a separate tank (2 m^3) with a propeller-type mixer. This tank is connected to an upstream tank by a recirculation pump. The turbid water returns to the mixing tank over a free surface weir, which controls the water level in the upstream tank. A gate with variable width and opening allows the controlled release of the turbidity current into the flume.

Measurements were made in the flume with three different configurations of the UVP transducers. Because the UVP instrument allows only one transducer to be connected at a time, the eight transducers used in the experimental set-up were connected to the UVP via a multiplexing unit.

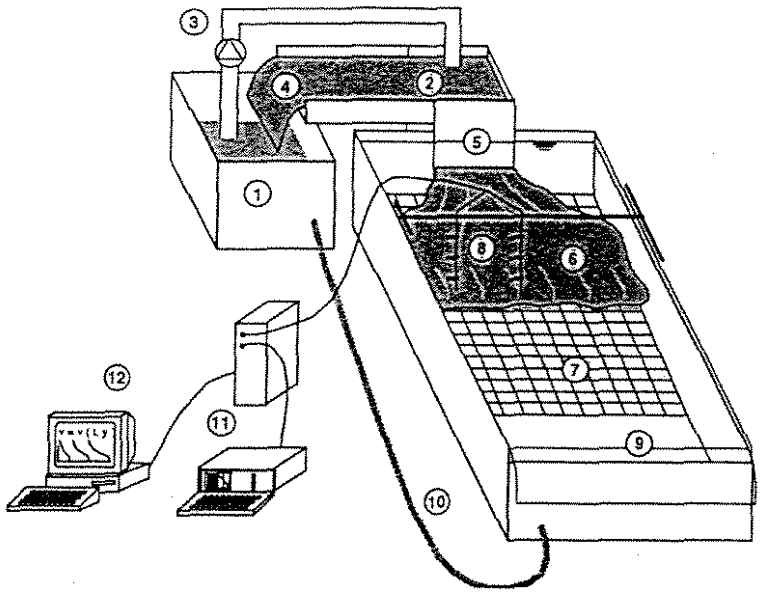

Figure 1:

Schematic drawing of the experimental installation, (1) mixing tank (2) upstream tank (3) recirculation pump (4) free surface weir (5) inflow gate (6) turbidity current (7) experimental flume (8) ultrasonic probes (9) sharp crested weir (10) flexible duct (11) UVP instrument (12) controlling computer

The beam directions and the penetration length were chosen in order to cover the interior of the advancing turbidity current. As the model is symmetric, the profiles were taken on the axis of symmetry and the flow -mapping region was situated on one side of the flume only. The arrangement of the transducers are described as follows:

- Vertical arrangement with 8 transducers looking with an angle of 60° against the main flow. The measurements give the projected vertical velocity profiles over 2 m flow length from the gate, the distance between the transducers was 25 cm.

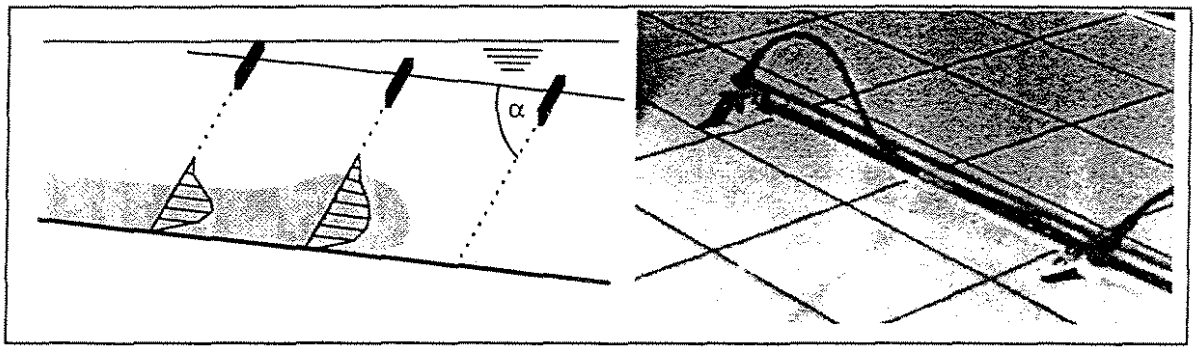

- Axial disposition with 8 transducers looking straight against the main flow. The measurements give the horizontal velocity profiles over the whole 3 m flow length from the gate, the distance between the transducers was 50 cm. The probes were installed 12 mm above the bottom and were slightly set off laterally in order to reduce interference by reflection of US from different transducers.

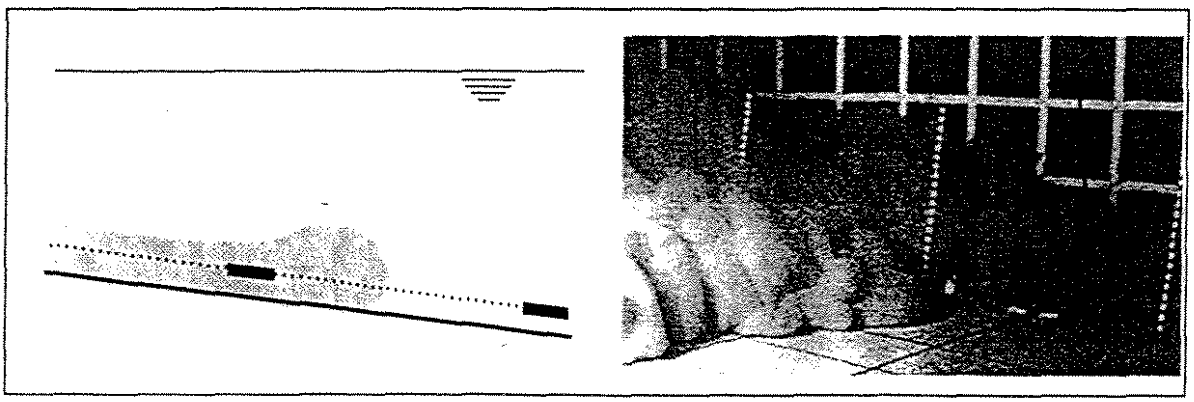

- Square grouping with 4 transducers on each side looking straight at and perpendicular to the main flow in the spreading part just after the inflow gate. The side of the square plane where the flow mapping took place was 62.5 cm long, the distance between transducers was 12.5 cm close to the inflow gate, and 25 cm elsewhere. The transducers were installed with plastic clamps 12 mm above the bottom on an aluminium frame.

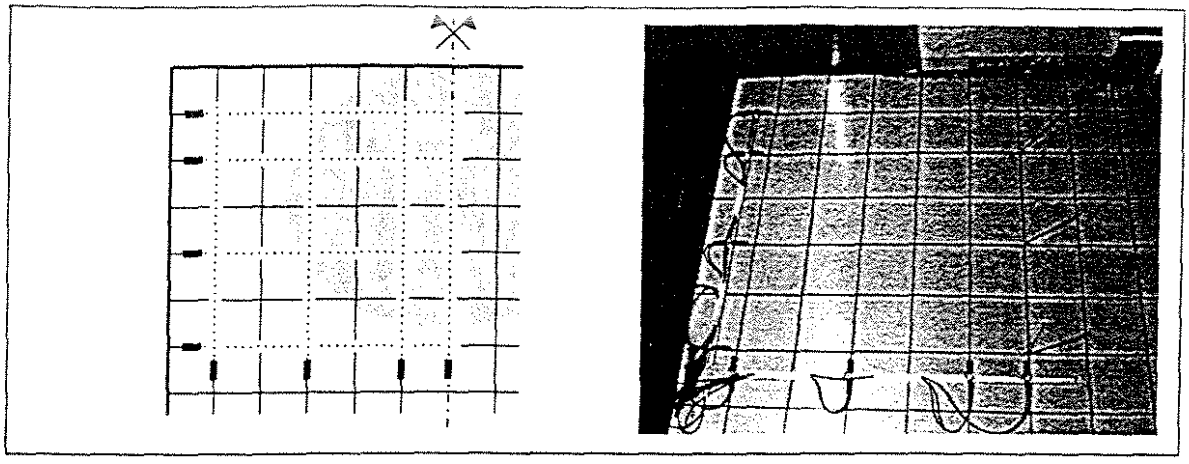

The echo of the flowing turbidity current was strong enough to allow rapid measurements, only 4 successive profiles were taken with each transducer, and the averaged profile is used as velocity profile at one location. The temporal resolution was therefore less than ½ second per profile. The duration to sweep all transducers was around 3 seconds and the cycle was repeated every 5 seconds, thus giving a quasi-instantaneous velocity information every 5 seconds. The vertical profiles were obtained with 8 measurements per profile, thus doubling cycle time, repetitions were made every 10 seconds.

3. Simulated turbidity current

All the experiments were conducted with fine homogenous clay as suspended matter. The density of the sediments is $\rho_s = 2'740$ kg/m^3. The particle size distribution ranges from $d_{10} \approx 0.002$ mm to $d_{90} = 0.1$ mm, with a mean particle diameter of $d_{50} \approx 0.02$ mm. The corresponding settling velocity calculated using Stokes law is $v_{ss} \approx 0.4$ mm/s for the representative particle size in calm water. In all experiments the clear water from the main reservoir of the hydraulic laboratory was used as the ambient fluid. The water-sediment mixtures were prepared in the mixing tank by adding the dry clay to the clear water. The density of the water-sediment mixture, ρ_m varied between 1'002 and 1'005 kg/m^3, and the mixture was considered to be a Newtonian Fluid.

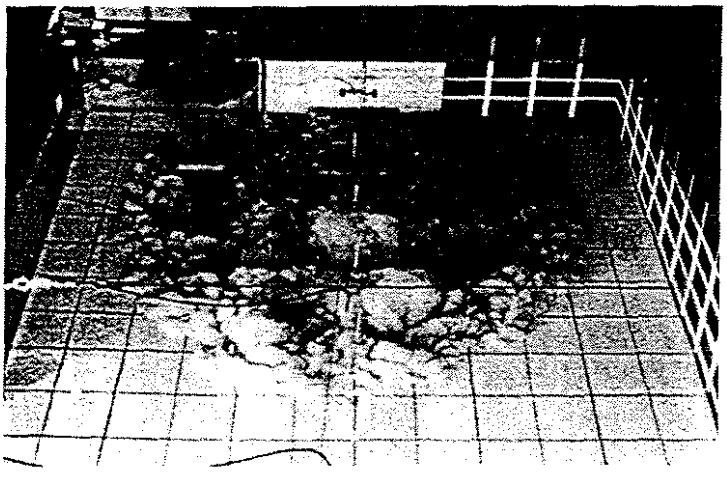

Figure 2:

Photograph of the expanding turbidity current in the experimental flume 25 s after opening of the gate, the current spreads out almost radial, 125mm x 125mm grid on PVC bottom

Figure 2 shows a photograph of the spreading turbidity current 25 seconds following its initial release. After its spreading to the total flume with, the current adjusted itself rapidly to a uniform flow advancing steadily within the tank. When the current reached the downstream end of the flume, the turbid water was evacuated by opening the bottom gate. During the total duration of the experiment the same turbid water flux was fed from the inflow gate.

4. Experimental results

The measured velocity profiles were compared a theoretical distribution, the result agrees well as shown in Figure 3. A bottom surface layer region, where the velocity distribution is logarithmic and a jet region, where the velocity is the half Normal (Gaussian) distribution.

Figure 4 shows the velocity distribution in the turbidity current expansion. Both calculated and measured values are plotted on the same graph. The results of the numerical modelling are presented by a surface of equal concentration where the maximum concentration gradient can be found.

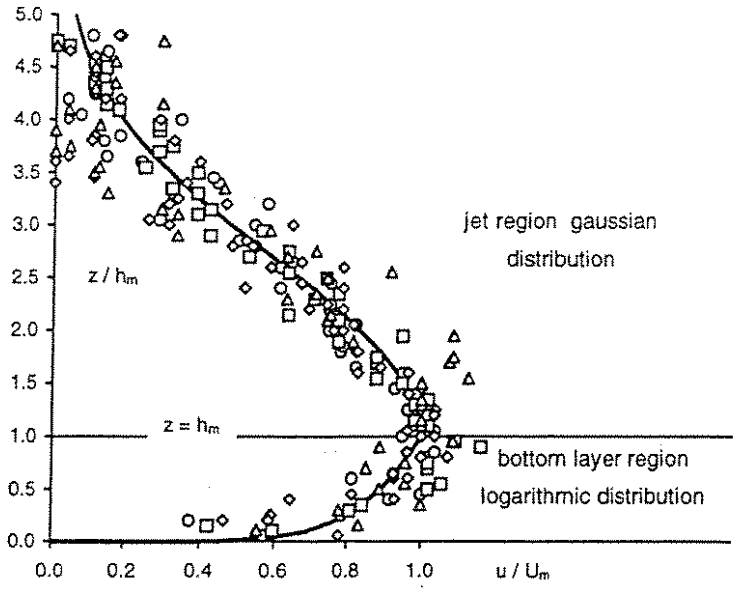

This surface fits well to the position of the interface between the turbidity current and the surrounding water. The velocity vectors are given on a fine grid in a plane parallel to the bottom. This plane is situated at 12 mm from the bottom, the same level as the one where the transducers were installed.

Figure 3:

Measured velocity values compared to theoretical vertical velocity distribution. Values from run n° 2, 80 ms between two succeeding measurements

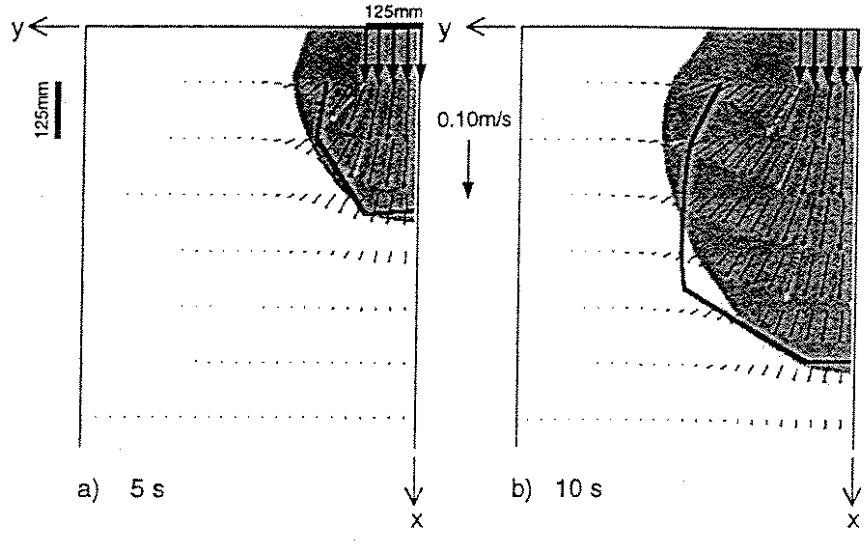

Figure 4:

Computed and measured 2D-flow field 12 mm from the flume bottom and limits of the spreading turbidity current a) 5 and b) 10 s after the opening of the gate; numerical simulation: black velocity vectors, turbidity current as a grey surface; physical model: white velocity vectors, limits of the turbidity current as a bold line.

5. Conclusions

Good experience with the ultrasonic echography for flow measurement in the laboratory has been acquired. The characteristics of the UVP instrument make it well adapted to operate in physical scale models with turbidity currents. The small ultrasonic transducers allow easy handling and undisturbed flow monitoring. It is possible to capture precise velocity profiles in very short a time.

Computer simulation has been used to predict the advancing 3D-turbidity current in the laboratory and validated with experimental results. Based on the numerical simulation, not only general conclusions can be drawn, but also the precise behaviour of turbidity currents can be predicted.

References

Boillat J.-L., De Cesare G. (1994). "Dichteströmungen im Bereich des Grundablasses des Stausees Luzzone – Modellversuche", *Proceedings of the Symposium "Betrieb, Erhaltung und Erneuerung von Talsperren und Hochdruckanlagen"*, pp. 183-192, Graz, Austria.

De Cesare G. (1998). "Alluvionnement des retenues par courants de turbidité", *PhD Thesis N° 1820 and communication du Laboratoire de constructions hydrauliques - LCH N° 7*, Lausanne, EPFL, Switzerland.

Fan J., Morris G. L. (1992). "Reservoir Sedimentation. II: Reservoir Desiltation and Long-Term Storage Capacity", *ASCE, Journal of Hydraulic Engineering*, Vol. 118, No. 3.

Graf W. H. (1984). "Storage losses in reservoirs", *International Water Power & Dam Construction*, Vol. 36, N° 4.

Rambaud J., Khalanski M. et al. (1988). "Expérience acquise dans les vidanges de retenues par Electricité de France et la Compagnie Nationale du Rhône", *Proceedings of XVIe congrès ICOLD*, Q.60-R.30, San Francisco.

Schleiss A., Feuz B., Aemmer M., Zünd B. (1996). "Verlandungsprobleme im Stausee Mauvoisin. Ausmass, Auswirkungen und mögliche Massnahmen ", Proceedings of Internationales Symposium «Verlandung von Stauseen und Stauhaltungen, Sedimentprobleme in Leitungen und Kanälen», *Mitteilungen der VAW* Nr. 142, Teil 1, pp. 37-58, Zürich, Switzerland.

Modeling and measurement of muddy debris-flows

Dr Jean-Louis Boillat, Erik Bollaert

Laboratory of hydraulic constructions, Swiss Federal Institute of Technology Lausanne, CH-1015 Lausanne, tel ++41 21 6932385, fax ++41 21 6932264, email secretariat.lch@epfl.ch

Summary

The physical modelling of a discharge control structure during muddy debris-flows has to take into account the particular shear behaviour of a muddy fluid, governed by the Herschel-Bulkley law. Determination of the main flow characteristics was obtained by vertical velocity profile measurements by means of a U.V.P (Ultrasonic Velocity Profiler). The transducer was mounted on the bottom of the channel, in a zone where the muddy flow is fully developed. The results were used to calibrate a theoretical model based on the principle of maximisation of entropy. An equivalent kinematic viscosity of the laminar muddy debris-flows was determined in order to calculate head losses. The empirical law obtained experimentally shows that this viscosity varies exponentially with the critical shear stress.

1. Introduction

Heavy rainfall on the catchment area of the Nant of Pissot, situated in the western part of Switzerland, produced a debris-flow during the night of the 13th to the 14th of August 1995. This event displaced about 50'000 m^3 of materials that finally accumulated on the alluvial deposition cone. Some 19'000 m^2 of vineyards were destroyed, the industrial zone was severely damaged and the national roadway RN9 was crossed by the flow, burying in that way 11 vehicles (Fig. 1). Fortunately, this natural disaster didn't make any victims.

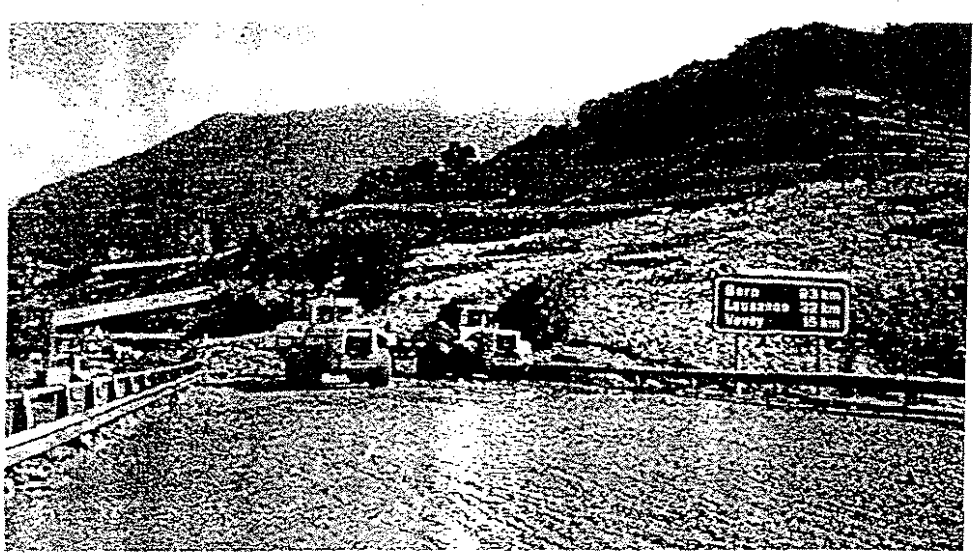

Fig. 1 View of the removal of debris on the RN9 after the avalanche of August 1995.

After the event of August 1995 several safety structures has been realized, namely two dumping basins, the first one with a volume of 20'000 m^3 at a height of 500 m a.s.l., and the second one with 5000 m^3 at a height of 380 m a.s.l., connected by a transition channel. Slightly downstream of the 500 dumping basin, at a height of 456 m a.s.l., the canal has been equipped by a discharge control structure. This device is one of the key elements of the concept established for the protection against debris-flows. Its function is to divert the debris-flow excesses lateral to the left bank in such way that water flows and moderate debris-flows still move straight ahead up to the dumping basin 380. The

discharge control structure consists of a channel contraction, a 35 m long lateral spillway on the left bank and a deviating balk wall directing the overflow to the left bank. This innovative device has been submitted to hydraulic tests on a scaled model [1].

The model, realized on a 1/50 scale, also reproduces a part of the upstream and downstream channel. Parallel to the physical model tests a study was undertaken concerning the similarity of the model fluid. The model tests were dedicated in a first stage to the hydraulic behavior of the system as well as to the simulation of granular debris-flows. In a second stage, the simulation of muddy debris-flows was performed, respecting the following order :

- study of the rheological similarity of the fluid model ;
- optimization of the geometry of the structure ;
- verification of the functionality of the discharge control structure – critical diversion discharge, diverted ratio – for different properties of the fluid model ;
- study of the behavior of the discharge control structure for different degrees of clogging of the channel aperture.

2. Modeling of muddy flows

The muddy debris-flow was simulated by means of a dilution of kaolinite into water. For volumetric concentrations between 20 and 30 %, the shear behaviour of the fluid is totally different from that of Newtonian fluids and follows the Herschel-Bulkley law [2], given by the following expression:

$$\tau = \tau_c + K \cdot \dot{\gamma}^n \quad \text{if} \quad \dot{\gamma} \neq 0 \qquad \tau \leq \tau_c \quad \text{if} \quad \dot{\gamma} = 0 \tag{1}$$

τ_c : *critical shear stress* [N/m^2]
$\dot{\gamma}$: *velocity gradient* [s^{-1}]
K et n : fluid parameters [-]

The critical shear stress, as well as the fluid parameters, have been obtained by rheological tests, and a relationship between the critical shear stress and the volumetric concentration of the water-kaolinite mixture could be adjusted as represented on Fig. 2:

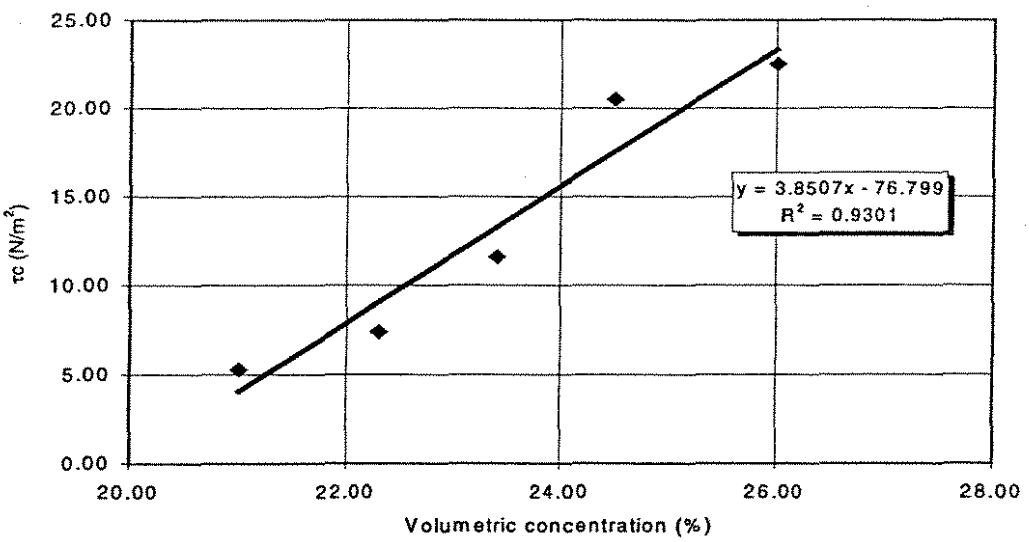

Fig. 2 Relationship between the critical shear stress and the volumetric concentration of the water-kaolinite mixture.

3. Comparison of experimental and theoretical velocity profiles.

The determination of the main flow characteristics has been obtained by vertical velocity profile measurements by means of a U.V.P (Ultrasonic Velocity Profiler). The transducer was mounted on the bottom, in the longitudinal axis of the upstream channel, in a zone where the muddy flow is fully developed. The UVP X-3-PS instrument functions by direct measurement in the fluid using ultrasonic waves with Doppler effect [3]. The analysis of the echo reflected by the particles that are moving in the

measurement zone allows to identify velocity and direction of flow as well as the position of the control volume. The installation was completed by an ultrasonic level meter intended to measure flow height simultaneously. The results were used to calibrate a theoretical model based on the principle of maximisation of entropy [4]. The corresponding velocity profile has the following form:

$$u(\xi) = \frac{u_{max}}{M} \cdot \ln\left[1 + \left(e^{M} - 1\right) \cdot \frac{\xi - \xi_0}{\xi_{max} - \xi_0}\right] \tag{2}$$

u :	*longitudinal component of flow velocity vector*	*[m/s]*
ξ :	*curvilinear co-ordinate of the lines of equal velocity*	*[-]*
u_{max} :	*maximum flow velocity*	*[m/s]*
M :	*parameter of entropy*	*[-]*

With:

$$\xi = \frac{y}{D-h} \cdot \exp\left(1 - \frac{y}{D-h}\right) \tag{3}$$

D :	*flow depth*	*[m]*
h :	*depth of maximum flow velocity*	*[m]*

In the above equations, D and h are measured values, while M is defined analytically. The parameter of entropy M has been determined as a flow constant on one hand, and as varying linearly with the flow depth on the other one. The results of the calibration of the theoretical velocity profiles are represented hereunder (Fig. 3) and show that a best fit is obtained by considering a linear variation of M with the flow depth. The data was collected for a frequency of 10Hz and a 0.748mm grid spacing along the axis of the transducer. This axis made an angle of 60° with the channel bottom, corresponding to one measurement every 0.648mm along the y-axis.

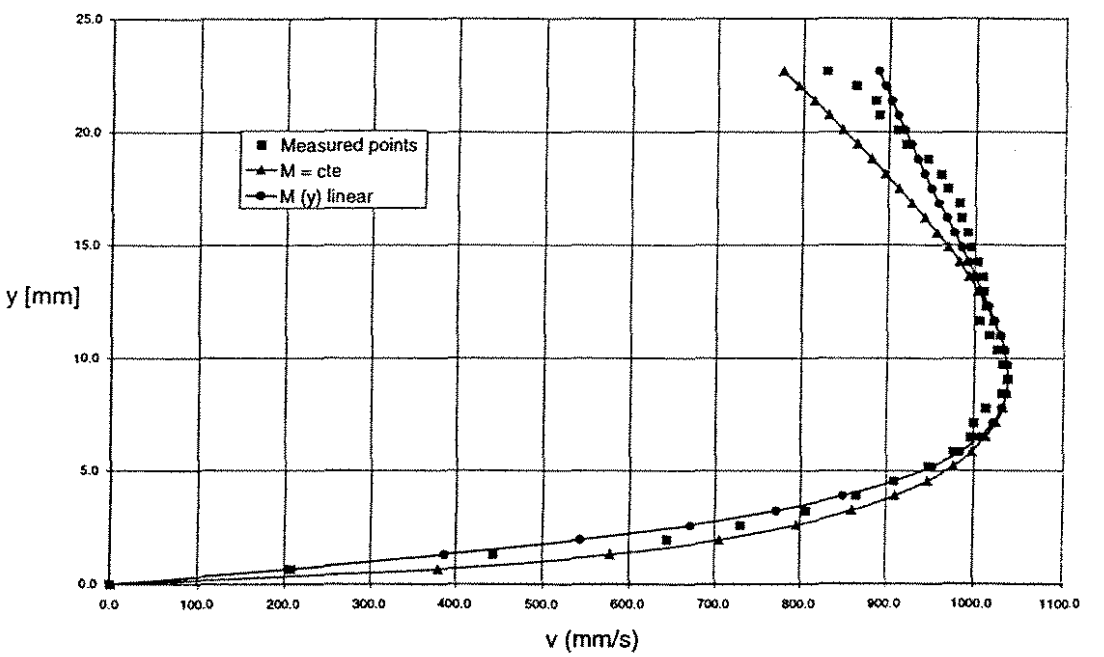

Fig. 3 Results of the calibration of the theoretical velocity profiles with M as constant and M varying linearly with the flow depth

This thermodynamic approach has been applied in order to determine an equivalent kinematic viscosity of the model flow and gives satisfactory results.

4. Hydraulic friction law for laminar muddy debris-flows

By the fact that all the observed muddy flows were laminar, an equivalent kinematic viscosity of muddy debris-flows was determined in order to calculate head losses. The empirical law obtained

experimentally shows that this viscosity varies exponentially with the critical shear stress. The friction coefficient f, determining head losses, is then expressed by the following relationship (Fig. 4):

$$f = \frac{45.8}{R} \qquad \text{for } R < 2300 \tag{4}$$

f :	*friction coefficient of Darcy-Weisbach [5]*	*[-]*
R :	*Reynolds number* $= u_m . D_h / v$	*[-]*
u_m :	*mean velocity based on (2)*	*[m/s]*
D_h :	*hydraulic diameter*	*[m]*
v :	*equivalent cinematic viscosity of flow*	*[m^2/s]*

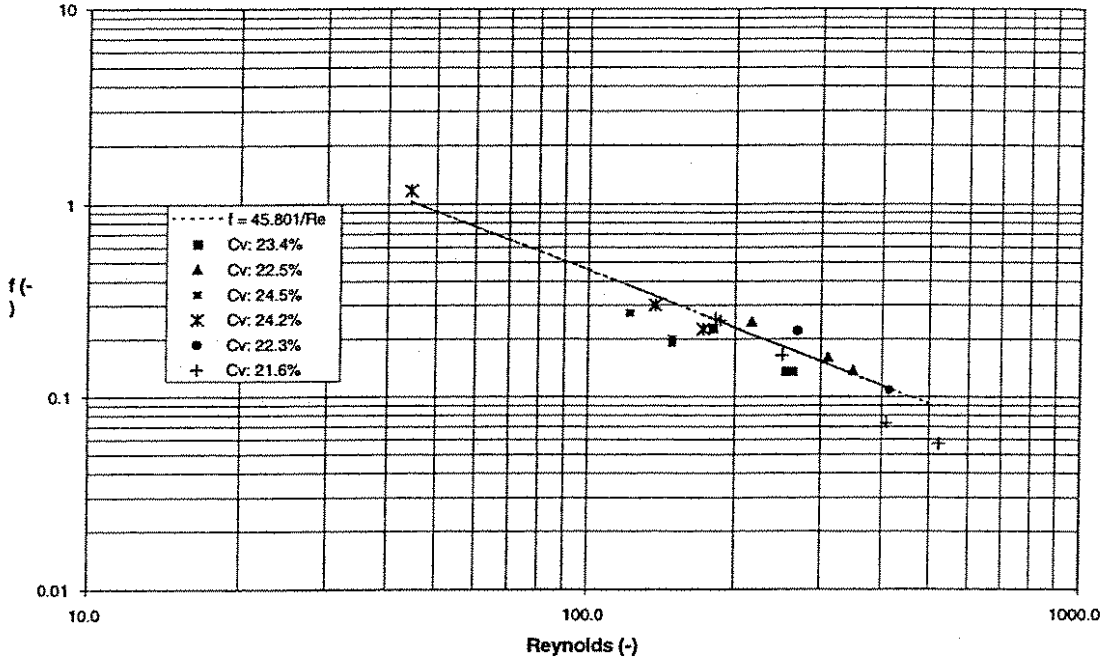

Fig. 4 Adjustment of the f(R) relationship over different volumetric concentrations

5. Conclusions

The physical modelling of a discharge control structure during muddy debris-flows took into account the shear behaviour of a muddy fluid following the Herschel-Bulkley law. The main flow characteristics were obtained through vertical velocity profile measurements by means of a U.V.P (Ultrasonic Velocity Profiler). The results were used to calibrate a theoretical model based on the principle of maximisation of entropy. An equivalent kinematic viscosity of laminar muddy debris-flows was then determined in order to calculate head losses. The empirical law shows that this viscosity varies exponentially with the critical shear stress. A friction coefficient f, determining the head losses following the Darcy-Weisbach equation, could be expressed in function of the Reynolds number of the muddy flow. This finally allowed the establishment of the "flow depth – discharge" relationship of the muddy flows at different volumetric concentrations. A reliable and detailed dimensioning of the discharge control structure could thus be achieved.

Bibliographical references

[1] Sinniger, R., Boillat, J.-L., "Modélisation de laves torrentielles granulaires et boueuses sur l'écrêteur 456 du Pissot", Rapport interne N°3, LCH-EPFL, mars 1998.

[2] Coussot, P., "Rhéologie des laves torrentielles boueuses" et "Lois d'écoulement des laves torrentielles boueuses", La Houille Blanche, mars 1994.

[3] MET-FLOW S.A.: Ultrasonic Velocity Profile Monitor – Operation Manual, Model UVP X-3-PS, May 1996.

[4] Chao-Lin Chiu, "Application of Entropy Concept in Open-Channel Flow.", Journal of Hydraulic Engineering, Vol.113, N°5, mai 1987.

[5] Sinniger, R., Hager, W., "Constructions Hydrauliques. Ecoulements stationnaires. Traité de Génie Civil, Vol.15", Ecole Polytechnique Fédérale de Lausanne, 1988.

2.ISUD
2nd International Symposium on Ultrasonic Doppler Methods
for Fluid Mechanics and Fluid Engineering
September 20-22, 1999
Paul Scherrer Institut, 5232 Villigen PSI, Switzerland

Liquid Flow Structure around Bubbles — Effect of Channel Width —

Hiroyuki MURAKOSO[1)], Yumiko SUZUKI[1)], Masanori ARITOMI[1)], and Michitsugu MORI[2)]

1) Research Laboratory for Nuclear Reactors, Tokyo Institute of Technology
2-12-1 Ohokayama, Meguro-ku, Tokyo, 152-8550 Japan
Tel: +81-3-5734-3059, Fax: +81-3-5734-2959, E-mail: murakoso@2phase.nr.titech.ac.jp

2) Tokyo Electric Power Co., 1-1-3 Uchisaiwai-cho, Chiyoda-ku, Tokyo, 100-0011 Japan
Tel: +81-45-585-8932, Fax: +81-45-585-8943

1. Introduction

To understand the fundamental mechanism of two-phase bubbly flows, a great number of experimental studies have been carried out. There are many measurement techniques for their flow structure. Quick closing valves is one of the most simple methods to measure average void fraction. To measure local void fraction, probe techniques and radiation techniques have been used for a long time. In recent years, a laser Doppler anemometer is widely used to measure void fraction, liquid velocity and its fluctuation. These methods have made a great contribution in clarifying the macroscopic flow structure of two-phase flows. However, there still does not exist a measurement technique which can easily measure the velocity profile around a gas-liquid interface, even though it is necessary to clarify the flow structure around the bubble surface in order to understand the microscopic mechanism of bubbly flows.

The authors have been trying to measure the velocity field in bubbly flows by using the ultrasonic Doppler-shift method. The measurement instrument, the Ultrasonic Velocity Profile Monitor (UVP), was originally developed to measure liquid flows. The system can measure an instantaneous velocity profile along a measuring line by the traveling time of its pulse and Doppler-shift frequency of signals reflected on micro-particles in liquid (Takeda, 1991). When it is applied to bubbly two-phase flow, the ultrasonic pulse is reflected on both micro-particles in liquid phase and gas-liquid interfaces.

The UVP was used to measure air-water bubbly upward flows in rectangular channels. Void fraction was less than 2 %, since it was hard to measure bubbly flows in high void fraction, which can easily induce multiple reflection on bubble surfaces. Measurement was carried out 9 times at each measurement condition, and more than 9000 velocity profiles were recorded. From the measured instantaneous velocity profiles, the position of the bubble surface was decided and the data was rearranged according to the distance from the bubble surface. In this paper, the data analysis method will be explained after describing the experimental equipment. Then, the velocity distribution around bubbles and the effect of channel width on the flow structure will be discussed.

2. Experimental Apparatus

The schematic diagram of the experimental apparatus is shown in Fig.1, which consists of a water circulation system, an air supply system, a test section and a measurement system. Working fluids are air and water. Micro particles (ca. 10μm diameter) of nylon powder were mixed in the water as reflector of ultrasonic pulses. Specific gravity of the powder is 1.02, and it can be said that tracer particles follow the liquid flow well.

Water flowed upward into the test section from the lower entrance of the test section. Water flow rate was controlled by a needle valve and it was measured by an orifice flow meter, both of which were located at the bottom part of the apparatus. Air was injected into the system through five needles (inner diameter: 0.1 mm) at the air-water mixing section, which were also located at the lower end of the test section. The air flow rate was regulated by a float flow meter and an air control valve. During experiments, water temperature was kept between 19 to 21 degree using a pre-cooler and thermo-couples. Also in parallel to the measurement by the UVP, the pressure drop was measured between pressure taps installed on the side wall to get average void fraction. All experiments were carried out under the atmospheric pressure.

Figure 2 shows the test section located between the upper tank and the air-water mixer. Two kinds of vertical test sections were used, both of which were made of Plexiglas with 10 mm wall thickness. The longer side length of the rectangular cross section was constant at 100 mm, and the shorter side length (channel width) was either 10 mm or 20 mm. An ultrasonic transducer was set on the outer surface with a contact angle of 45 degrees toward the liquid main flow direction. Gap between the transducer and the wall was filled with ultrasonic jelly to prevent the reflection of ultrasonic pulses on the wall. Under each experimental condition, measurement was carried out 9 times continuously and more than 9,000 velocity profiles in the channel were obtained along the measuring line.

The experimental conditions are tabulated in Table 1. Also, the UVP configurations used in this study were summarized in Table 2.

Table 1 Experimental conditions

Water superficial velocity (10 mm channel width)	0.12	–	0.18	m/s
Air superficial velocity (10 mm channel width)	0.00235	–	0.00384	m/s
Average void fraction (10 mm channel width)	0.09	–	0.83	%
Bubble diameter (10 mm channel width)	2.7	–	3.1	mm
Water superficial velocity (20 mm channel width)	0.10	–	0.18	m/s
Air superficial velocity (20 mm channel width)	0.00349	–	0.00748	m/s
Average void fraction (20 mm channel width)	0.98	–	2.01	%
Bubble diameter (20 mm channel width)	2.9	–	3.2	mm

Table 2 Specification of the UVP in this study

Basic ultrasonic frequency	4 MHz
Maximum measurable depth	91 – 189 mm
Velocity resolution	5.6 – 2.8 mm/s
Time resolution	16.4 – 32.8 msec
Spatial resolution in water	0.74 mm
Measurement points	128
Number of profiles	1024
Ultrasonic beam diameter	5 mm

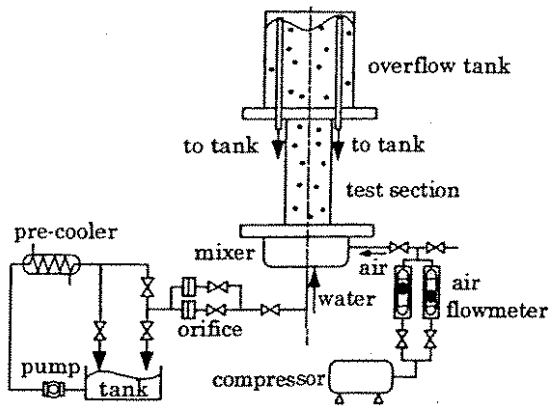

Fig.1 Schematic diagram of the experimental apparatus

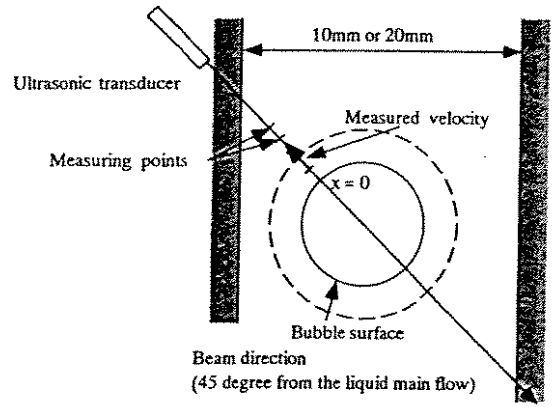

Fig.2 Test section

3. Data Processing method

The UVP system records information about the velocity field as a set of 1,024 instantaneous velocities at 128 positions. In this study, measurement was carried out nine times continuously under each flow rate condition. Therefore, 9,216 (1024 × 9) velocity data were obtained at each measurement position. When the UVP is used to a measurement of bubbly flows, ultrasonic pulses are reflected on bubble's surfaces and micro particles in liquid. Therefore, velocity profiles measured by the UVP include velocities of both liquid phase and bubble's interface. Since it is not possible to know which pulse is reflected on a bubble surface at present, distinction of bubble's interface velocities and liquid velocities was made using the threshold $T(x)$.

$$T(x) = C \times V_S(x) \qquad \text{(Eq.1)}$$

where the value $T(x)$ is defined as the product of a constant C and the time-averaged velocity $V_S(x)$ of the liquid single-phase flow (Fig.3).

According to this manner, 9,216 velocity profiles were divided into two groups, Group (a) and (b). If a bubble exists on the measuring line when a ultrasonic pulse is emitted from the transducer, the velocity profile recorded at that moment is selected as Group (b). If bubbles do not exist on the measuring line, the velocity profile is put into Group (a). By averaging velocities of Group (a), the time-averaged velocity profile of liquid main flow can be obtained. From the set of Group (b), it is possible to get velocity profiles around bubble surface if the relative coordinate is adopted whose origin is set on the bubble's surface.

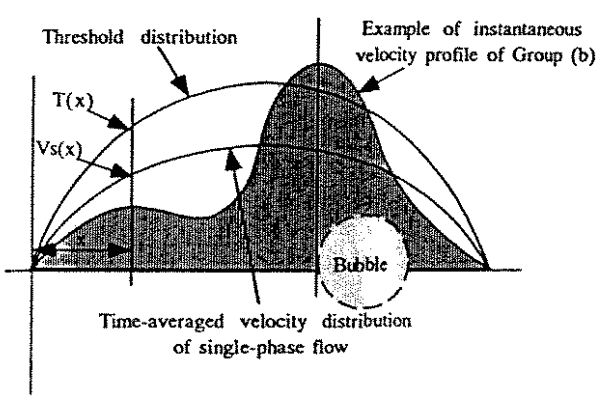

Fig.3 Schematic diagram of the threshold and instantaneous velocity

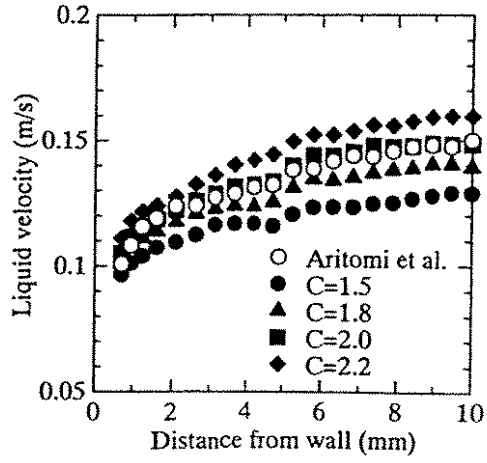

Fig.4 Comparison of liquid velocity distribution in the channel (Group (a))

Figure 4 shows the time-averaged liquid phase velocity profile obtained from Group (a). When the threshold is set larger, a small amount of instantaneous velocity profile is transferred to Group (b) and as a result, the mean velocity of Group (a) increases and an appropriate threshold can not be decided from this result.

In the previous research, our group developed a velocity measurement system for bubbly flows with the UVP (Aritomi et al., 1996, 1997 and Zhou et al., 1998). In Fig.4, time-averaged liquid phase velocity profile obtained using the system is plotted by open circles. The velocity profile has a good correlation with the mean velocity distribution of Group (a) if the constant C is set between 1.5 to 2.2 according to the liquid flow rate.

4. Results and Discussion

In Fig.5, normalized relative velocity distributions around bubbles for both 10 and 20 mm channel width are shown. Relative velocity of gas and local liquid velocity is normalized by that at the bubble's surface. Recently, Suzuki et al.(1999) has reported the velocity distribution around bubbles in upward bubbly flow for 10 mm channel width. According to their report, the flow structure around bubbles could be divided into three regions (Fig.5(a)). For 20 mm channel width, the same trend was observed (Fig.5(b)). Relative velocity has large gradient near bubbles and it becomes almost constant in the region more than 9 mm away from a bubble. The region with large velocity gradient was named the 'boundary region'. The area, where the velocity is relatively uniform, was called the 'main flow region', and the area between the 'boundary region' and the 'main flow region' was called the 'buffer region'. As seen in Fig.5, thickness of the boundary layer did not change according to the configuration of the test section. Since the flow is dominated by the relative velocity of gas and local liquid velocity in the boundary region, thickness of the region does not change even if the test section is widened. On the other hand, distance from the bubble surface to the main flow region is broadened when the test section's width is doubled. In the experiments in the channel of 20 mm width, relative velocity tended to decrease in the region more than 20 mm away from a bubble. This tendency would be considered the effect of the wall existence.

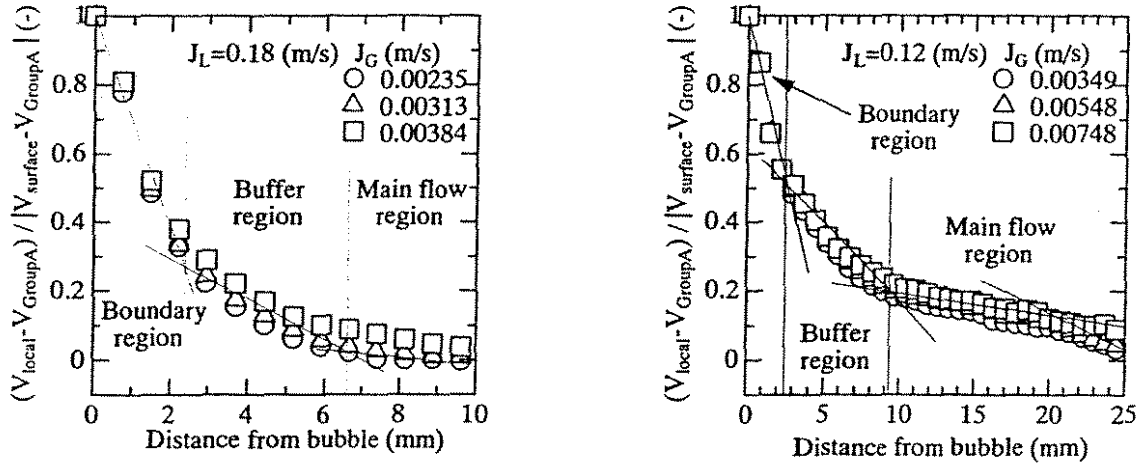

(a) 10 mm channel width (b) 20 mm channel width

Fig.5 Relative velocity distribution around bubbles

References

Takeda, Y.,: Nuclear Engineering and Design, Vol. 126, 277 (1991).
Aritomi, M. et al.,: Journal of Nuclear Science and Technology, Vol. 33, 915 (1996).
Aritomi, M. et al.,: Journal of Nuclear Science and Technology, Vol. 34, 783 (1997).
Zhou, S. et al.,: Journal of Nuclear Science and Technology, Vol. 35, 335 (1998).
Suzuki, Y. et al.: Proceedings of the 7th International Conference on Nuclear Engineering (ICONE-7), Tokyo, ICONE-7163 (1999.4).

2.ISUD
2nd International Symposium on Ultrasonic Doppler Methods
for Fluid Mechanics and Fluid Engineering
September 20-22,1999
Paul Scherrer Institut, 5232 Villigen PSI, Switzerland

Effect of control volume of UVP method on turbulent pipe flow measurement

Tsuyosi TAISHI , Hiroshige KIKURA , Masanori ARITOMI
Tokyo Institute of Technology, 2-12-1 Ohokayama, Meguro-ku, Tokyo, 152-8550 Japan

1. Introduction

Measurement of an instantaneous velocity profile of the turbulent flow has long been demanded in fluid dynamics, fluid engineering and other engineering fields involving a fluid flow. Various flow visualization techniques have been used for measurement of flow characteristics and sophisticated image processing procedures such as Particle Image Velocimetry (PIV) or Particle Tracking Velocimetry (PTV) are now available. They require, however, experienced know-how for successful measurement and data treatment, and are still expensive and time costuming for measurement. Ultrasonic Velocity Profile (UVP) method has been developed by Takeda at Paul Scherrer Institut in Switzerland [1]. It utilizes a pulsed echo-graphic technique of ultrasound and can measure a velocity profile on a measuring line instantaneously. Since the spatial information of the flow field is obtained from its traveling time, this method has various advantages over other flow measuring methods for measurement.

Although UVP method can be adapted for various liquid flow velocity measurements, it is necessary for the measurement of turbulent flow to consider the effect of measuring control volume. That is, UVP method has large measuring control volume compared with other conventional methods. Even for LDA measurement of turbulent flow, there have still been several attempts described in literature to obtain the influence of the effective volume size. Therefore, the effective volume size of UVP method for velocity profile measurement on the turbulent pipe flow was studied in the work.

Reynolds stress measurement on the turbulent pipe flow using one-component measurement is available [2][3]. Considering the effective volume size, the Reynolds stress was investigated by mean of UVP method.

2. Effect of control volume and Reynolds stress measurements

2.1 Mean velocity

The principle of UVP is to detect and process the echoes of ultrasonic pulses reflected by micro-particles crossing the measuring control volume. If the control volume was negligibly small the mean velocity U would be obtained by

$$U(x_c) = \sum_{i=1}^{N} U(x_c, t) \ . \qquad (1)$$

where x_c the position of the measuring control volume. However, the measuring

control volume is of a finite size and also velocity gradients exist across it.

Thus, considering the UVP measuring control volume and measurement period,

$$< U_{MVx_c} >= \frac{1}{Vm\ \tau_w}\int_t\int_V U(x_c, t)dVdt \qquad (2)$$

where, Vm is the measuring control volume τ_w is measurement period. It is well known that an error in turbulence measurements is induced specially in region of high velocity gradients.

For the UVP method, the control volume is disk shape of the height h and diameter D. Considering this disk control volume and expressing the time averaged velocity in a truncated Taylor series expansion around its value at the center of the measuring control volume

$$Uc_v = U(y_c) + \frac{1}{2}G\left(\frac{\partial^2 U}{\partial y^2}\right)_{x=x_c} + \text{h.o.t.} \qquad (3)$$

$$G = \left(\frac{h^3}{12\cos^3\theta} + \frac{2}{3}R^2 h\frac{\sin^2\theta}{\cos\theta} + \frac{R^3}{8}\pi\sin^3\theta + \frac{h^2 R\pi\sin\theta}{8\cos^2\theta}\right)\Big/\left(\frac{h}{\cos\theta} + \frac{\pi}{2}R\sin\theta\right)$$

where, y is direction of radius (distance from the wall) and R is D/2.

2.2 Reynolds stress

In the present study measurements were carried out for the Reynolds stress $\overline{uv}$. To estimate these quantities using UVP method it requires independent measurements of the u and v-velocity components and also at angle α and $-\beta$ with respect to the x-axis. It is often common practice to set α and $-\beta$. Using coordinate transformations, the instantaneous signals can be expressed in term of the velocity components (Fig.1).

$$\tilde{U} = \overline{U} + u \qquad (4)$$

$$\tilde{V} = \overline{V} + v \qquad (5)$$

$$\tilde{Q} = \tilde{U}\cos\alpha + \tilde{V}\sin\alpha \qquad (6)$$

And the fluctuating signals in the fluctuating velocity components on two measuring lines are:

$$q_1 = v\cdot\cos\alpha + u\cdot\sin\alpha \qquad (7)$$

$$q_2 = v\cdot\cos\beta - u\cdot\sin\beta \qquad (8)$$

With the prior knowledge of the u and v-velocity components, and if $\alpha=\beta$, the following expressions provide the Reynolds stress $\overline{uv}$.

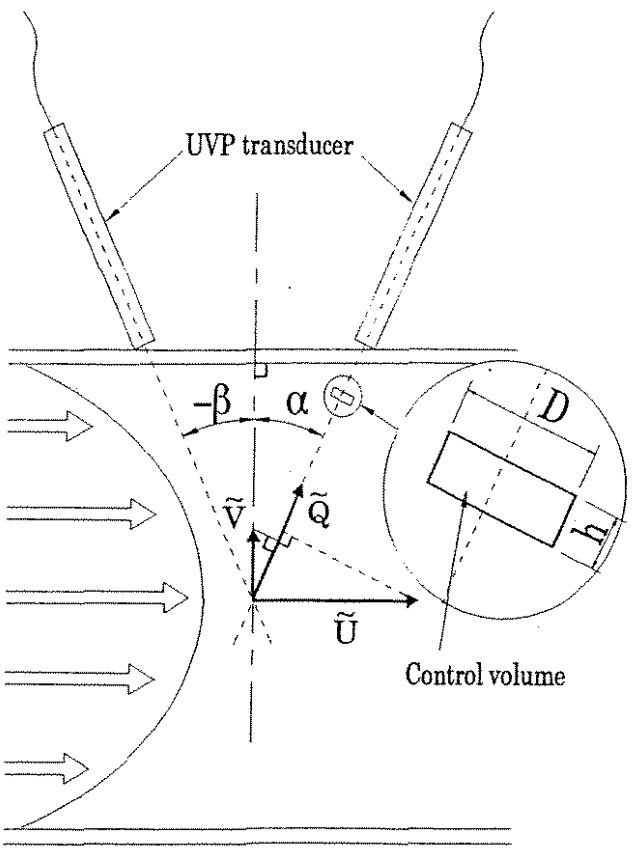

Fig.1 Control volume arrangements for measuring the Reynolds stress

$$\overline{uv} = \frac{\overline{q_1^2} - \overline{q_2^2}}{2\sin 2\alpha} = \frac{q_1'^2 - q_2'^2}{2\sin 2\alpha} \qquad (9)$$

where, q' = standard deviation of the measuring line direction.

It should be notes that the above-described method is applicable only for steady flows.

3. Experimental set-up

A schematic diagram of the experimental apparatus employed in this study, is shown in Fig.2. Both water upward and downward flows can be investigated in the apparatus, which consists of a water circulation system, an air supply system, a test section and a measurement system. An air supply system is used for the two-phase flow and is composed of an air compressor, an air regulator for controlled to presser, an laminar flowmeter, and an air-water mixing section including injected needles (inner diameter: 0.1mm). In the present study, the downward flow for a single-phase turbulent pipe flow is studied. The water is contained in a storage tank, and is pumped up to an overflow tank by a centrifugal pump. Then it is fed into the test section through the contraction under a constant pressure. Flow rate is controlled by a needle valve and is monitored by two orifice flowmeters, one is used for Re<8000 and other one for Re≧8000. They are located downstream of the test section. During the experiments, water temperature is kept about 20 degrees using a sub-cooler. The flow measuring system consists of the UVP monitor (X-3 PS-i model) and a personal computer which records the flow rate and temperature data. Setting parameters of UVP measurement in present experiments are shown in Table1.

The test pipe made of Plexiglas of total 6m length is located vertically, and it is inner diameter is 50mm. The test section is located at 80 pipe inner diameters downstream of the entrance. Turbulence mixing is promoted by the "Tripping ring" mounted at the inlet pipe and thus to reduce the length required for fully developed turbulent flow.

The test section is shown in Fig.3. The UVP transducer is set on the surface of outer wall with a contact angle of θ degrees perpendicular to the flow direction. Wall thickness of pipe in this section is 1mm, because permeability of the ultrasonic beams are good. The test section is set in an aquarium filled with water to get easy and firm coupling between the wall and transducer. As a reflector material, nylon powder is suspended in water about 0.0058%vol which has a median diameter of about 80 μm.

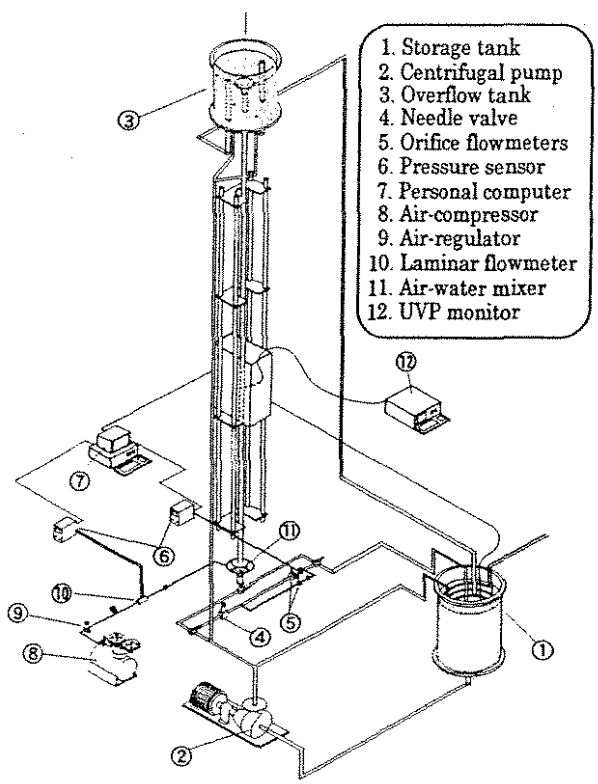

Fig.2 Schematic diagram of experimental apparatus

Table1 Parameters of UVP measurement

Basic ultrasonic frequency	4MHz
Maximum measurable depth	586mm
Velocity resolution	0.46mm/sec
Time resolution	147msec
Spatial resolution	0.37mm
Measurement point	128
Number of profiles	20000
Ultrasonic beam diameter	2.5mm

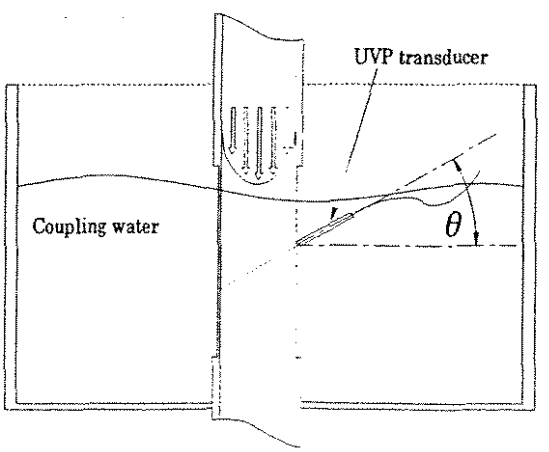

Fig.3 Test section

4. Experimental results

The error induced by the effect of measuring control volume is shown in Fig.4, which are based on the Direct Numerical Simulation [4]. Due to the error, depend on a curvature of velocity gradient, there are slightly different in the buffer region of $Y^+>30$ and $Y^+<2$. In region of $2<Y^+<30$, there are observed obvious deviation (max 5% at θ =15°), and are increased with increase of θ. Further, the measuring control volume is crossed into the wall in the extremely near wall region. Therefore, nearest measuring point from the wall is $Y^+>3.6$ at θ =15°. Measured mean velocity distribution in the present experiment at Re=5300 is shown in Fig.5. This velocity profile is sufficiently practical in $Y^+>30$ region. However, in $Y^+<3.6$ region is not accurately due to various effects as mentioned above and diffusion of ultrasonic pulse reflection from the wall and the error in $3.6<Y^+<30$ region is included by the effect of control volume.

The Reynolds shear stress profile over the pipe radius along with the data of DNS is shown in Fig.6. The present results are slightly smaller than those of DNS data in the region of $0.2 < r/R < 1.0$ and show a different near-wall profile.

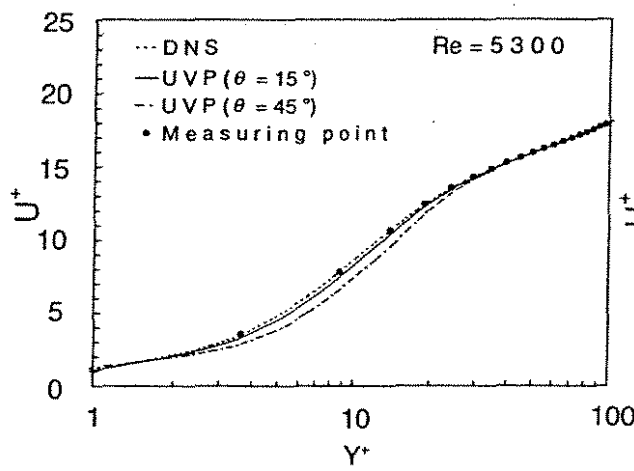

Fig.4 Effect of control volume on mean velocity profile

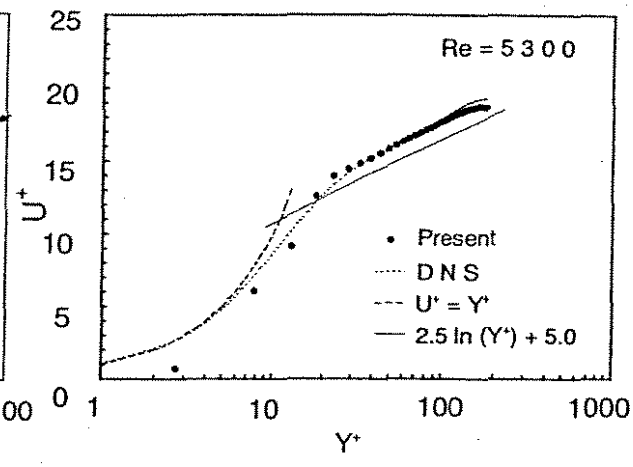

Fig.5 Mean velocity profile

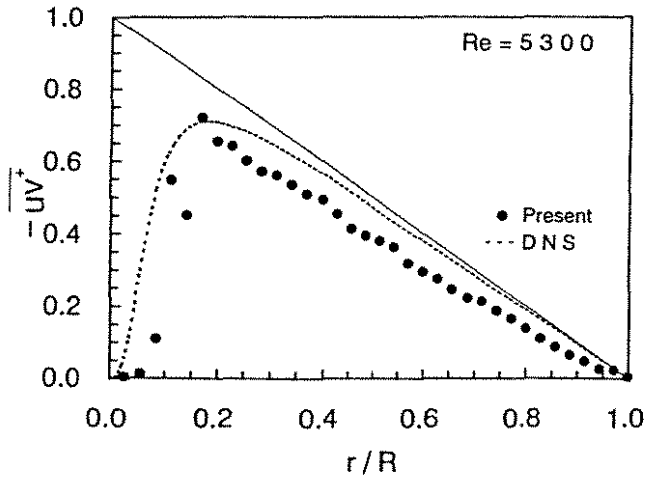

Fig.6 Reynolds stress

References

[1] Y.Takeda, *Experimental Thermal and Fluid Sci.*, Vol. 10 (1995), pp. 444-453.

[2] F.Durst, A.Melling and J.H.Whitelaw, London : Academic Press (1976), pp.345-346.

[3] C.Tropea, *Experiments in Fluids,* Vol. 1, Technical notes, (1983), pp. 209-210.

[4] J.G.M.Eggels, *et al., J. Fluid Mechnics,* Vol. 268 (1994), pp. 175-209.

2. ISUD
2nd International Symposium on Ultrasonic Doppler Methods
for Fluid Mechanics and Fluid Engineering
September 20-22, 1999
Paul Scherrer Insitut, 5252 Villigen PSI, Switzerland

The structure of flow over the heated rotating plate.

M., Kuze[1], N., Furuichi[2], and M., Kumada[1]

1. Department of Mechanical Engineering, Gifu university, 1-1 Yanagido, Gifu 501-1193, Japan
2. Paul Scherrer Insitut, CH5232 Villigen PSI, Switzerland

1.INTRODUCTION

A flow over the rotating plate is often studied to understand the instability mechanisms present in a three-dimensional boundary layer. This configuration can realize a wide range of Reynolds number so that many investigations have been also reported about laminar-turbulent transition[1] [2]. On the other hand, it is well known that a flow structure over the heated rotating disk is affected with the natural convection and centrifugal force of rotation plate. However, in this flow field, there is three-dimensional boundary layer as mentioned above so that it is difficult to clarify the mechanism in quantitatively. Especially, Ogino et al.[3] showed the vortex structure when the free convection govern the flow field. To clarify the relation between the free convection and a flow by centrifugal forced, it is necessary to measure a velocity profile over a flow field.

In this investigation, we measured velocity field on a heated rotating disk with attention to the three-dimensional boundary layer. Especially, we discuss about a relation between a radial flow by centrifugal force and an axial flow by natural convection.

2.EXPERIMENTAL EQUIPMENT AND METHOD

Experimental equipment is shown in Fig.1. The rotating plate with heater and thermocouple integrated(Cu-Co) inside has a diameter of 170mm and made of copper. The heater (200V-20A) was fixed by an adhesive with high thermal conductivity onto the copper and covered by thin insulation. The heater was connected with the transformer through the slip ring as shown in Fig.2. Rotational unit was connected with the motor by a rubber belt and maximum rotation speed is 200rpm.

The UVP monitor used in this experiment is model X3-PS, and a basic frequency of transducer is 4MHz. A Nylon powder (a diameter of 50 μm, density is 1.02) was used as a tracer. The schematic of

the measuring line is shown in Fig.3. The transducer was set to measure three components of velocity (circular, radius, and axis direction) to clarify the three-dimensional structure. The control parameter of a flow is $Re=\Omega r^2/\nu$ (where Ω is a angular velocity, r is distance from center of the disk and ν is a kinematic viscosity) as rotation and $Gr=d^3 g\beta'(\theta-t)/\nu^2$ as natural convection (where θ is a temperature of the surface of the disk and t is a temperature of a water, d is a diameter of the disk).

3.RESULTS AND DISCUSSION

A mean velocity profiles of v_r-component are shown in Fig.4(a)-(c). Rotating speed is 50rpm and Re=0 to 3.1×10^4. A difference of temperature are (a)0℃, (b)20℃ ($Gr=5.96\times10^8$), and (c)40℃ ($Gr=2.14\times10^9$). This velocity component is generated by the centrifugal force of rotating plate and velocity component is clearly decreased due to free convection generated by temperature gradient. When the rotation speed is 50rpm and difference of temperature is 20 degree, the velocity component of centrifugal force can be observed at 5mm upward from the surface of the plate, however it can not be observed above this region. When a difference of temperature is 40 degree, velocity component can be observed only at 1mm from the surface. In a case of fast angular velocity, v_r-component can be observed at the upper region of surface of the plate. As a result, it can be considered that the radial direction is controlled by Reynolds number more than Grashof number at where Reynolds number is large (r is large).

Those results clearly show that natural convection affects to a velocity component of centrifugal force largely. We will measure velocity component of circular and axial direction for various rotation speed and a difference of temperature and will clarify the structure of three-dimensional boundary layer and relation between free convection(Gr) and flow of rotation plate(Re).

REFERENCES

[1] Balachandar, S. Streett, C. L. and Malik, M. R., J. Fluid Mech., 242, p323, 1992

[2] Littell, H. S. and Eaton, J. K., J. Fluid Mech., 266, p175, 1994

[3] Ogino, F., Inamuro, T., Saito, Y. and Saito, A.,, 34th National Heat Transfer Symposium of Japan. p605, 1997 (in Japanese)

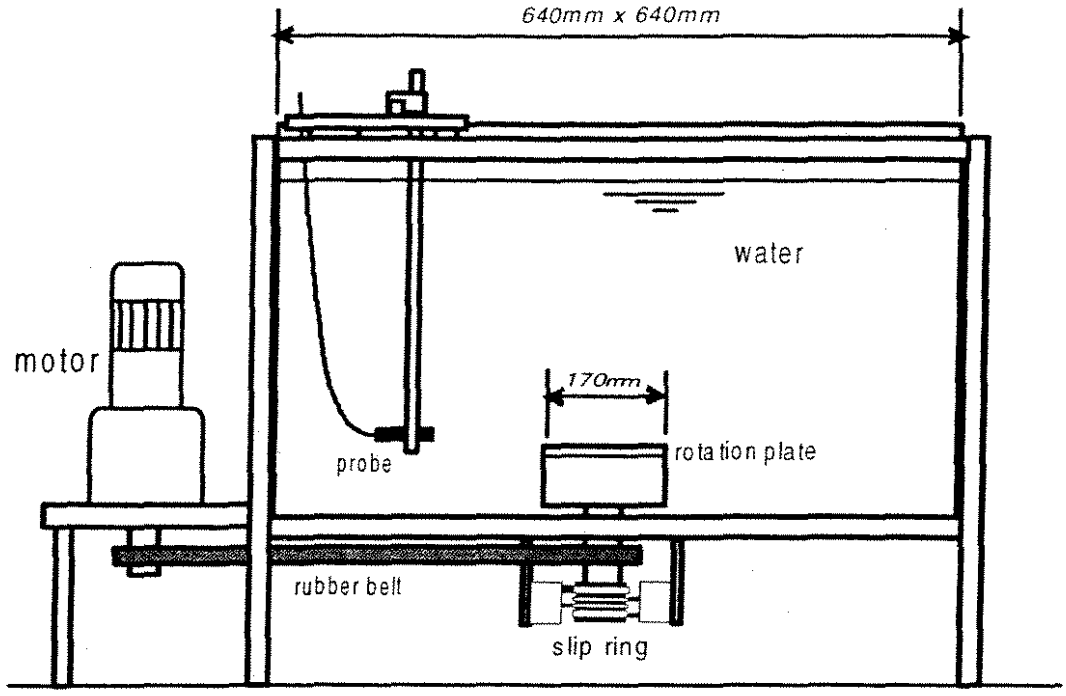

Fig.1 Experiment equipment

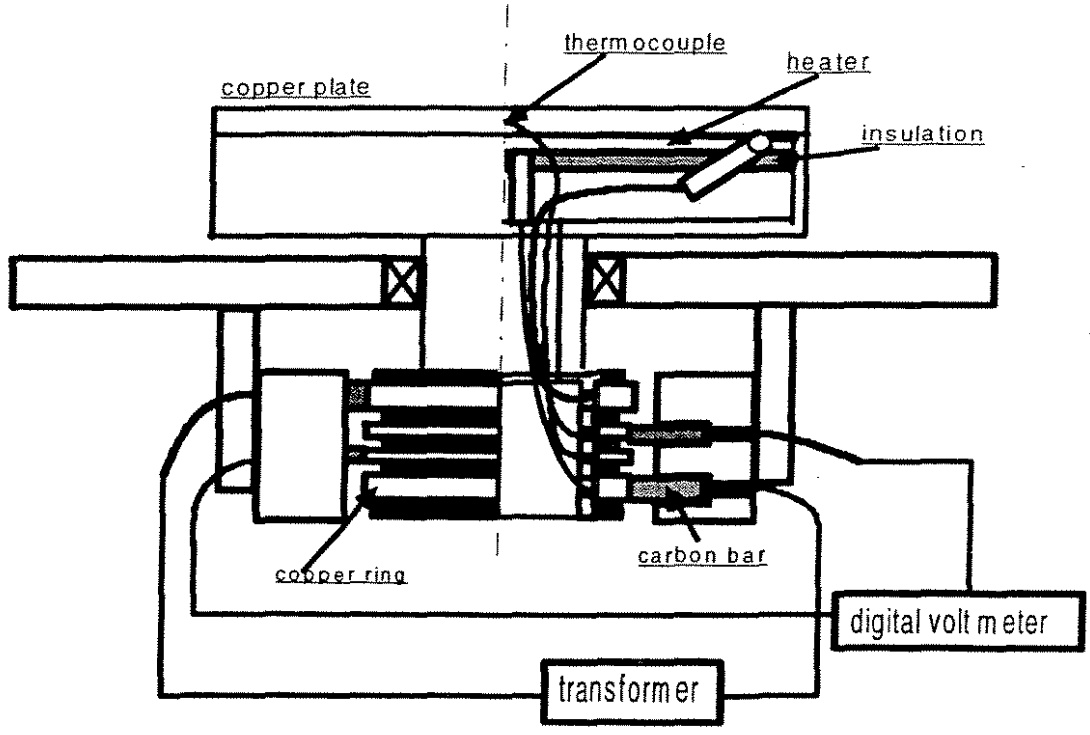

Fig.2 Slip ring detail

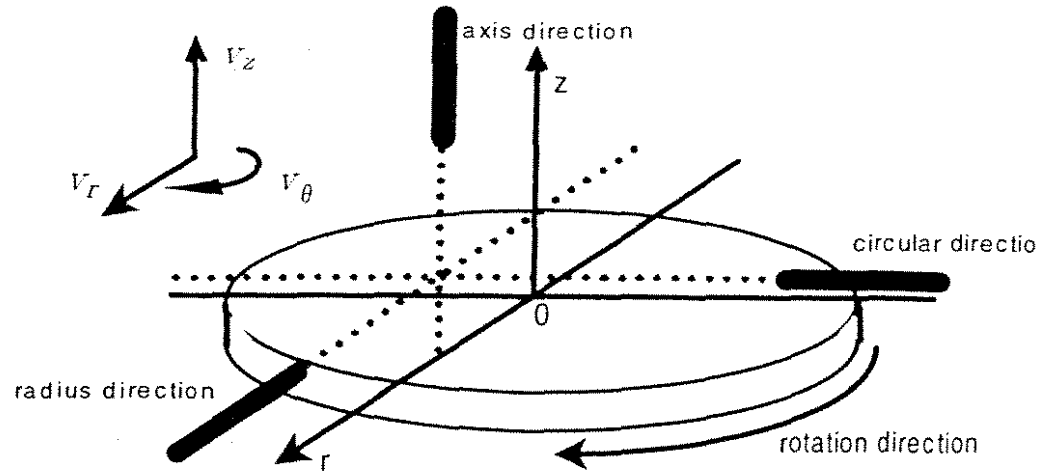

Fig.3 Probe directions

(a) 50r.p.m Gr=0

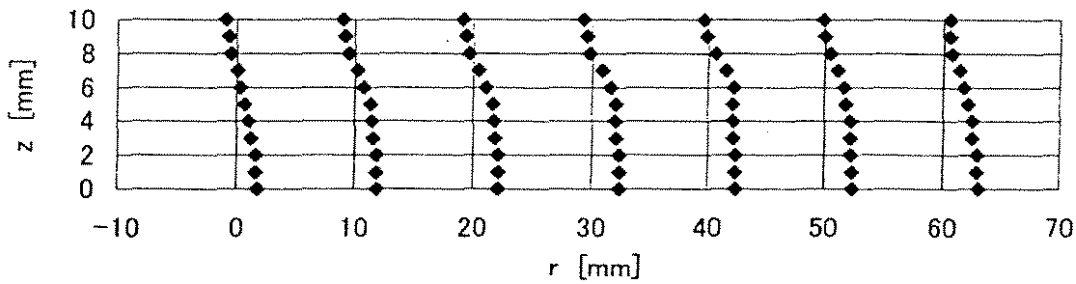

(b) 50r.p.m $Gr=5.96\times10^8$

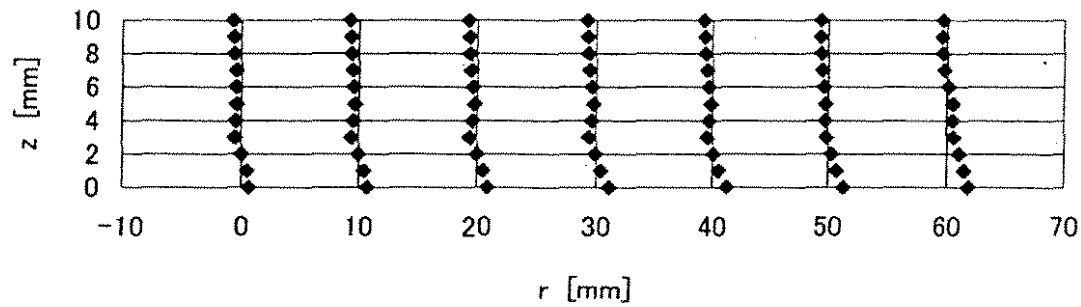

(c) 50r.p.m $Gr=2.14\times10^9$

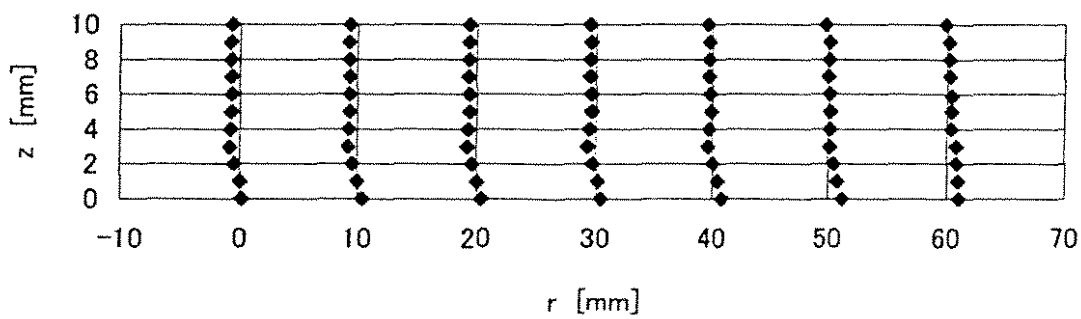

Fig.4 Mean velocity profile of v_r-component

PAUL SCHERRER INSTITUT

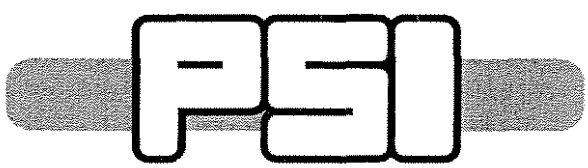

Paul Scherrer Institut
CH-5232 Villigen PSI
http://www.psi.ch

Phone 056 310 21 11
Fax 056 310 21 99